University of California, San Diego
Department of Structural Engineering
Structural Systems Research Project

Report No. SSRP – 2000/11

Assessment of Hoop Strains in the Flexural Plastic Hinge Region of Typical Bridge Columns

by

Yael D. Hose
Graduate Research Assistant
University of California, San Diego

Danielle Brestel
Graduate Research Assistant
University of California, San Diego

Frieder Seible
Professor of Structural Engineering
University of California, San Diego

Robert K. Dowell
ANATECH Corporation

Final Research Report for Caltrans under Contact No. 59A0232

Department of Structural Engineering
University of California, San Diego
La Jolla, California 92093-0085

Revision A
May 2001

Technical Report Documentation Page

1. Report No.	2. Government Accession No.	3. Recipient's Catalog No.
SSRP 2000/11		

4. Title and Subtitle	5. Report Date
ASSESSMENT OF HOOP STRAINS IN THE FLEXURAL PLASTIC HINGE	FINAL OCTOBER 2000
	6. Performing Organization Code

7. Author(s)	8. Performing Organization Report No.
Hose/Brestel/Seible/Dowell	UCSD / SSRP 2000/11

9. Performing Organization Name and Address	10. Work Unit No. (TRAIS)
Department of Structural Engineering School of Engineering University of California, San Diego La Jolla, California 92093-0085	11. Contract or Grant No.

12. Sponsoring Agency Name and Address	13. Type of Report and Period Covered
California Department of Transportation Engineering Service Center 1801 30th St., West Building MS-9 Sacramento, California 95807	Final Report – Revision A
	14. Sponsoring Agency Code

15. Supplementary Notes

Prepared in cooperation with the State of California Department of Transportation.

16. Abstract

Prior to the 1990's, the use of A615 steel for the construction of highway structures in California was widespread. Some of these structures used stick welding for the transverse column reinforcement. A sampling of these welded hoops was later tested and found to have an average strain capacity of approximately 4.2%, with a standard deviation of 1.2%. This capacity is well below the 9% strain that is typically assumed in today's standard design at design displacement ductility capacities of around 4. The purpose of this report is to investigate hoop strain levels measured in laboratory experiments in the plastic hinge zone of ductile columns and compare them to theoretical strains obtained using Mander's model at various ductility levels to see how realistic hoop strain levels based on current design approaches are. The results of the investigations show that typical current bridge column designs have adequate transverse confinement to prevent hoop strains from exceeding 2% to 3% at a displacement ductility level of 4. Furthermore, there is approximately twice the amount of transverse steel required to prevent hoop strains from exceeding 4%. The research shows that strains around the circumference of the transverse reinforcement remain well below strain levels assumed in current section analysis design models. These results indicate that expected hoop strain levels at the design ductility of typical bridge columns are still well below the reduced strain capacity levels of stick-welded hoops. As part of this research project, a method was developed to allow the designer a quick assessment of other questionable circular confined columns to determine the amount of transverse steel required to prevent weld failure.

17. Key Words	18. Distribution Statement
Hoop strains, plastic hinge, welded hoops	Unlimited

19. Security Classification (of this report)	20. Security Classification (of this page)	21. No. of Pages	22. Price
Unclassified	Unclassified	123	

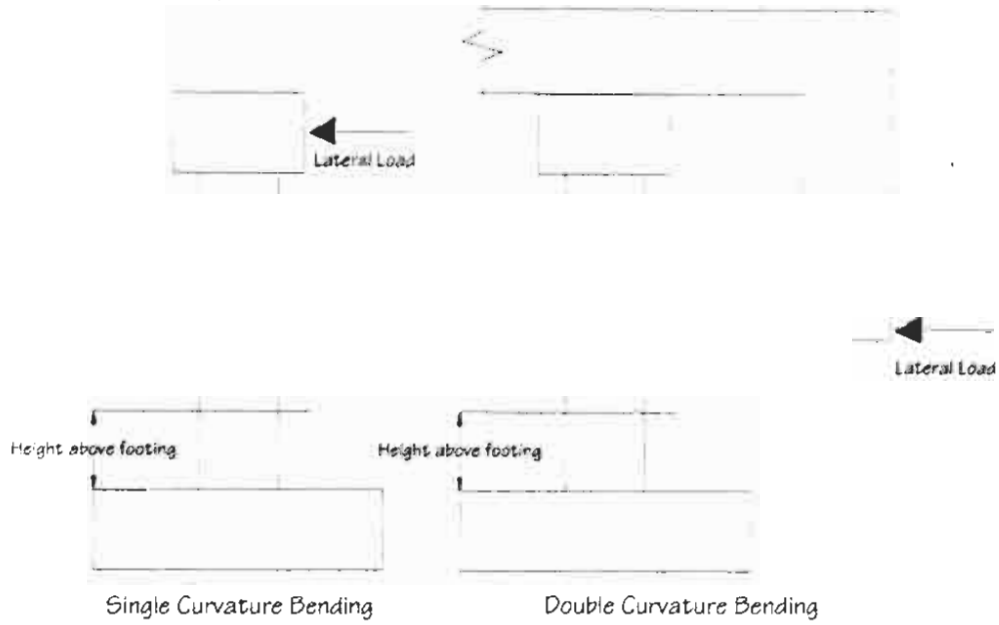

Figure 2.2: Flexure and shear test setups

Table 2.1: Test Matrix

Report #	Reference #	Test Unit	Scale	Cross section	Transverse Reinforcement
SSRP 97/05	[7]	TU1	40%	Circular	Spiral
		TU7	40%	Circular	Spiral
SSRP 97/06	[15]	RDS1	40%	Rectangular	Double spiral
		RDS6	40%	Rectangular*	Double spiral
SSRP 94/14	[16]	Col 1	Full	Circular	Spiral
		Col 2	Full	Circular	Spiral
SSRP 96/07	[10]	L1	Full	Circular	Hoops
		L1-R	Full	Circular	Hoops w/ fiberglass jacket
SSRP 93/01	[18]	R5	40%	Rectangular	Stirrups
		R6	40%	Rectangular**	Stirrups w/ steel jacket
SSRP 94/08	[13]	Col 1	40%	Circular	Hoops
		Col 2	40%	Circular	Hoops
SSRP 91/06	[3]	TU3	40%	Circular	Hoops
		TU4	40%	Circular	Hoops w/ steel jacket
SSRP 99/08	[11]	VP1	25%	Circular	Spiral
		VP2	25%	Circular	Spiral
TR 97/07	[5]	Carbon Jacket	40%	Circular	Hoops w/ carbon-fiber jacket
NIST	[17]	Flexure	Full	Circular	Spiral
		Shear	Full	Circular	Spiral

* Flared Column

** Elliptical steel jacket placed on column from base to 48 inches above base

TABLE OF CONTENTS

spiral ruptured in the second cycle of ductility 6, however, extensive shear deformation was evident. Additional information on TU7 can be found in Sections 2.8 and 4.7.7 of [7]. It should be noted that TU5 from this experimental program was not one of the columns explicitly evaluated in this chapter. However, it was used in the validation of the new analytical model in Chapter 4. TU5 and TU7 were designed identically except the curvature rods going through the column in TU7 were split, sleeved, and lubricated.

2.1.2 40% Scale Flexural Flared Rectangular Columns with Interlocking Spirals (SSRP 97/06 [15])

The test objectives for RDS1 and RDS6 were to investigate the influence of concrete flares on the structural behavior of the columns, to verify the potential seismic performance issues associated with flared columns, and to develop solutions to properly analyze, design, and retrofit these columns. RDS1 and RDS6 were rectangular in cross-section and contained a double cage consisting of longitudinal reinforcement and transverse spirals placed in a figure eight pattern. Both columns were scaled to 40%, tested in single bending, and subjected to quasi-static loading. RDS1, a prismatic reference column with a constant rectangular cross-section the entire height of the column, failed at a displacement ductility level of 12 by buckling of the longitudinal reinforcement which led to rupture of the transverse spirals and eventually rupture of the longitudinal reinforcement. Additional information about RDS1 can be found in Section 6.1 of [15]. RDS6 consisted of a design that decoupled the concrete flare from the cap-beam connection by a 2-inch soffit gap while also providing increased transverse reinforcement in the flared region. RDS6 failed at a displacement ductility level of 10 by buckling and rupture of the longitudinal reinforcement. Additional information on RDS6 can be found in Section 6.6 of [15].

2.1.3 Full-Scale Flexural Circular Columns with Spiral Confinement Reinforcement (SSRP 94/14 [16])

The test objectives for Columns 1 and 2 were to investigate the flexural integrity of longitudinally loaded cap-beam/column connections in current bridge design practice. The columns were designed with #18 column longitudinal bars that were anchored

LIST OF FIGURES

buckling and rupture of the longitudinal reinforcement. Additional information on R5 can be found in Sections 4.2.1, 5.1.2.1, and 5.4.2.5 of [18]. R6 was designed based on R5 and was retrofitted with a steel jacket. It failed at a displacement ductility level of 7.7, due to shear degradation at a location above the steel jacket. Additional information on R6 can be found in Sections 4.2.2, 5.1.2.2, and 5.4.2.5 of [18].

2.1.6 40% Scale Shear Circular Columns with Hoop Confinement Reinforcement (SSRP 94/08 [13])

The test objective for Column 1 was to investigate the flexural response of columns with low longitudinal steel ratios, while Column 2 investigated whether shear strength was influenced by the longitudinal steel ratio. Both columns were scaled to 40%, tested in reversed curvature, and subjected to quasi-static loading. Column 1 was designed to evaluate ductile response and the distribution of cracking for a column at the lower end of the feasible longitudinal reinforcement ratio range. The column suffered a combined flexure-shear failure at a displacement ductility level greater than 10 when longitudinal reinforcement in the upper and lower plastic hinge regions buckled and several hoops along the large diagonal flexural-shear cracks (that spanned the entire column height) fractured. Additional information on Column 1 can be found in Section 4.1 and Chapter 5 of [13]. Column 2 was under-reinforced for shear to investigate the shear strength of columns with low longitudinal reinforcement ratios, and failed at a displacement ductility level of 4 in shear. Additional information on Column 2 can be found in Section 4.2 and Chapter 5 of [13].

2.1.7 40% Scale Flexural Circular Columns with Hoop Confinement Reinforcement and a Steel Jacket Retrofit (SSRP 91/06 [3])

The test objective for columns TU3 and TU4 in this study was to investigate the use of a steel jacket retrofit program to enhance the plastic hinge regions of these continuously reinforced columns. Both columns were scaled to 40%, tested in single bending, and subjected to quasi-static loading. TU3, the control column without a steel jacket, failed at a displacement ductility level of 5 by means of confinement failure. Additional information about TU3 can be found in Sections 4.1.2.1, 3.1.4, 4.3, and 4.5 of

LIST OF TABLES

SUMMARY

Prior to the 1990's, the use of A615 steel for the construction of highway structures in California was widespread. Some of these structures used stick welding for the transverse column reinforcement. A sampling of these welded hoops was later tested and found to have an average strain capacity of approximately 4.2%, with a standard deviation of 1.2%. This capacity is well below the 9% strain that is typically assumed in today's standard design at design displacement ductility capacities of around 4. The following report investigates actual experimental and analytical strain demands in hoop reinforcement of various bridge columns to see how realistic hoop strain levels based on current design approaches are. Current design approaches based on Mander's model to determine transverse reinforcement/confinement amounts are known to be very conservative when compared to large or full-scale laboratory test data. The purpose of this report is to investigate actual hoop strain levels measured in laboratory experiments in the plastic hinge zone of ductile columns and compare them to theoretical strains obtained using Mander's model at various ductility levels. The results of the investigations show that typical current bridge column designs have adequate transverse confinement to prevent hoop strains from exceeding 2% to 3% at a displacement ductility level of 4. Furthermore, there is approximately twice the amount of transverse steel required to prevent hoop strains from exceeding 4%. The research shows that strains around the circumference of the transverse reinforcement remain well below strain levels assumed in current section analysis design models. These results indicate that expected hoop strain levels at the design ductility of typical bridge columns are still well below the reduced strain capacity levels of stick-welded hoops. As part of this research project, a method was developed to allow the designer a quick assessment of other questionable circular confined columns to determine the amount of transverse steel required to prevent weld failure.

welded hoop was placed in several components of the "Orange Crush" interchange (SR-57/I-5). A sampling of these welded hoops was later tested and found to have an average strain capacity of approximately 4.2%, with a standard deviation of 1.2%. This capacity is well below the 9% strain that is assumed as the limiting hoop strain value in today's standard design based on section analyses using the Mander model [9].

1.2 Research Objective:

In May of this year, a study was performed [8] to investigate the strain capacity of an array of bar samples representing different conditions found for transverse reinforcement in typical bridge columns. Initially, #8 continuous reinforcing bar samples using A706 and A615 steel were pulled to compare straight bars versus hoop segments. The results indicate that there is no significant difference between pulling straight bars or hoop segments as measured by the strain at peak stress. Phase II of the study investigated A706 and A615 #8 straight bar samples, spliced straight bar samples, hoop bar samples, and spliced hoop bar samples. Both stick-welds and flash welds were tested for the spliced bars. The results, reported in terms of "average strain" and "standard deviation" for the strains obtained from the pull tests of each group, are summarized in Table 1.1and show that welded #8 bars can experience significant failure strain reductions depending on the welding procedure and heat treatment. While in general the currently specified and used A706 steel seemed to outperform A615 steel and splices, the standard deviations in the A706 tests were significantly higher. Thus statistically, both steel types show similar performance. More information regarding the testing procedure and results from these tests can be found in [8].

In addition to the above pull tests, sample pulls from the I-5/SR-14 and Orange Crush projects were investigated and reported. Samples of the #8 A706 continuous, stick-welded, and flash welded hoops were extracted from various existing columns of the ramps at the I-5/SR-14 separation. Also, #14 stick-welded main reinforcement samples were removed from the columns for testing purposes. For the Orange Crush project, all the samples were #8 A615 stick-welded hoops. Table 1.2 shows the findings from these pull tests.

the hoop strains occurring in plastic hinge regions at high ductility levels, well-calibrated analytical tools are required.

Current design methods use sectional moment-curvature analysis tools that are based on the Mander equal energy model [9], which equates the work done on the confined concrete core up to failure with the strain energy capacity of the hoop or spiral reinforcement. The Mander model has consistently been found to be conservative by large-scale flexural testing. This conservatism is reasonable for design but not for the detailed assessments required in this study. To overcome the deficiencies in current analytical tools, a new model was developed by Dowell of ANATECH Corp. of San Diego as part of this study. In the Dowell model, the expansion of the concrete core is explicitly considered during each increment of a moment-curvature analysis, which enables reliable hoop strains to be determined at any ductility level. The Dowell model, which is presented in Chapter 3, was calibrated using experimentally observed hoop strain data and was used to assess the hoop strains in the Orange Crush columns in Chapter 4 to determine whether their displacement capacities were sufficient.

The purpose of this report is to show that the hoop strains assumed in design, which are based on the Mander model, are not actually occurring in experiments or refined analyses. The objective of this research is to establish a relationship between column ductility levels and strain in the transverse reinforcement. This information will be used to determine whether or not the capacity of the welds in structures that have A615 or A706 stick-welded confinement hoops exceed the expected demands placed on them.

1.3 Research Tasks:

1.3.1 Experimental Review

As part of the Caltrans Seismic Safety Bridge Research Program, over 200 large or full-scale bridge columns with various design and retrofit details have been tested to

equates the axial work done on the confined concrete core up to failure with the strain energy capacity of the hoop or spiral reinforcement. Mander assumes that the ultimate concrete compressive strain capacity derived from this energy balance approach occurs when the spiral/hoop necks and fractures at an ultimate strain of 12% [9]. Although the Mander model is used extensively for the design of bridge columns, it has been found to be conservative by large-scale flexural testing. The Mander model is conservative because (1) it assumes that 100% of the axial work done on the column is transferred to strain energy in the hoops, whereas at large axial strains only about 60% efficiency is noted, and (2) it does not include a strain gradient (flexure) in the energy balance equation.

The ductility capacity of a member in the Mander model is only provided at hoop fracture, and hoop strains at lesser ductility levels are not determined. To overcome these deficiencies, a new method is presented in Chapter 3 that calculates the hoop strains at each increment of a moment-curvature analysis. The method uses a similar energy balance approach as developed by Mander, but the energy balance is applied at each curvature or axial strain increment and to each fiber, rather than to the entire section. This allows the tangent Poisson's ratio at each curvature increment and for each element to be determined, which directly affects the concrete core expansion and the hoop strains. The theory of the new model, developed by Dowell at ANATECH Corp. of San Diego, is presented in Chapter 3.

1.3.3 Design analysis

In Chapter 4, the modified moment-curvature analysis tool, discussed above, was validated with experimental data and then applied to the bridge columns in the Orange Crush Interchange to evaluate hoop strain demands. The initial case study evaluation consisted of comparing the analytical model with experimental results. Two columns that were part of a research program to investigate the effects of relocating the plastic hinge region in flexural bridge columns were assessed [7]. Also evaluated were two full-scale circular bridge column-superstructure connection tests [16]. Once the analytical model

ASSESSMENT OF HOOP STRAINS IN THE FLEXURAL PLASTIC HINGE REGION OF TYPICAL BRIDGE COLUMNS

1 Introduction

Rather than designing structures with excessive strength, the emphasis in current seismic bridge design is the concept of ductility, which allows a structure to undergo large inelastic deformations imposed by seismic forces without any degradation in strength. The basis of this design philosophy consists of predefining locations in the structure, called plastic hinges, which are suitably designed and detailed as regions where large inelastic deformations and energy dissipation can occur. All other locations or members are capacity protected against inelastic deformations by designing them with a strength which is greater than the maximum possible force developed from column plastic hinging [12]. This ensures that the damage is controllable and occurs at designated locations in the bridge columns where inspection and repair are possible without traffic interruption.

Since by design the inelastic action is limited to these plastic column hinge regions, they become the critical sections of the columns that will see the highest forces and strains. For circular bridge columns, typically transverse spirals or hoops are used to confine these regions. The amount of transverse reinforcement in the plastic hinge regions is based on achieving specific design displacement ductility levels. The design objective is to ensure that the deformation capacity of these elements is greater than any demand they would see during a seismic event.

1.1 Problem Statement:

Although current construction of highway structures in California requires the use of A706 steel, prior to the 1990's the use of A615 steel with stick welding for the transverse reinforcement was widespread. Between 1991 and 1996, this type of A615

Table 1.1: Strain capacities from bar samples under various conditions

Sample Type	A706		A615	
	Average Strain (%)	Standard Deviation (%)	Average Strain (%)	Standard Deviation (%)
Continuous Straight	13.61	1.09	10.06	0.79
Continuous Hoop	12.17	0.65	9.47	0.68
Continuous Straight, Heated samples	12.40	1.20	9.60	0.85
Continuous Hoop, Heated samples	9.42	1.67	5.85	1.99
Stick-welded Straight, Standard pre-heating	7.74	2.63	3.80	0.82
Stick-welded Hoop, Standard pre-heating	7.21	3.69	3.08	0.76
Stick-welded Straight, No pre-heating	5.50	0.94	3.82	0.74
Stick-welded Hoop, No pre-heating	6.79	2.19	3.05	0.61

Table 1.2: Strain capacities from sampling projects

Sample Type	I-5/SR-14 sampling project A706 Steel			Orange Crush sampling project A615 Steel		
	# of samples	Average Strain (%)	Standard Deviation (%)	# of samples	Average Strain (%)	Standard Deviation (%)
#8 continuous hoop	6	12.47	2.10	--	--	--
#8 stick-welded hoop	21	5.85	2.86	58	4.21	1.23

Results from Table 1.2 show that the stick-welded hoops extracted from the Orange Crush columns are well below the capacity of 9% that was assumed in the design. However, results from recent laboratory tests of a variety of modern columns indicate that there is a significant reserve in ductility capacity and hoop strain capacity in columns designed by current confinement standards. These experimental results show reliable hoop strains only at low displacement ductility levels of loading. Therefore, to determine

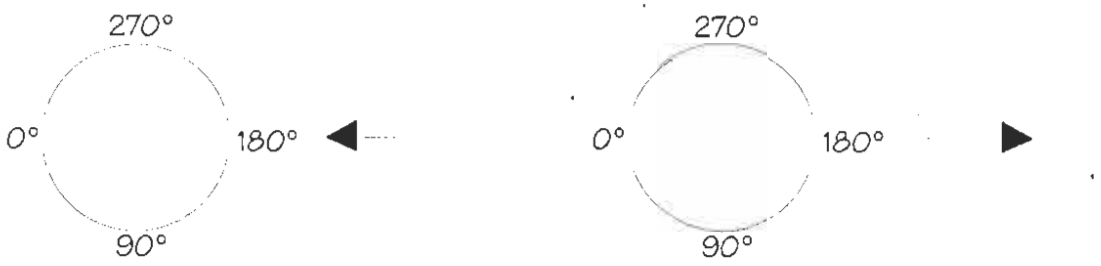

a) Push Loading **b) Pull Loading**

Figure 2.1: Degree locations around the circumference of the columns

Although strains were often measured at various locations up the height of the column, only the largest strain values representing the critical section were recorded. The location up the column height where the largest strain value was observed, at a given ductility level, was noted. For most of the columns, the location of the highest hoop strain occurred within a column diameter of the critical section, which is defined by the lowest capacity over demand ratio. In some cases, however, the location where the highest strain was measured fell outside this region. These cases typically occurred in columns that experienced extensive shear degradation. High strains are often seen up the entire column height for shear dominated columns. To see the full strain profiles for these columns outside the critical region, which are well below the values reported at the critical location in this chapter, the provided test report references should be consulted.

The flexural columns were tested in single curvature bending, while most of the shear critical columns were tested in double curvature bending. Figure 2.2 shows the flexure and shear test setups. The test matrix summarizing the experiments that were evaluated in this assessment is given in Table 2.1.

failure under simulated seismic loads at the UCSD Charles Lee Powell Structural Research Laboratories over the past decade. Thus a comprehensive database of bridge column hoop strains in flexural plastic hinge regions exists. Results from previously completed experiments conducted at UCSD as well as test results from other institutions on bridge columns designed to current seismic standards and details were reviewed. The results from these experiments were compiled to develop a relationship between the measured strains in the confinement steel at various column displacement ductility levels. The intent is to show actual hoop strain levels in flexural plastic hinge zones and to demonstrate existing capacity reserves in current Caltrans designs. Experimental strain demands on the transverse reinforcement in these columns at various ductility levels are demonstrated to be considerably lower than the design strain levels obtained from Mander's model.

Since most experimental testing is conducted on scaled specimens, particular attention was paid to the review of tests on large or full-scale bridge columns. The gathered experimental and analytical evidence is also used to support opinions on whether scaling of the test column from the full-scale prototype effects the relationship between ductility and transverse reinforcement strain. Furthermore, in the test specimen the effect of size and spacing of the transverse reinforcement on the hoop strains is evaluated. For experimental columns that were not designed according to Caltrans design specifications, it is determined if the strain in the confinement steel would be affected if related back to Caltrans design specifications. Finally, for the experimental columns that have reinforcement properties such as steel grade and deformed/smooth bar characteristics that vary from the typical columns constructed with A615 deformed bar reinforcing steel, the effect that differences in these physical properties have on the transverse strains are investigated.

1.3.2 Analytical Review

As discussed in Section 1.2, current design methods use sectional moment-curvature analysis tools that are based on the Mander equal energy approach [9], which

The Structural Systems Research Reports (SSRP) and Test Reports (TR) are from tests conducted in the Charles Lee Powell Structural Research Laboratories of the Department of Structural Engineering at UCSD. The NIST report is from a study conducted at the National Institute of Standards and Technology, a division of the Department of Commerce. The number corresponding to the reference associated with each particular column is provided. All columns were tested quasi-statically except for column VP1, which was loaded dynamically at a rate of 13 inches/sec (0.33 m/s), as part of the velocity pulse project described in Section 2.1.8. It should be noted that the columns in Table 2.1 are not reported in any specific order.

The selection of test columns evaluated in this report focused on columns with (1) current typical confinement ratios, (2) large or full-scale, (3) circular and rectangular cross-sections and (4) conventional hoop reinforcement and jacket retrofits, to cover a wider variety of typical bridge column cases. In the Section 2.1.1 through Section 2.1.10, brief summaries explaining test objectives, test scale, loading characteristics and failure modes for each test are presented. The sections in the appropriate references where additional information can be found are also given. An overview of the key design characteristics of each test column that are provided in Section 2.1.1 through Section 2.1.10 are depicted in Table 2.2 and Table 2.3.

2.1.1 40% Scale Flexural Circular Columns with Spiral Confinement Reinforcement (SSRP 97/05 [7])

The test objectives for TU1 and TU7 were to determine the effects of relocating the plastic hinge away from supporting members such as cap beams and footings. Both columns were scaled to 40%, tested in single bending, and subjected to quasi-static loading. TU1, the reference column designed by conventional standards, failed in the third cycle of displacement ductility 8 when the longitudinal reinforcement buckled and eventually ruptured. Additional information on TU1 can be found in Sections 2.2 and 4.7.1 of [7]. TU7 had a reduced effective column length and was designed to test the effect of relocating the plastic hinge region two feet from the column base on the shear capacity of the column. TU7 ultimately failed when the longitudinal bars buckled and the

was validated with experimental data, a case study assessment using as example columns of the Orange Crush was performed to determine the probable expected hoop strains in the columns.

straight into the cap beam. Other goals of this study were to determine capacity levels and the critical failure load of these connections as well as the development length of the #18 bars. Both columns were full-scale, tested in flexure, and loaded in the quasi-static range. Column 1, constructed with an "as built" cap beam, failed at a structure displacement ductility level of 3 by joint/cap deterioration in shear. Additional information about Column 1 can be found in Chapter 5 of [16]. Column 2, constructed with a more heavily reinforced cap beam, failed at a displacement ductility level greater than 4 by buckling and fracture of the longitudinal reinforcement. Additional information on Column 2 can be found in Chapter 9 of [16]. For these columns, spiral strains were measured only at 10 inches above the joint.

2.1.4 Full-Scale Flexural Circular Columns with Hoop Confinement Reinforcement and a Fiberglass Jacket Retrofit (SSRP 96/07 [10])

The test objectives for L1 and L1-R were to investigate the seismic performance of shear-dominated bridge columns with "as built" and "as repaired" (fiberglass jacket) conditions. Both columns were full-scale, tested in single bending, and subjected to quasi-static loading. L1, the "as built" control column, failed suddenly in shear just prior to the first peak of displacement ductility 1.5. Additional information on L1 can be found in Chapter 4 of [10]. L1-R, which consisted of the L1 column design retrofitted with a fiberglass jacket, developed its maximum flexural strength and achieved a displacement ductility level of 6 without strength degradation. Additional information on L1-R can be found in Chapter 5 of [10].

2.1.5 40% Scale Flexural Rectangular Columns with Stirrup Confinement Reinforcement and a Steel Jacket Retrofit (SSRP 93/01 [18])

The test objectives for R5 and R6 were to investigate the behavior of pre-1971 rectangular bridge columns and study the effectiveness of providing oval steel jackets as a retrofit strategy to enhance flexural strength and ductility. Both columns were scaled to 40%, tested in single bending, and subjected to quasi-static loading. R5, which was designed with continuous reinforcement in the plastic hinge region and served as the control column without a steel jacket, failed at a displacement ductility level of 3 by

2 Experimental Review

An extensive amount of large-scale experimentation of flexural bridge columns has been conducted at UCSD and other institutions. The results from some of these experiments, designed to be close to current Caltrans specifications, were reviewed to evaluate the actual strain demands that can be expected in the transverse reinforcement at various displacement ductility levels. Furthermore, some of these test results were used in the validation of the moment-curvature analytical tool (developed in Chapter 3) and is presented in Chapter 4. The following chapter describes the method of extracting hoop strain data from the past experimental studies and gives background information about each test that was assessed. The results are presented and comparisons of the results to support opinions on the effects that scaling, as well as size, spacing, and properties of the transverse reinforcement have on the hoop strains are provided.

2.1 Background Information

After collecting the reference material containing transverse strain data that would be relevant to this study, the column design details and material properties were logged. Strain gage data around the circumference of the section was then extracted from graphs in the reference reports in both the push and pull directions at various displacement ductility levels. In this report, degree location (i.e. 0°, 45°, 90°...) refers to the location around the circumference of the column. Typically the 0° and 180° locations represent the extreme compression and tension faces of the column. Figure 2.1 shows the locations of the strain gages around the circumference of the columns. In this study, when the columns are loaded in the push direction, the 0° gage location is in compression, while the 180° gage location is in tension. Conversely, when the columns are loaded in the pull direction, the 0° location is in tension and the 180° location is in compression.

[3]. TU4 was designed similarly to TU3 but with a steel jacket provided in the plastic hinge region. It failed at a displacement ductility level of 8 due to low-cycle fatigue fracture of the longitudinal bars. Additional information on TU4 can be found in Sections 4.1.2.2, 3.1.3, 4.3, and 4.5 of [3].

2.1.8 25% Scale Flexural Circular Columns with Spiral Confinement Reinforcement Subjected to Large Velocity Pulse Loading (SSRP 99/08 [11])

VP1 and VP2 were part of an experimental program to investigate the behavior of reinforced concrete columns subjected to near field velocity pulse loading under various strain rates. The study was a multi-institutional collaborative research program funded by the Pacific Earthquake Research Center (PEER) and conducted at the University of California, San Diego (UCSD) and the University of California, Irvine (UCI). VP1 and VP2 were part of Phase 1, which evaluated the behavior of ductile columns. VP1 was a dynamic actuator test loaded at a loading rate of 0.33 m/sec (13 in/sec), while VP2 was a quasi-static test. Both columns were first subjected to a large asymmetric pulse, and then followed by the standard cyclic loading history. The overall failure mechanism for these columns was similar and consisted of bulging of the concrete core in compression, which caused buckling of the longitudinal reinforcement, and eventually spiral and longitudinal bar fracture within the plastic hinge region. Additional information for these columns can be found in [11].

2.1.9 40% Scale Flexural Circular Column with Hoop Confinement Reinforcement and a Carbon-Fiber Jacket Retrofit (TR 97/07 [5])

The test objectives for TR 97/07 were to assess the effectiveness of a continuous carbon-jacket retrofit system for post earthquake repair of bridge columns. The "as built" and carbon jacket retrofit columns were scaled to 40%, tested in single bending, and loaded quasi-statically. The "as built" column failed at a displacement ductility level of 1.5 due to longitudinal bar buckling. Additional information on the "as built" column can be found in Section 3.1 of [5]. The carbon-jacketed column reached the design ductility level while only experiencing marginal splitting of the jacket, but no column failure. Additional information on the carbon-jacketed column can be found in Section 3.2 of [5].

2.1.10 Full-Scale Flexural and Shear Circular Columns with Spiral Confinement Reinforcement (NIST [17])

The test objectives for the NIST experiments were to determine the effects of scaling bridge columns and the effectiveness of standard design details at that time to achieve reasonable ductility capacity. The test program also included the identification of symptomatic problems in detailing practices that existed in 1989. The Flexure and Shear columns were full-scale, tested in single bending, and subjected to quasi-static loading. The Flexure column failed at a displacement ductility level of 6 due to buckling and rupture of the longitudinal reinforcement and rupture of the transverse reinforcement. Additional information about the Flexure column can be found in Section 3.2 of [17]. Although the axial loads on the two columns were the same, the column height in the Shear column was reduced while the transverse reinforcement was almost doubled. The Shear column was essentially a squat column that was adequately detailed for shear. It failed at a displacement ductility level of 8 due to longitudinal bar buckling, but had significantly more shear cracks than the Flexure column as observed by photographs provided in [17]. Additional information on the Shear column can be found in Section 3.3 of [17].

2.2 Column Parameters and Reinforcement Details

The main design parameters that include basic dimensions, concrete material properties, and axial load ratio information for each column are presented in Table 2.2. The reinforcement details and material properties are given in Table 2.3.

Table 2.2: Column Parameters

Report #	Test Unit	L' (ft)	D (in)	Cover (in)	f'_c Day of Testing (ksi)	P (kips)	$P/A_g f'_c$ (%)
SSRP 97/05	TU1	12	24	1	6	400	14.7
	TU7	5*	24	1	5.1	200	8.68
SSRP 97/06	RDS1	13	24x36	1	4.81	400	9.63
	RDS6	13	24x36	1	4.79	400	9.67
SSRP 94/14	Col 1	25	60	2	6.1	600	3.48
	Col 2	25	60	2	4.34	600	4.89
SSRP 96/07	L1	12	72	2.5	4.29	300	1.72
	L1-R	12	72	2.5	4.29	300	1.72
SSRP 93/01	R5	12	19.25x28.75	0.75	4.85	400	14.9
	R6	12	19.25x28.75**	0.75	5.25	400	13.8
SSRP 94/08	Col 1	7.5	24	0.8	4.35	113	5.7
	Col 2	7.5	24	0.8	4.37	113	5.7
SSRP 91/06	TU3	12	24	0.8	4.73	400	18.7
	TU4	12	24	0.8	5.52	400	16
SSRP 99/08	VP1	6	16	0.5	5	0	0
	VP2	6	16	0.5	4.38	0	0
TR-97/07	Carbon Jacket	12	24	0.5	6.07	400	14.57
NIST	Flexure	30	60	2	4.14	1000	8.54
	Shear	15	60	2	5.2	1000	6.8

* L' = L_{eff}: plastic hinge was relocated 2 ft up from column/footing interface. L_{total} = 7 ft

** Elliptical steel jacket was placed on column changing cross-section. See reference.

Table 2.3: Reinforcement Parameters

Report #	Test Unit	ρ_l (%)	$d_{b,l}$ (in)	# bars	$f_{y,l}$ (ksi)	ρ_s (%)	d_{sp} (in)	s (in)	$f_{y,t}$ (ksi)
SSRP 97/05	TU1	2.66	0.875	20	66	0.87	0.375	2.25	Gr 60
	TU7	2.66	0.875	20	67	0.87	0.375	2.25	Gr 60
SSRP 97/06	RDS1	1.53	0.75	30	68.5	0.44	0.375	2	68.5
	RDS6	1.53	0.75	30	70.8	0.44	0.375	2	Gr 60
SSRP 94/14	Col 1	4.07	2.257	20	77.5	0.89	0.75	3.5	62.3
	Col 2	4.07	2.257	20	70	0.89	0.75	3.5	66.8
SSRP 96/07	L1	1.33	1.693	24	73.8	0.09	0.5	12	43.3
	L1-R	1.33	1.693	24	73.8	0.09	0.5	12	43.3
SSRP 93/01	R5	5.03	1*	14	47.7	0.17	0.25	5	51
			0.875*	28	40.6				
	R6	5.03	1*	14	47.7	0.17	0.25	5	51
			0.875*	28	40.6				
SSRP 94/08	Col 1	0.53	0.5	12	67	0.29	0.25	3	52.3
	Col 2	1.06	0.5	24	67	0.17	0.25	3	52.3
SSRP 91/06	TU3	2.53	0.75	26	45.7	0.174	0.25	5	51
	TU4	2.53	0.75	26	45.7	0.174	0.25	5	51
99/08	VP1	1.2	0.5	12	64.6	0.52	0.178	1.25	Gr 80
	VP2	1.2	0.5	12	64.6	0.52	0.178	1.25	Gr 80
TR-97/07	Carbon Jacket	5.1	1.128**	16	Gr 60	0.17***	0.25	5	50
			0.75**	16	70.5				
NIST	Flexure	2	1.693	25	68.9	0.633	0.625	3.5	71.5
	Shear	2	1.693	25	68.9	1.479	0.75	2.125	63.1

* Columns had 28 #7's around the perimeter of the column with two additional rows of 7 #8's directly outside the main longitudinal reinforcement cage on the 19.25"edges of the column

** Columns had bundled longitudinal bars: 14 #8 and then 14 #7 directly inside the #8's

*** Number shown for transverse reinforcement ratio does not include carbon jacket

2.3 Experimental Transverse Reinforcement Strain Results

As described in Section 2.1, the strains measured by gages on the transverse reinforcement were extracted for each test unit described in the previous section from figures in the reference reports. Tabular results of these strain values for each test are supplied in Appendix A. In these tables, strain values at various locations around the circumference of the transverse reinforcement for each column are provided for increasing ductility levels. The location up the height of the column where the highest strains were observed is also given and is understood to be where all the strain values were extracted from unless otherwise noted. Typically, these peak hoop strain values fell

within a column diameter of the critical section, defined by the lowest capacity over demand ratio.

Appendix B presents the tabular results, which were compiled to compare hoop strain and displacement ductility levels at different locations around the column perimeter. The strain results at various locations around the circumference of a column provide a better understanding of the behavior of the column during testing. Typically, gages placed on the transverse reinforcement in the direct line of loading along the tension or compression generators (i.e. 0° and 180° gages) provide data for maximum strains seen during flexural response, while strains measured on the sides of the column (90° and 270°) indicate shear strain. Graphs representing the strain versus displacement ductility level for various circumference degree locations using the tabular results in Appendix B are given in Appendix C. These figures isolate locations around the circumference and show strains values as the displacement ductility levels increase. In Appendix D, graphs that depict the circumferential strain profiles for the columns at each displacement ductility level are provided. These graphs isolate each displacement ductility level and show the strain values as they vary around the column.

2.3.1 Test Comparisons

Although the graphs in the appendices present the results for all of the experimental columns investigated, graphs showing comparisons of various parameters are provided in this section in order to more clearly observe trends or behavioral characteristics between the experimental columns. For clarity in these graphs, only displacement ductility levels of 1, 2, 3, 4, 6, 8 and 10 and degree locations of 0, 90, 180, and 270 are presented. As stated in the Section 2.3, results for the columns that are not included in Figure 2.3 through Figure 2.9 can be found in their respective tables in Appendix A.

Figure 2.3 shows a comparison of all the flexural tests assessed in this report whether they required the use of jacket retrofits or other methods to obtain their ductility.

The strain gages for most cases remained intact up to a displacement ductility level of 4, demonstrating that hoop strain values extracted from these experiments were relatively low (below a value of 0.004). Hoop strains at the 0° location are shown in Figure 2.3a, while the strains at the 90° location are depicted in Figure 2.3b. Since the strain values are extremely low in these flexural columns, the difference between strains measured at the extreme tension and compression side of the column (0° location), as opposed to the out of plane shear faces of the columns (90° location), is not as apparent. However, typically for flexure columns the higher strains are observed on the compression side of the column at the 0° location in the direct line of loading.

With the development of a full flexural plastic hinge as indicated by full cover concrete spalling in the hinge region, slip in the hoop reinforcement can also occur. The effect of this hoop reinforcement slip can be seen in Figure 2.3Figure 2.4 in the form of hoop strain reductions at high ductilities.

Figure 2.4 presents a comparison of the hoop strains at the 0 and 90 degree locations for the experiments that were designated as shear columns. Although most of these columns were designed for shear with reduced shear spans, the failure mechanism for some of these columns was due to combined flexure-shear behavior at high displacement ductility levels. This is due to an increased amount of transverse reinforcement provided in these columns based on current shear design requirements. Although it is expected that the 90° location have higher strains in columns dominated by shear behavior, TU7 and Column 2 in these figures show higher strains in the direct line of loading at the 0° location. Despite being shear columns, TU7 and Column 2 were designed with sufficient transverse reinforcement such that adequate flexural ductility could be achieved. Both of these columns ultimately suffered flexure-shear failures. Maximum recorded hoop strains in the shear dominated columns reached approximately 1% at a displacement ductility level of 3.

A comparison of all the full-scale columns is given in Figure 2.5, while the results for the 40% scale columns, no matter what the governing failure mode was, are shown in

Figure 2.6. From these figures it is apparent that the scale of these experiments does not affect the ultimate behavior and, consequently, hoop strain values observed during testing. It has always been under debate whether scaling of the large-scale experimental tests in the laboratory influences behavior of the columns. It is the opinion of the authors of this report that if all parameters of the prototype column are scaled accordingly at a 40% scale, where conventional rebar and aggregates can still be used, the difference in overall response and behavior of the scaled column to that of the full-scale column is insignificant, especially for flexural columns. The only situation where scaling could come into play is in the case of shear dominated columns, if the concrete aggregate size is not scaled appropriately. The larger rocks could influence the shear-sliding plane that develops in these columns.

Furthermore, the size and spacing of the transverse reinforcement in scaled or full-scale columns has little effect on hoop strains. As long as the same longitudinal and transverse reinforcement ratios are used, the strains observed in the experiments are ultimately the same. This is also true with the new analytical model, which is described in Chapter 3. In sectional moment-curvature analytical models (when the longitudinal steel is well distributed), the longitudinal and transverse reinforcement details can be smeared around the column section, providing almost identical results to analyses which have the longitudinal steel modeled discretely. The size and spacing of the longitudinal and transverse reinforcement, however, significantly influences when longitudinal buckling is initiated and what buckling mode shape occurs. Therefore, although size and spacing of the reinforcement does not effect overall hoop strains prior to longitudinal steel buckling, anti-buckling checks should be performed to ensure that the chosen reinforcement details are sufficient.

Figure 2.7 shows a comparison of all the circular columns that were assessed in this report. The strains observed in the columns with rectangular cross-sections were similar to the circular columns. Several tests evaluated in this report were retrofitted with steel or composite jackets to enhance flexural strength. In these tests, both the internal transverse reinforcement and external jackets were gaged. A comparison between hoop

and jacket strains for these columns is shown in Figure 2.8. The results demonstrate that the internal and external measured strains were relatively the same. Usually strain gages within the column are lost quite early, while the gages placed on jackets remain reliable throughout the duration of the test. The results from Figure 2.8 indicate that it is reasonable to use the strain data from the jackets at high levels of displacement ductility to represent internal strain levels when the gages are lost.

A comparison between the different types of jacket retrofits is depicted in Figure 2.9 to demonstrate that confining strains measured in the jackets were similar to internal hoop strains despite what type of jacket material was used. However, it should be noted that strains in the steel jacket were well below the yield strain, thus linear elastic action consistent with the carbon-fiber jacket characteristics are to be expected.

From the evaluated hoop strain data it can be observed that (1) hoop strains were only reliably measured to displacement ductility levels $\mu_\Delta = 3$ or $\mu_\Delta = 4$ in conventionally reinforced columns and up to $\mu_\Delta = 6$ or $\mu_\Delta = 8$ in jacketed columns, (2) hoop strains were very low (<1%) even at ductility levels of $\mu_\Delta = 4$, and (3) the highest hoop strains were recorded in columns with high shear forces in combination with the flexural loads.

In order to extrapolate maximum expected hoop strain levels from design displacement ductility levels of $\mu_\Delta = 4$ to 6, appropriate analytical models need to be developed first which can be calibrated and verified with the existing hoop strain data and subsequently be used to extrapolate to the desired design displacement ductilities.

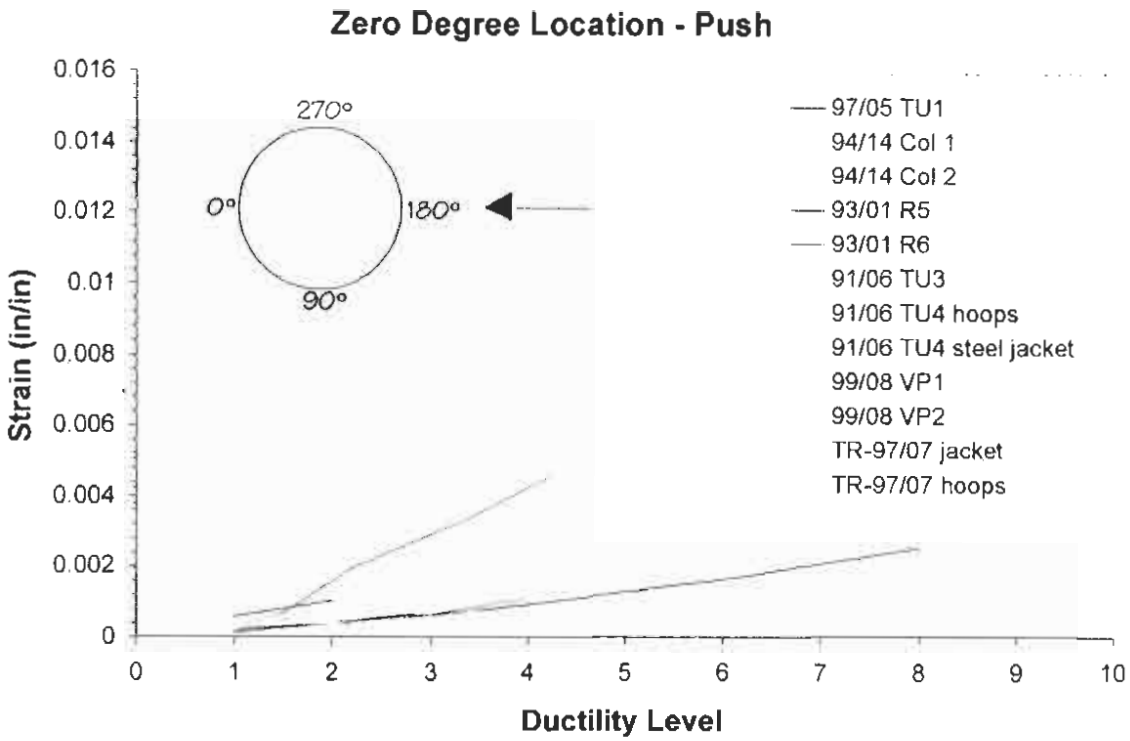

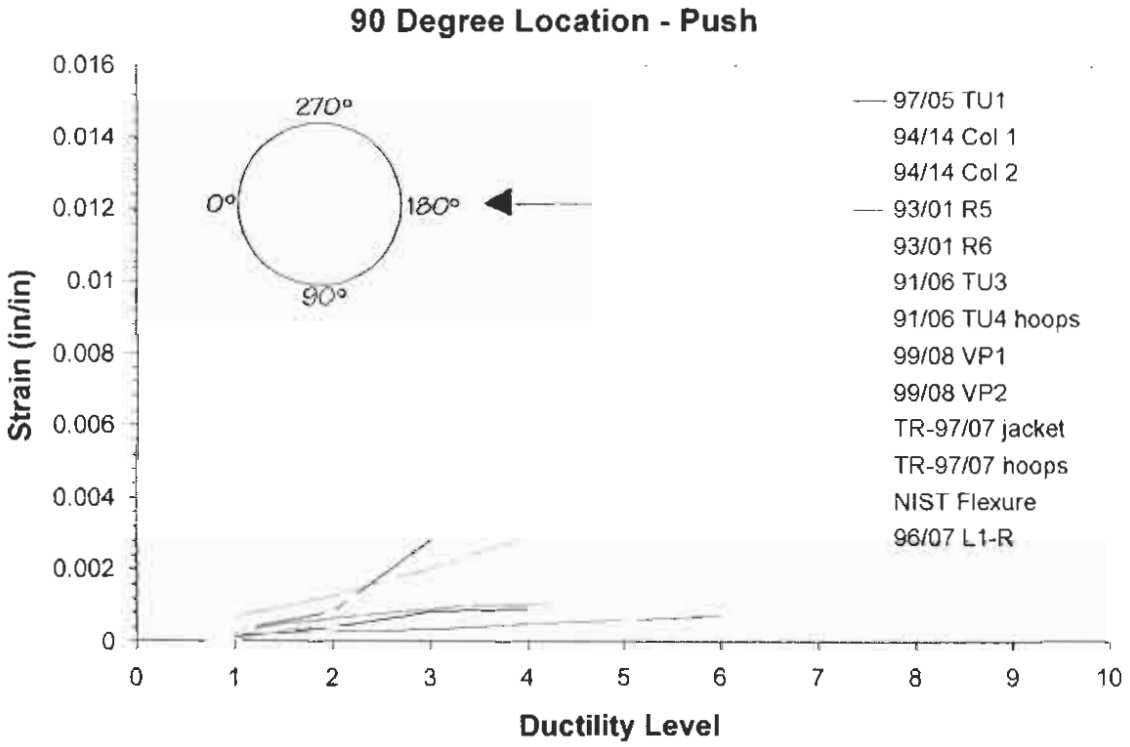

Figure 2.3: Comparison of flexure columns at zero and 90 degree locations

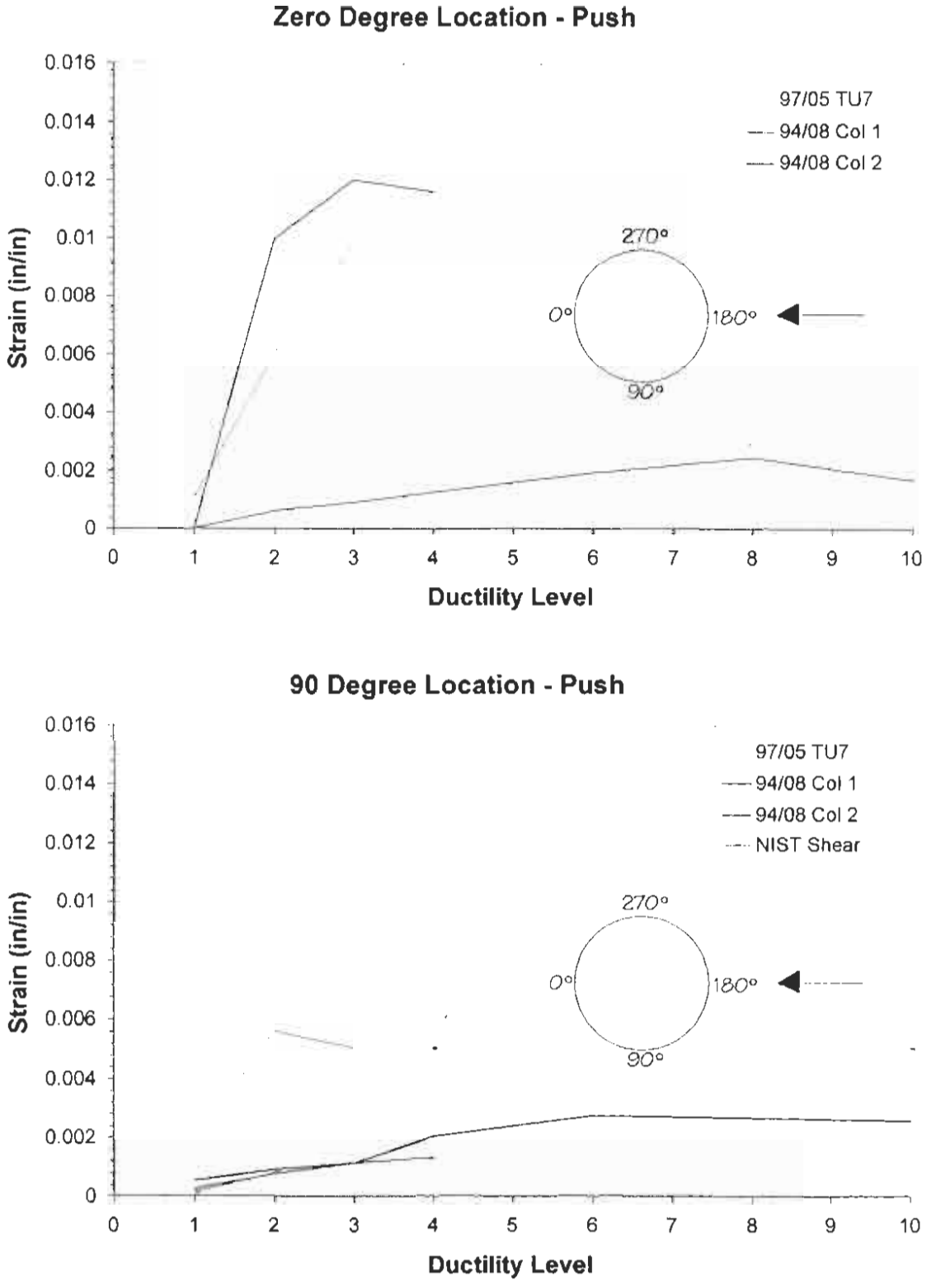

Figure 2.4: Comparison of shear columns at zero and 90 degree locations

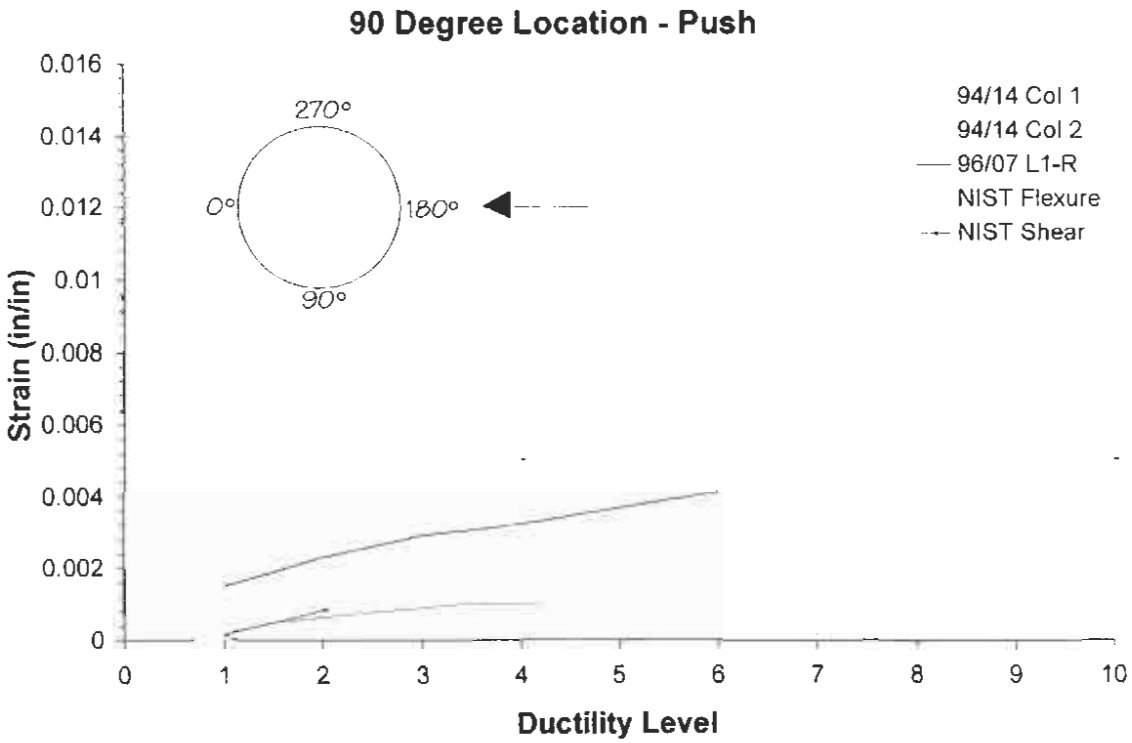

Figure 2.5: Comparison of full-scale columns

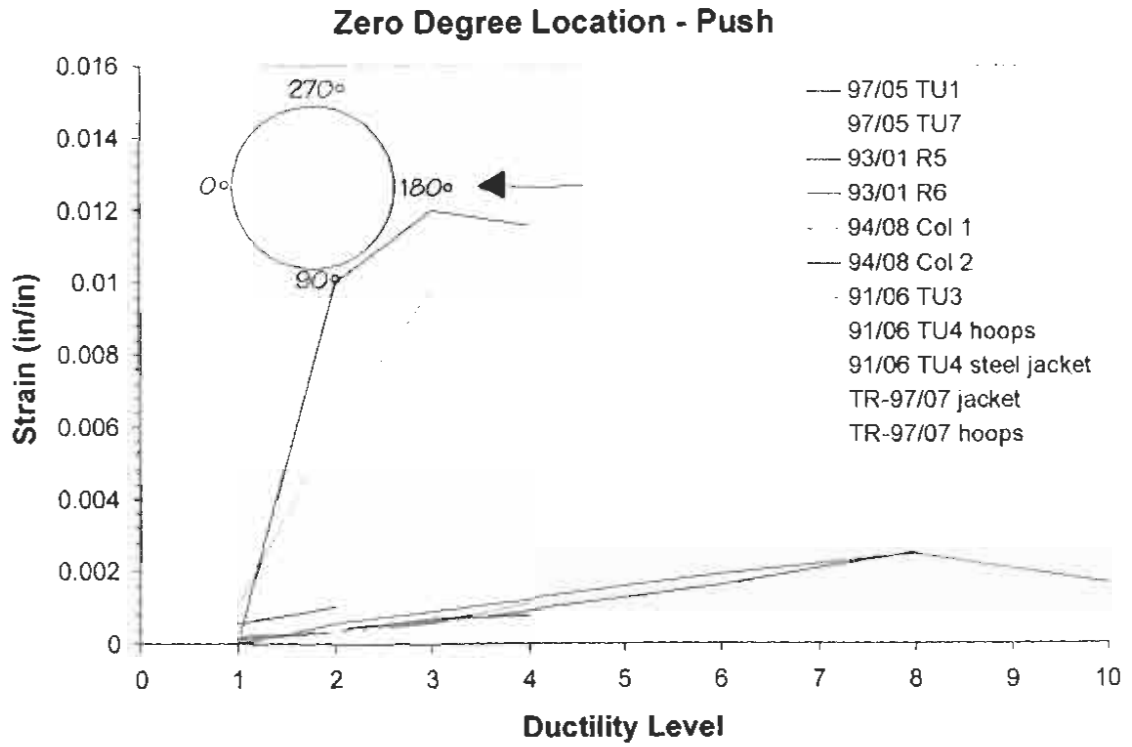

Figure 2.6: Comparison of 40% scaled columns

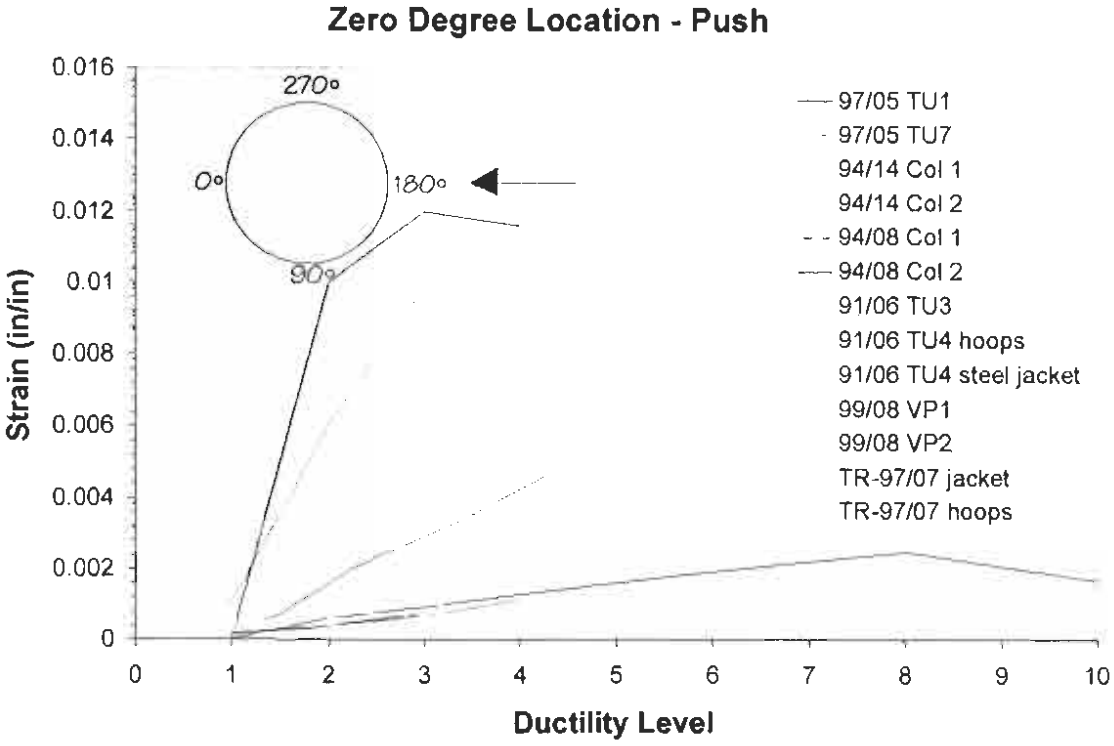

Figure 2.7: Comparison of circular columns

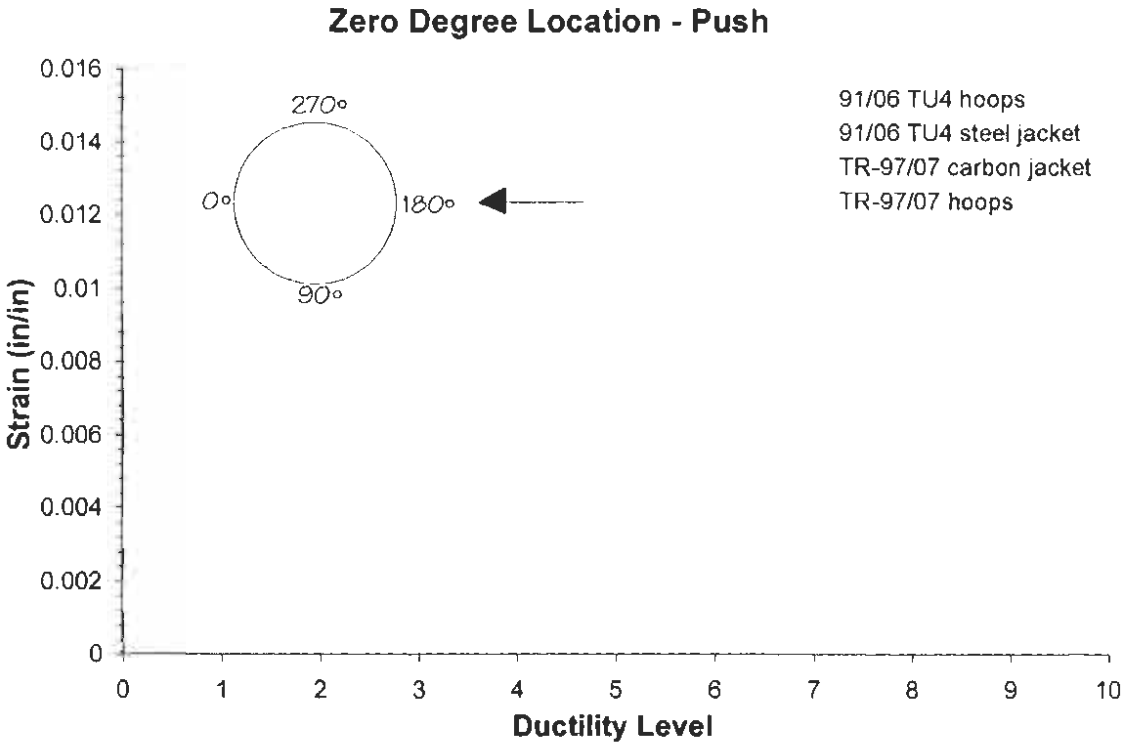

Figure 2.8: Comparison of hoops versus jacket strains

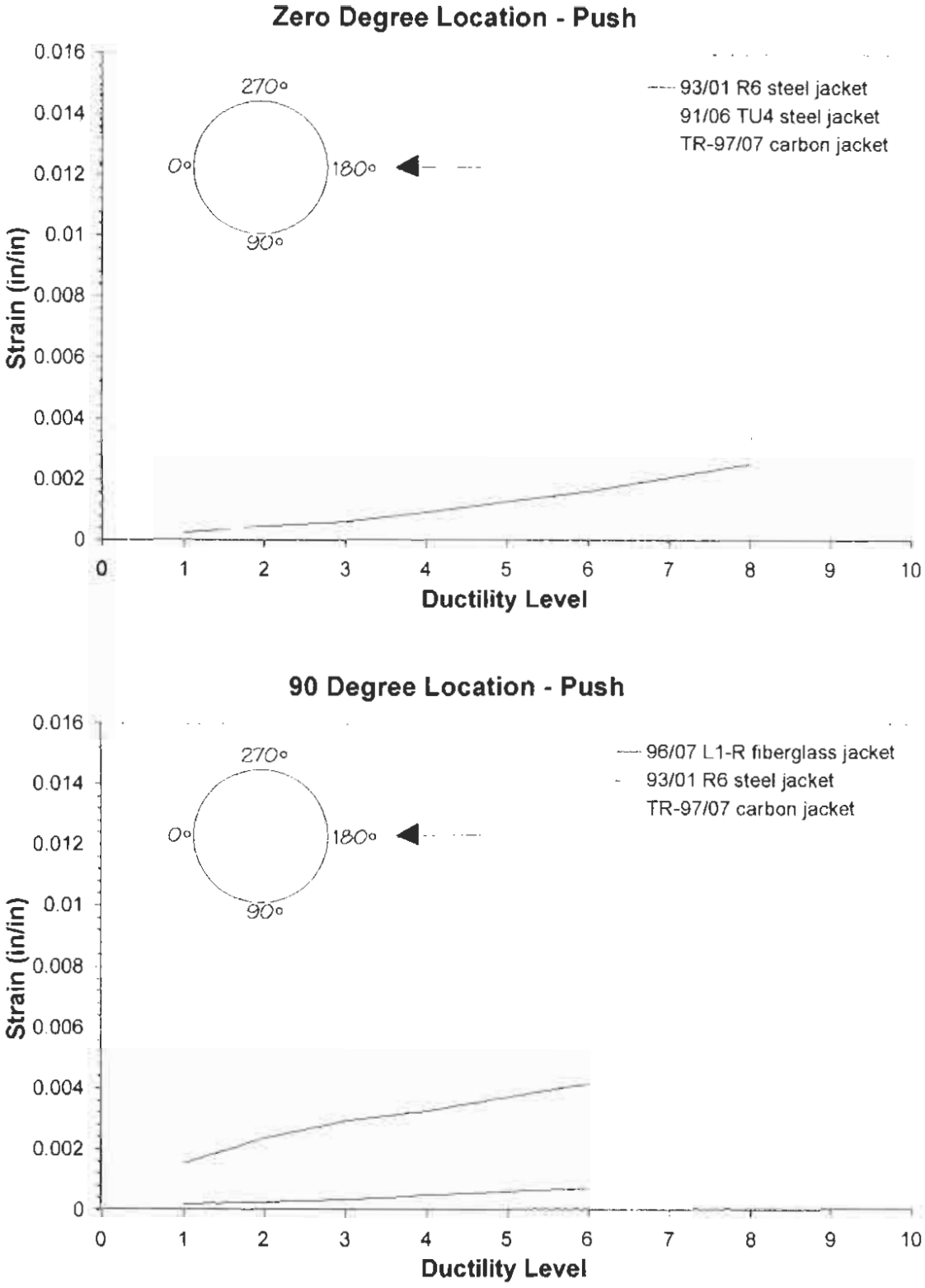

Figure 2.9: Jacket performance at zero and 90 degree locations

3 Analytical Review

3.1 Introduction

The purpose of the analysis presented in this section is to provide a rational method to determine maximum spiral or hoop strains at given ductility levels for reinforced concrete columns. The Mander model [9] has been used almost exclusively to determine both the curvature and displacement ductility capacity of columns and is based on the theory that the axial work done on the confined core concrete to failure is equal to the strain energy capacity of the hoops or spirals. In this way the ultimate compressive strain capacity of the concrete, which signals first hoop fracture, can be determined. Mander verified his model through extensive comparisons of tests on axially loaded columns with different volumes of transverse steel [9].

Mander extended the use of this model to flexure by assuming that the ultimate compressive strain capacity derived from the balanced energy approach for an axially loaded column could be used as the termination criteria for flexure. From a moment-curvature analysis of the critical section the peak compressive axial strain of the confined core concrete is monitored and the analysis is terminated when the axial strain capacity is reached, allowing the curvature and displacement ductility capacities to be determined. The compressive strain capacity is found prior to the analysis from the equal energy approach discussed above. An ultimate curvature is determined and the curvature ductility capacity of the section is found from dividing the peak curvature by the idealized yield curvature [14]. To obtain the displacement ductility capacity of a column an equivalent plastic hinge length is required as discussed in [14].

While the Mander approach has been used extensively for the design of bridge columns, it is understood to be conservative as has often been shown by large-scale flexural testing at UCSD and elsewhere. Note that the Mander model defines ductility capacity only when the compressive strain capacity of the concrete is reached prior to the

tensile strain capacity of the longitudinal reinforcement, otherwise ductility capacity is a function of the tensile strain capacity of the primary flexural steel.

The Mander model provides the ductility capacity only at hoop fracture (or at ultimate hoop strain as discussed later) and does not yield any information about the hoop strains at smaller ductilities. Also, as mentioned above, the method is conservative for flexural columns, making it a reasonable tool for production design work but not necessarily a good tool for detailed assessment or prediction analysis. The particular problem at hand requires that the ductility capacity corresponding to reduced hoop strain demands of 0.02, 0.03 and 0.04 be determined. Or, conversely, that the hoop strains be found at a given design ductility level. The Mander model cannot answer these questions. Therefore a new model is required which is capable of calculating the hoop strains as a function of curvature and displacement ductility.

In the following a new method is presented for calculating hoop strains at each increment of a moment-curvature analysis for flexural columns or an axial force-strain analysis for axially loaded columns. The expanding core concrete stretches the hoop material, which in turn confines the concrete within and limits the dilation. With linear-elastic hoop material, such as carbon fiber wrap, the confining stresses continue to build and the dilation and hoop strains are kept to a minimum. For the more traditional confinement material of steel, however, the hoops yield early and provide essentially no additional confinement to the core concrete, allowing dilation and hoop strains to increase rapidly. The method developed herein utilizes a similar energy concept presented by Mander, but the energy balance is applied at each curvature or axial strain increment and to each fiber, rather than to the section as a whole. This allows the current tangent Poisson's ratio to be determined for each element, which directly affects the core concrete expansion and hoop strains and, ultimately, the displacement capacity of the member. The new method presented here has been implemented in the moment-curvature program ANDRIANNA [4].

3.2 Theory

3.2.1 Mander Model

In the Mander model, the axial work done on the confined core concrete (beyond the unconfined response) is equated to the strain energy capacity of the hoops to fracture. The idea is that any axial load that is beyond the unconfined concrete capacity is being supported by the hoop reinforcement; if the hoops were removed the concrete would dilate rapidly and the member would fail.

In his model the ultimate strain capacity and confining stress as well as the shape of the stress-strain curve are calculated prior to a moment-curvature analysis. This approach assumes that the transverse steel has yielded (making it unsuitable for elastic hoop material where confining stresses continue to build until failure) and that dilation is symmetric around the hoop (true only for axially loaded columns). At first glance this seems an overly crude approximation for flexure, but it can provide reasonable results for columns with steel hoop reinforcement because the hoop steel yields at low ductility and, for the remainder of the loading, the confinement stresses are constant where the spiral has yielded. On the tension side of the column the concrete has cracked and, therefore, the assumed shape of the compressive stress-strain curve does not affect the response of the tension fibers.

The confining stress f_l is found from a free-body diagram of half the section with twice the hoop tension force T balanced by the confining stress f_l in the concrete multiplied by the diameter D and hoop spacing S (Figure 3.1). This is written as

$$2T = f_l DS \tag{1}$$

allowing the confining stress to be found

$$f_l = \frac{2T}{DS} \tag{2}$$

which may be given in terms of the hoop stress σ_h and hoop area A_h as

$$f_l = \frac{2\sigma_h A_h}{DS} \tag{3}$$

The transverse steel volumetric ratio is given as

$$\rho_h = \frac{4A_h}{DS} \tag{4}$$

Combining Equations 3 and 4 for f_l and ρ_h allows the confining stress to be given in terms of the transverse volumetric ratio and hoop stress

$$f_l = \frac{1}{2}\rho_h \sigma_h \tag{5}$$

In the Mander model the hoop stress is set to yield which allows the confining stress to be written

$$f_l = \frac{1}{2}\rho_h \sigma_{hy} \tag{6}$$

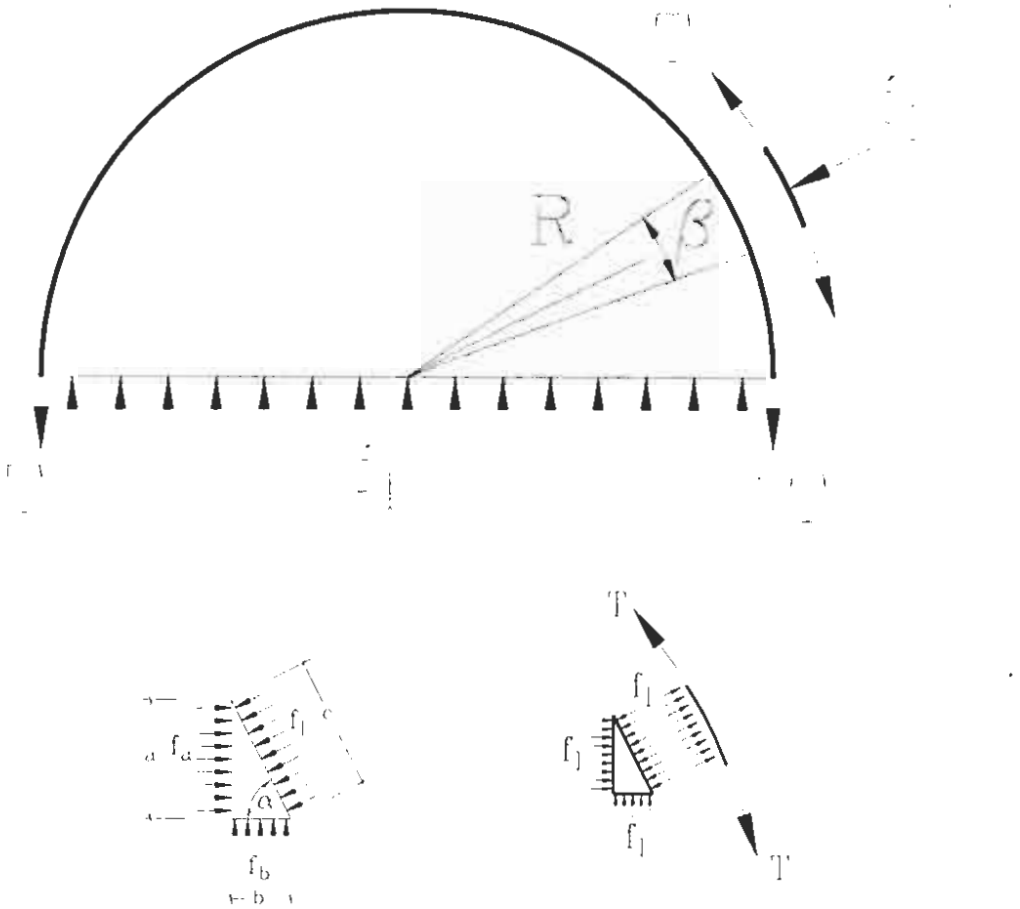

Figure 3.1: Free-body diagrams of hoop and confined concrete

3.2.2 New Model

It is of particular interest to the development of the proposed model that the same confinement expressions shown above can be developed at the element level by using the free-body diagrams shown in the lower region of Figure 3.1. In the upper sketch of Figure 3.1 the hoop tension force is constant around the entire perimeter and is representative of an axially loaded column. A column in flexure, however, has a hoop tension force which varies around the section due to increased expansion of the concrete on the compression side of the neutral axis, with the greatest dilation at the extreme concrete compression fiber. The free-body diagrams at the lower right side of Figure 3.1 represent a portion of the hoop steel and confined concrete over a small angle β. The horizontal component (toward the center of the hoop) of the tension force T is equal to

$T\beta/2$. The total horizontal force is $T\beta$, which must be balanced by the local confining stress f_l. To find the stress f_l applied to the concrete the force $T\beta$ is divided by the hoop arc length within the angle β and the hoop spacing S. This results in the same confinement stress derived in Equation 2 of

$$f_l = \frac{T\beta}{(R\beta)S} = \frac{T}{RS} = \frac{2T}{DS} \tag{7}$$

or written as

$$f_l = \frac{1}{2}\rho_h \sigma_h \tag{8}$$

which are the same confinement expressions developed from the half-section free-body diagram in Equation 5. Note, however, that this represents the local confining stress, which depends on the current hoop stress at a point on the perimeter.

In Figure 3.1, the hoop region of interest is shown at an arbitrary angle α from the horizontal to demonstrate that the confining stress f_l at any given angle is equal to the horizontal and vertical confining stresses on the element. The lower left sketch shows the applied confining stress f_l coming from the hoop steel (at the angle α) and the required stresses, f_a and f_b, for force equilibrium on the left and bottom of the element. Note that it is not assumed that f_a and f_b are equal to f_l; which is demonstrated in the following paragraphs. The lengths a and b are given in terms of the length c and angle α as

$$\begin{aligned} a &= c(\sin\alpha) \\ b &= c(\cos\alpha) \end{aligned} \tag{9}$$

Summation of horizontal forces gives

$$f_l c(\sin\alpha) = f_a a \tag{10}$$

Placing a from Equation 9 into the above expression shows that $f_a = f_l$.

Similarly, summation of vertical forces gives

$$f_l c(\cos\alpha) = f_b b \tag{11}$$

and placing b from Equation 9 into the above expression results in $f_b = f_l$. This is indicated in the lower right sketch of Figure 3.1 where the confining stress f_l is the same in all directions for the element. Therefore at all points along the hoop reinforcement the confining stress in the adjacent concrete element is the same in the two principal directions and is equal to

$$f_l = \frac{1}{2}\rho_h \sigma_h \tag{12}$$

where σ_h is the current stress in the hoop reinforcement at the given location around the perimeter.

The proposed model allows confining effects to develop incrementally as the concrete expands into the surrounding material. This requires a dilation rate for each element at each increment of axial strain or curvature. It is well known that increasing the confining stress reduces the dilation of concrete. To properly account for this a rational model was developed to relate the dilation rate, or tangent Poisson's ratio μ_t, to the current confining stress f_l. A state dependent energy balance approach is performed at each axial deformation increment $\Delta\varepsilon_l$ for each element within the confined boundary. The axial work done for the increment of axial strain $\Delta\varepsilon_l$ is equated to the energy

expended by the confining stresses σ_2 and σ_3 as they move through the dilation strain increments $\Delta\varepsilon_2$ and $\Delta\varepsilon_3$, respectively, written as

$$\sigma_1'\Delta\varepsilon_1 = \sigma_2\Delta\varepsilon_2 + \sigma_3\Delta\varepsilon_3 \tag{13}$$

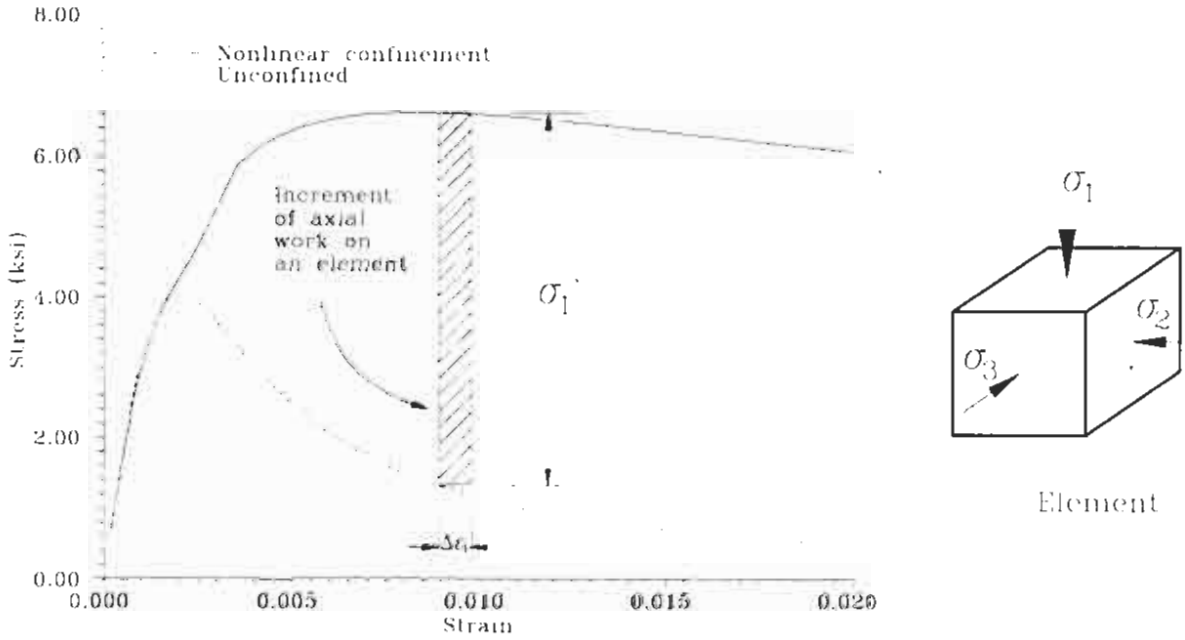

Figure 3.2: Incremental energy balance for an element

where σ_1' is the difference between the current confined axial stress σ_1 and the unconfined axial stress (Figure 3.2). With confining stresses the same in both directions the above energy expression may be written as

$$\sigma_1'\Delta\varepsilon_1 = 2f_1\Delta\varepsilon_d \tag{14}$$

which allows the tangent Poisson's ratio μ_{tn} (change in dilation strain divided by the change in axial strain) to be expressed as

$$\mu_{tn} = \frac{\sigma_1'}{2f_1} \tag{15}$$

It is important to note that as the confinement level approaches zero the dilation rate becomes unstable, indicating sudden expansion for unconfined concrete. The total tangent Poisson's ratio is the summation of elastic and nonlinear parts, given as

$$\mu_t = \mu_{tn} + \mu_e \tag{16}$$

where μ_e may be taken as 0.2. Thus Poisson's ratio is written

$$\mu_t = \frac{\sigma_1'}{2f_l} + \mu_e \tag{17}$$

The elastic component μ_e is required so that initially realistic expansion occurs, as the nonlinear term μ_{tn} is approximately zero until just before the unconfined concrete strength is reached (σ_1' is approximately zero in this range as indicated in Figure 3.2). As discussed in the following section, the energy transfer mechanism from axial deformation to dilation is not 100 percent efficient and in recognition of this an efficiency factor Σ is applied to the nonlinear portion of Poisson's ratio. Thus the final ratio used in the present study is written

$$\mu_t = \Sigma \frac{\sigma_1'}{2f_l} + \mu_e \tag{18}$$

It was found from reviewing the results of the axially loaded Mander column tests [9] that at larger axial strains a more efficient energy transfer mechanism develops yet still not 100 percent. This variation in efficiency is included in the model by making the efficiency factor Σ a function of axial strain, with constants η and J determined from experiment, in this case the axially loaded Mander column tests [9]. The form of the following equation for Σ was chosen so that the efficiency of the energy transfer mechanism approaches 100 percent as the axial strain increases without bound.

$$\Sigma = \left(\frac{1}{1 + \frac{1}{\eta \varepsilon_l + J}} \right) \tag{19}$$

When the axial strains are small, J is the dominant parameter, but as the strains reach large values η becomes the dominant parameter, allowing accurate modeling through the entire range of hoop strains. The determination of these parameters is discussed more fully in Section 3.3.1

3.3 Axial Load Analysis

3.3.1 Single Fiber Analysis and Comparison to Mander Experiments

In developing his confined concrete model, Mander tested many columns in axial deformation control [9]. Various combinations of longitudinal and hoop steel were tested within the same 59 inch high, 19.7 inch diameter column geometry. It was clearly shown that the amount of hoop reinforcement was the most important factor influencing the axial strain capacity of the columns. Therefore, in the following the analyses will be compared to columns in Test Series 1 (Columns 1 through 6 in [9]) which had the same amount of longitudinal reinforcement and a varied amount of transverse reinforcement. Table 3.1 shows the test matrix for the Mander columns that were used in this study. All of the columns in this test series were loaded at the fast strain rate of 0.0133 strain/sec. It should be noted that Mander also tested two identical columns with different strain rates (Column *b* at the fast strain rate of 0.0133 strain/sec. and Column *a* at the slow strain rate of 0.0000027 strain/sec). A comparison of results from these tests indicates an 80 to 100 percent increase in hoop strains under dynamic loading (fast strain rate). However, this is only one available data point from Mander's work [9] and additional static and dynamic tests will be required to verify that columns loaded at a high strain rate have higher hoop strains.

Table 3.1: Mander axially loaded columns in Test Series 1

Column	Diameter	Cover	ρ_l	ρ_s	f'_c (ksi)
3	500 mm (19.7 in)	25 mm (1 in)	1.23% 12 D16 (0.63 in)	1% R12 (0.5 in) @ 109 mm (4.3 in)	28 MPa (4.06 ksi)
4	500 mm (19.7 in)	25 mm (1 in)	1.23% 12 D16 (0.63 in)	0.6% R10 (0.4 in) @ 119 mm (4.7 in)	28 MPa (4.06 ksi)
5	500 mm (19.7 in)	25 mm (1 in)	1.23% 12 D16 (0.63 in)	2% R10 (0.4 in) @ 36 mm (1.4 in)	28 MPa (4.06 ksi)

The above expression for the rate of dilation (Equation 17) was used to calculate the hoop strain versus axial strain for Column 5 (assuming constant confinement pressure based on yield of the transverse steel). It was found that measured hoop strains were much less than the dilation strains based on Equation 17 and that Mander's equal energy approach significantly overestimates the hoop strains (Figure 3.3). This has also been recognized by others who have noted that only 15 percent of the axial strain energy is transferred to the hoops [2]. Good correlation was obtained using the dilation rate from Equation 18 (see Figure 3.3) with efficiency constants η and J of 20 and 1/3, respectively, indicating that at small strains the energy transfer was only 25 percent efficient (similar to in [2]). By the end of the test, at an axial strain of 0.058, the efficiency of the energy transfer mechanism had increased to over 60 percent. Figure 3.3 depicts the calculated and measured axial and hoop strains and also shows the hoop strains from a 3-D nonlinear finite element analysis of Column 5 which utilized ANATECH concrete and reinforcement material models [1] in conjunction with the general purpose finite element program ABAQUS [6]. The finite element results demonstrate a known weakness of plasticity based concrete models; the dilation rate is not large enough for members with steel confinement. Also the finite element analysis terminated at an axial strain of less than 0.02 due to large element distortion.

Mander verified his energy balance model by comparing measured and predicted axial strains at first hoop fracture. It was assumed that the strain limit to be used in calculating the strain energy capacity of the hoops was the rupture strain. It should be

recognized, however, that at strains beyond ultimate stress the bar begins necking and the strain increases rapidly until a local fracture occurs. Therefore, when computing the strain energy capacity of the hoops it is more realistic to use the strain at ultimate stress rather than the fracture strain, as most of the hoop length will be at the lesser strain. Mander reported that the hoop steel for Column 5 had an ultimate strain of 0.14 and fracture strain of 0.22. If Mander had used his ultimate rather than the fracture strain he would have found that the energy transfer mechanism is not 100 percent efficient, but approximately 64 percent efficient (ratio of ultimate to fracture strain) at the end of the test, which is very similar to that found above.

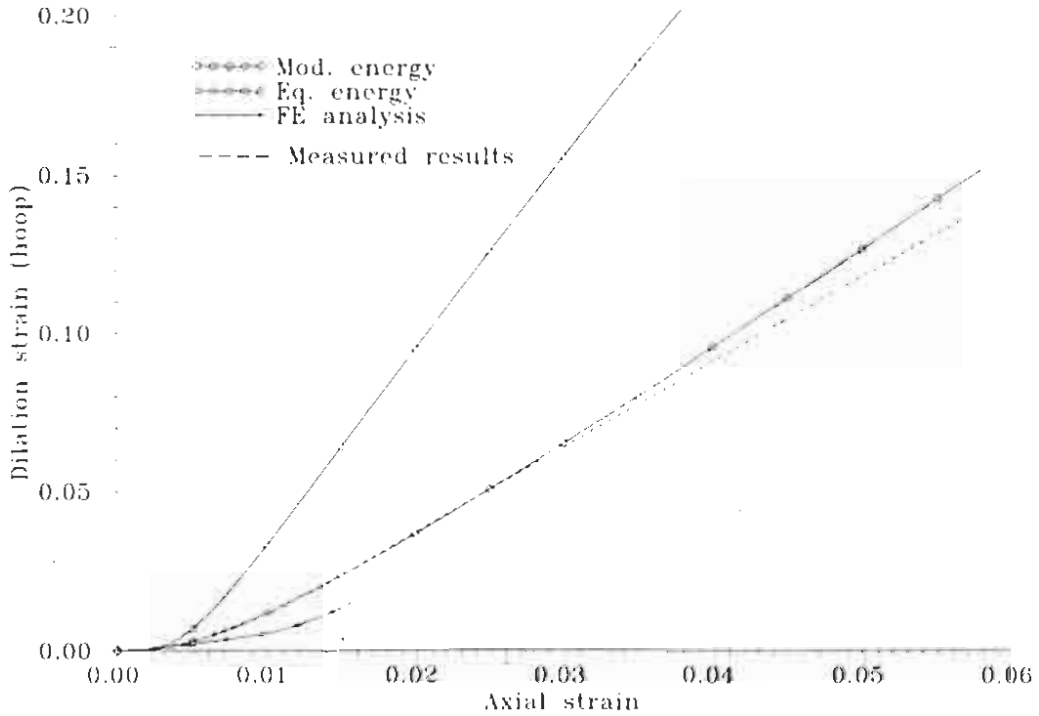

Figure 3.3: Comparison of dilation strains using equal energy, modified energy and finite element approaches for Mander Column 5 [9]

Using the same efficiency parameters η and J developed for Column 5, with hoop steel ratio of 2 percent, additional analyses were conducted for Columns 3 and 4 which had hoop steel ratios of 1 percent and 0.6 percent, respectively (Figure 3.4). The results show that the rational approach is realistically modeling the hoop strains at small and large axial strains for various amounts of transverse steel, with increased volume of hoop steel (increased confining stress) resulting in reduced hoop strains.

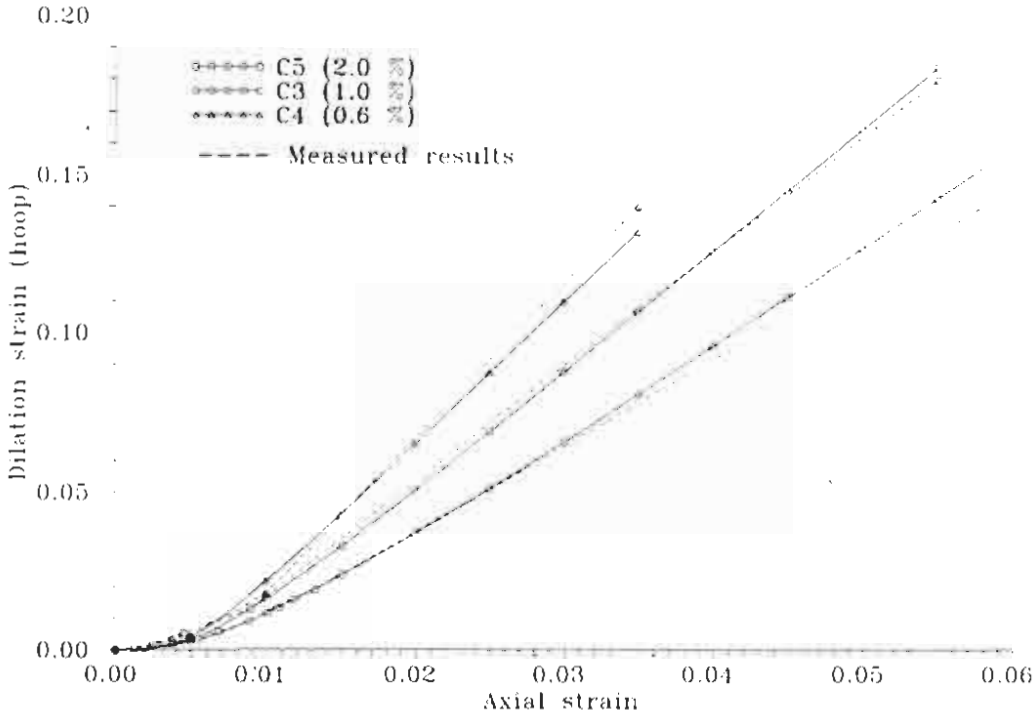

a) **Complete results**

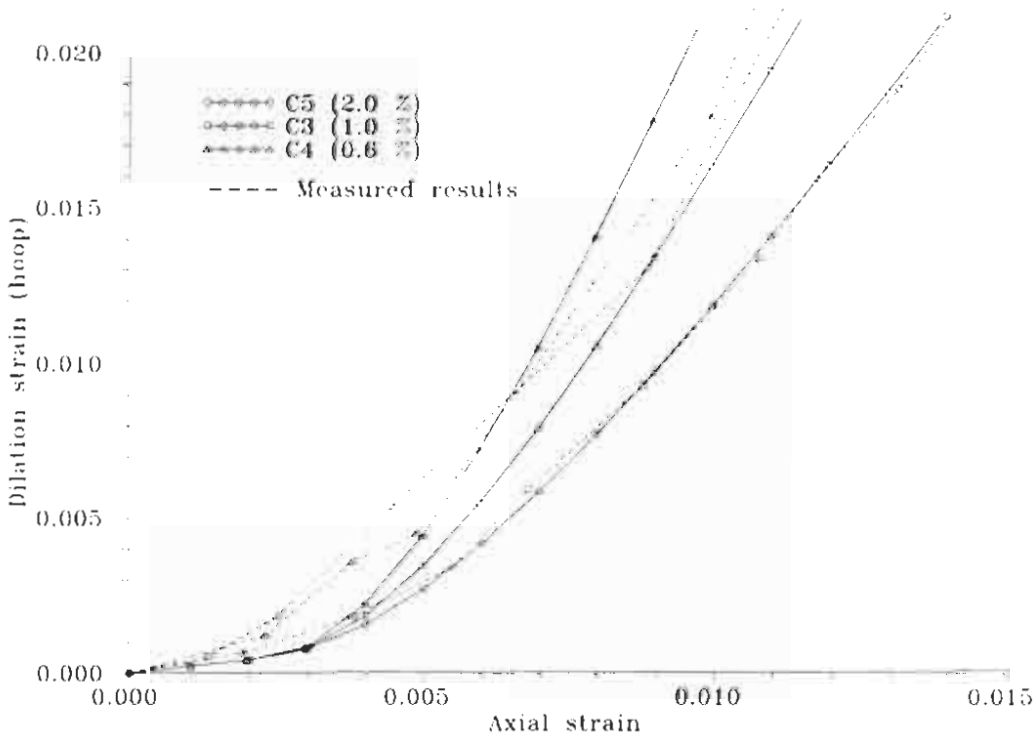

b) **Small strain region**

Figure 3.4: Axial stress versus dilation strain for Mander axial column tests [9]

It should be noted that the "measured" hoop strains in the figures are found from two sources. Up to axial strains of 0.01 to 0.02, depending on the test, the results are from measured strain gage readings. The second source of "measured" hoop strains are interpreted from the fact that the hoops failed at a measured axial deformation (hence strain). The second source is also based on the assumption that the average hoop strain is the strain at ultimate stress (reported as 0.14 for Columns 4 and 5 and 0.18 for Column 3 in [9]). One can see that this last point looks reasonable because the slope (dilation rate) at the end of the measured strain gage data is similar to the slope to the last data point (Figure 3.4a).

3.3.2 Section Analysis

The analysis shown in Section 3.3.1 consists of a single concrete fiber (with assumed constant confining pressure based on yield of the hoops) loaded with axial strains and responding with dilation strains, which are equivalent to hoop strains. The following section extends this approach to a complete section analysis under axial deformation control (no curvature or moment). The analysis procedure is given in the following steps:

(1) Increment axial strain for all elements
(2) Determine increment in dilation strain for all elements
(3) Calculate hoop strains around confined perimeter
(4) Determine hoop stresses from hoop strains (elastic or nonlinear hoop material)
(5) Assign confining stresses to all elements based on current hoop stresses
(6) Based on confining stress and axial strain determine axial stress for all elements
(7) Calculate new Poisson's ratio for all elements using confinement and axial stresses
(8) Return to (1) above

Mander's Column 5 [9] is used to compare results from the complete section and single fiber analyses. The dimensions and properties for this column were defined in Table 3.1. The section definition is shown in Figure 3.5, which indicates the longitudinal reinforcement and the confined and unconfined concrete elements. Also the confined

boundary (representing the hoop location) is clearly shown with a 30x30 grid of elements resulting in 560 confined concrete fibers. Figure 3.2 compares the dilation or hoop strains from the single fiber and the complete section analyses, which shows almost identical behavior. However, prior to yield of the transverse hoop steel the complete section analysis dilates more rapidly than the single fiber analysis (see Figure 3.2b) because the confining stresses are lower which increases the dilation rate given in Equation 18. This also affects the axial stress-strain response as shown in Figure 3.7. Initially, the axial stress-strain path follows the unconfined response until the concrete expands enough to activate the hoop steel, which increases the axial stress and directs the stress-strain path away from the unconfined curve and toward the constant confinement response.

In addition to the Mander Column 5 [9] analysis with steel hoops (nonlinear material behavior), an analysis was conducted assuming linear-elastic hoop material (no yield) with the same stiffness as the elastic stiffness of the steel hoops (see Figure 3.8). It is clear from Figure 3.8 that the column with elastic hoop material has the same response as the column with nonlinear hoop material until the hoops yield at an axial strain of about 0.004. With the elastic hoop material the axial stresses (Figure 3.8a) and confining stresses (Figure 3.8c) continue to build which results in reduced dilation strains (Figure 3.8b). The nonlinear confinement steel develops confinement stresses, which stay constant once the hoops yield (Figure 3.8c).

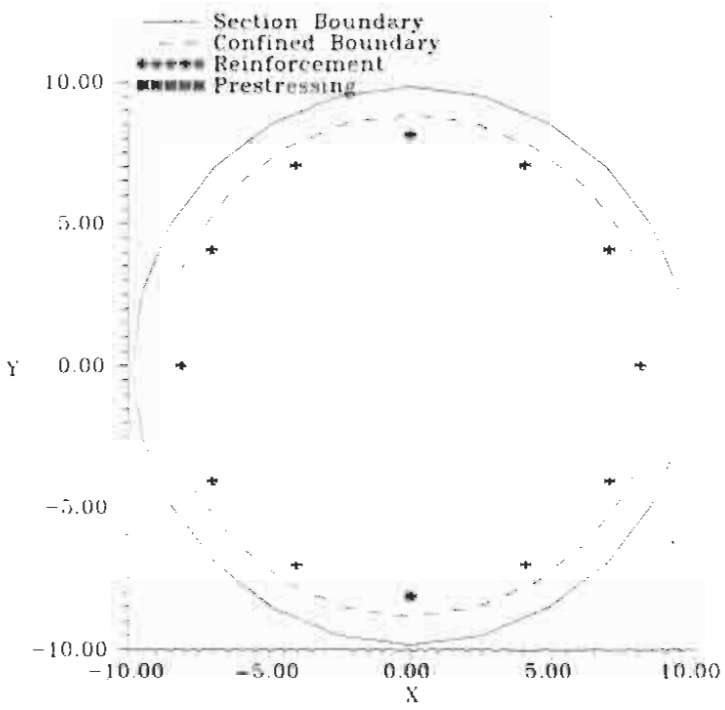

(a) General section definition

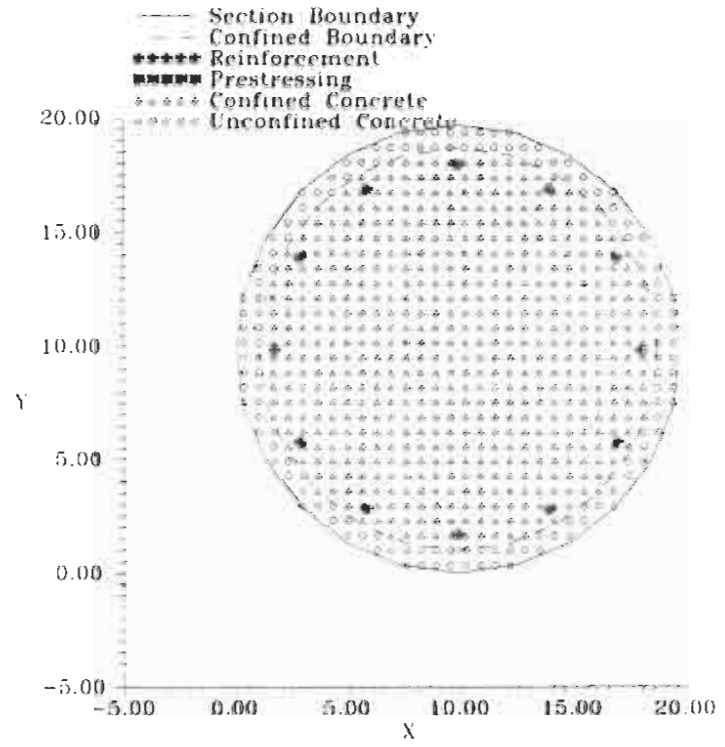

b) Discretized section with 30x30 grid

Figure 3.5: Definition of Mander column for axial force-strain analysis

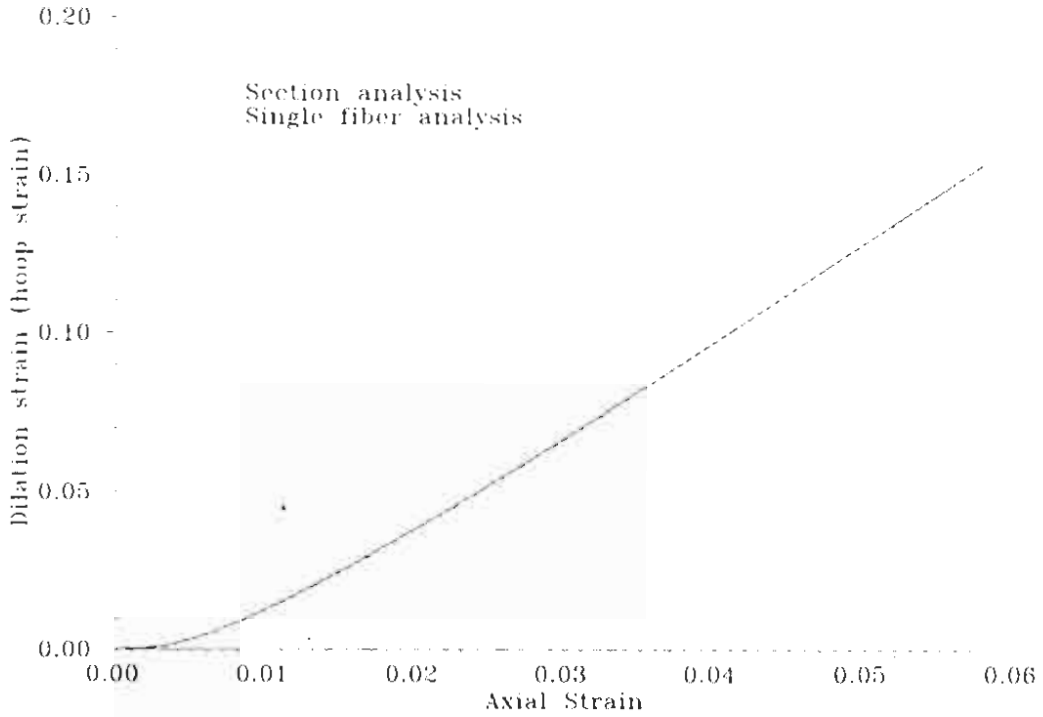

a) Complete results

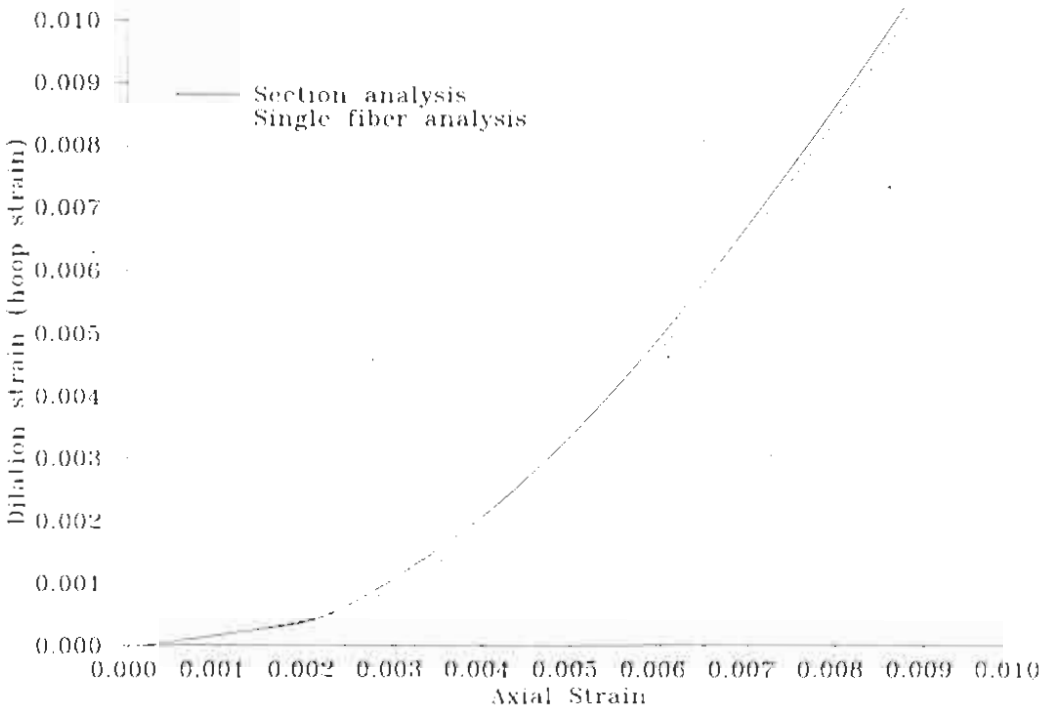

b) Small strain region

Figure 3.6: Comparison of dilation strains from single fiber and complete section analyses for C5

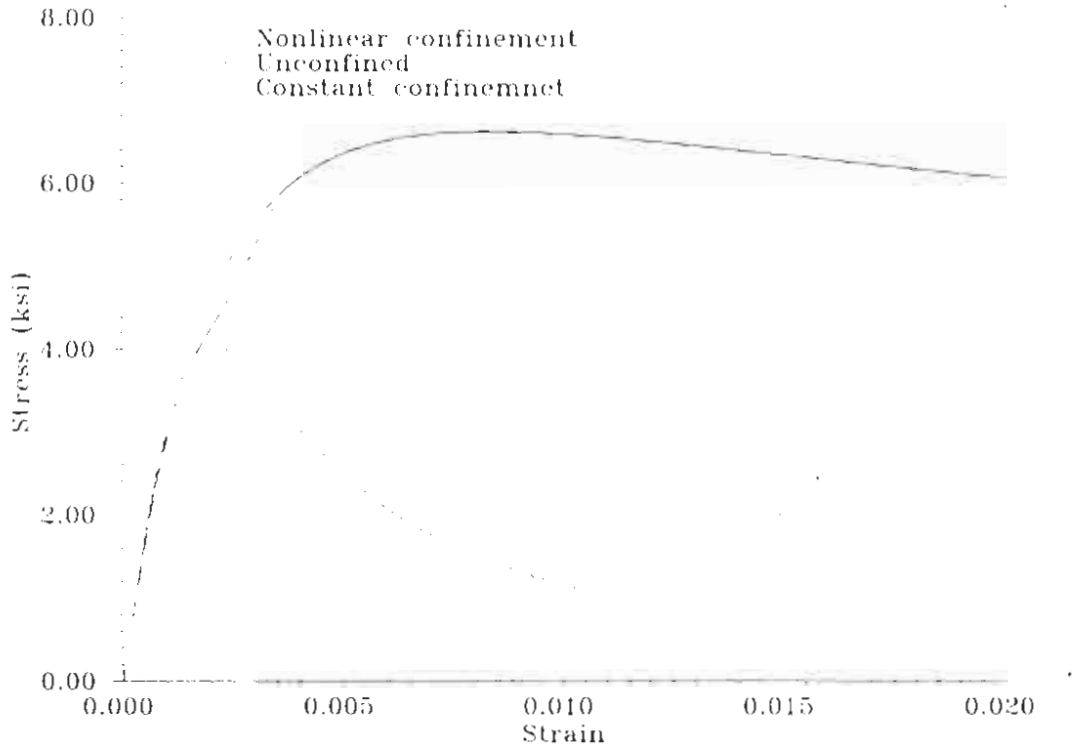

Figure 3.7: Axial stress-strain responses from constant and nonlinear confinement

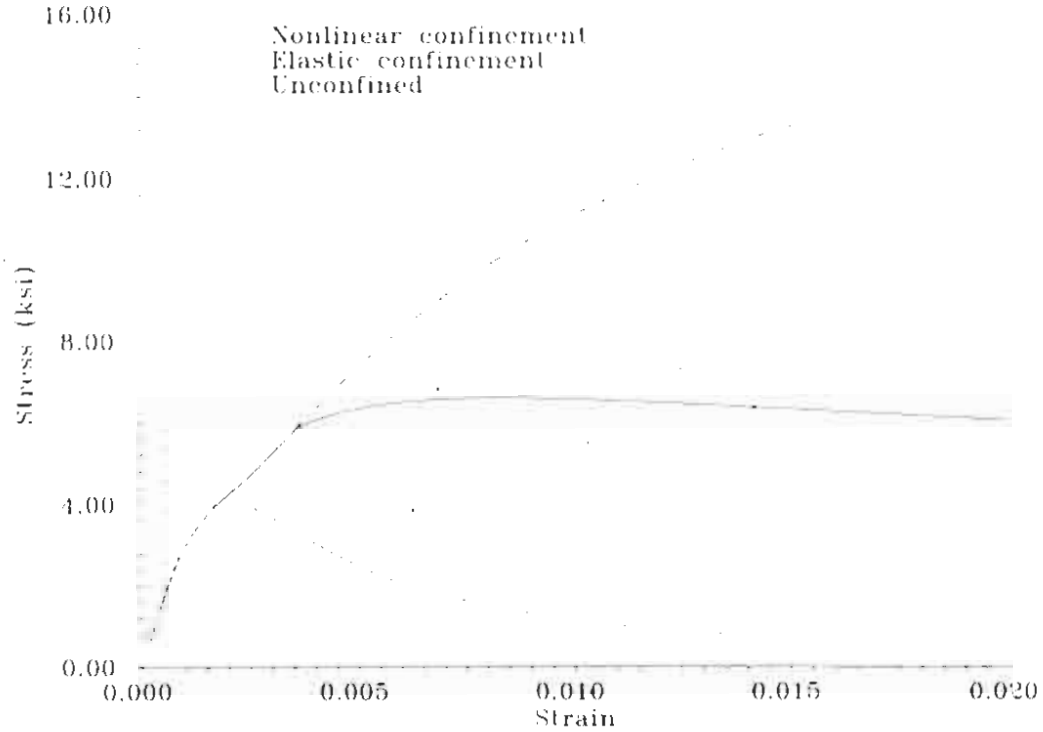

a) Axial stress versus axial strain

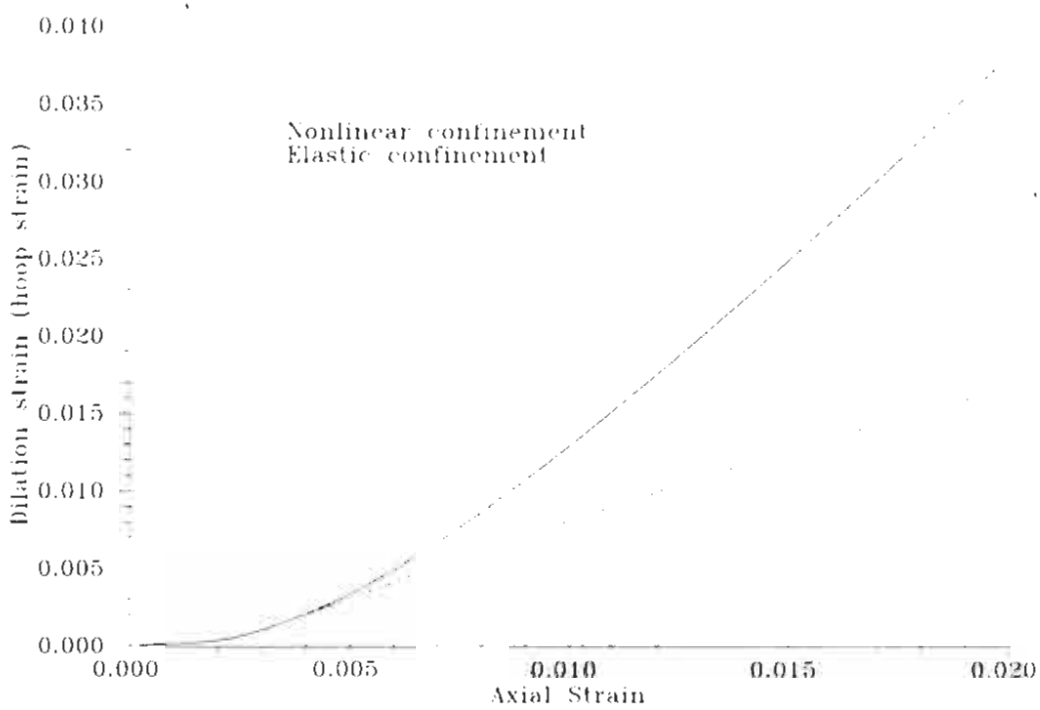

b) Dilation strain versus axial strain

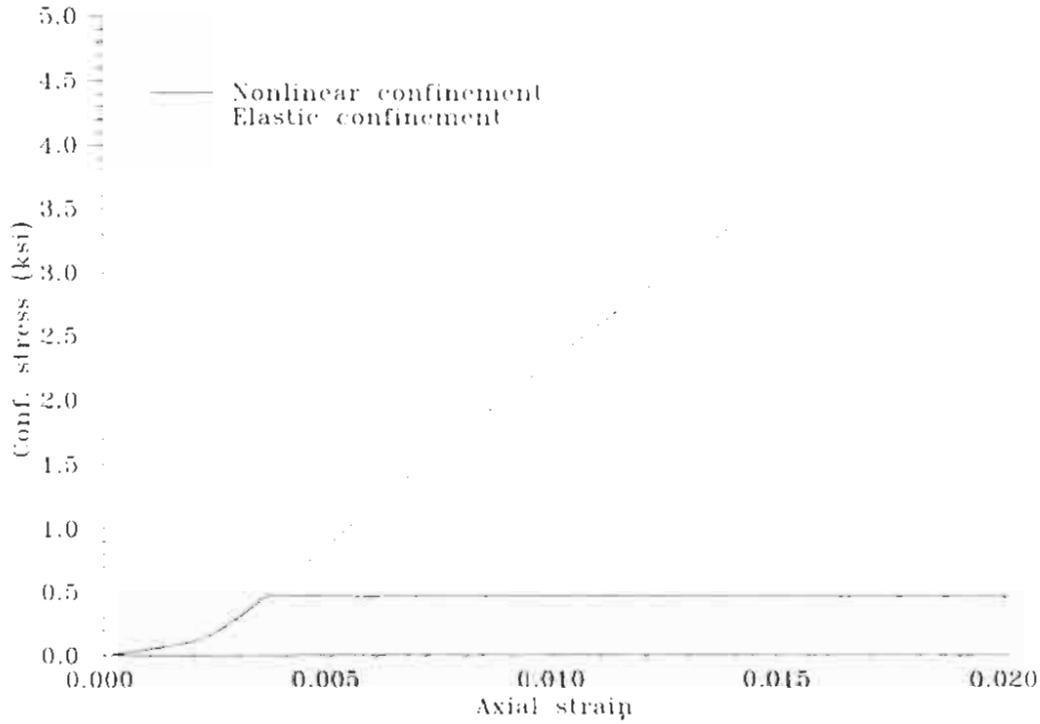

c) Confining stress versus axial strain

Figure 3.8: Column 5 analyses using nonlinear hoop material (steel) and elastic hoop material (carbon shell)

3.4 Flexure Analysis

3.4.1 Theory

To determine the hoop strains in flexure a similar procedure to that outlined in Section 3.3.2 for axially loaded columns is conducted, except that each fiber undergoes different increments of axial strain which are consistent with the curvature increment and distance between the fiber centroid and current neutral axis. With varying axial strains across the section, the dilation strains also vary for each element. Actually, for all elements in a given row, which are the same distance from the neutral axis and have the same confining stress, the axial and dilation strains are the same. The extreme confined elements are monitored for each row and the change in hoop strain at a given row location is equated to the increase in dilation strain for that row of elements. It is clear from Mohr's circle that because the dilation strains of the confined concrete are the same in two principal directions (confining pressure is the same as noted previously), the hoop strain is equal to the dilation strain. This is regardless of the angle of the hoop steel with respect to the principal directions (see Figure 3.1). The hoop strains are calculated at the ends of each row of confined elements and the current hoop stresses are determined from either a linear-elastic or nonlinear stress-strain material relation, depending on the type of confinement. Since steel hoops are modeled as elastic-perfectly-plastic, the modulus of elasticity and yield stress are required during input, while only the modulus of elasticity is needed for a purely elastic carbon fiber shell. The current confining pressure is calculated from Equation 5 for each row, based on the hoop stress at that location. Each element is then assigned a confining pressure, which allows a new tangent Poisson's ratio to be found for the next increment of curvature from Equation 18.

Since no axial strains develop at the neutral axis there are no dilation strains and, consequently, no hoop strains or stresses (or confinement effects). At locations on the compressive side of the neutral axis, the axial strains increase linearly with distance from the neutral axis (plane sections remain plane). However, dilation or hoop strains increase more rapidly (see upper right sketch in Figure 3.9), depending on the ability of the hoop material to confine the concrete. The force equilibrium at various locations on the

compression side of the neutral axis is shown in Figure 3.9. At the neutral axis there is no tension force in the hoop and, consequently, no confining stresses in the concrete. At sections above the neutral axis the hoop tension force increases until, at some point, the hoop yields and the confining stress remains constant (for elastic hoop material there is no yield and the confining stress would continue to increase).

Note that this approach assumes that there is perfect bond between the hoops and the confined core concrete. Some relative slip is possible which would make the actual response less critical. However, it is not advised to allow for such slip in the analysis as test results only sometimes indicate slip and redistribution of hoop strains at large ductility. As mentioned previously, the energy approach used in the present study is performed for each element at each increment of loading allowing the hoop strains and stresses around the section to vary properly. Test results show high hoop strains on the compression and tension sides of the column. This is primarily because the hoops yield at the compression toe in one direction of loading and then yield on the opposite side of the column when the loading direction is reversed. The analysis presented in this report is based on a monotonic moment-curvature approach and therefore yielding at the hoop reinforcement occurs only on the compression side of the column. If reversed loading was applied in the model then large hoop strains would develop on both sides of the column as in the cyclic tests.

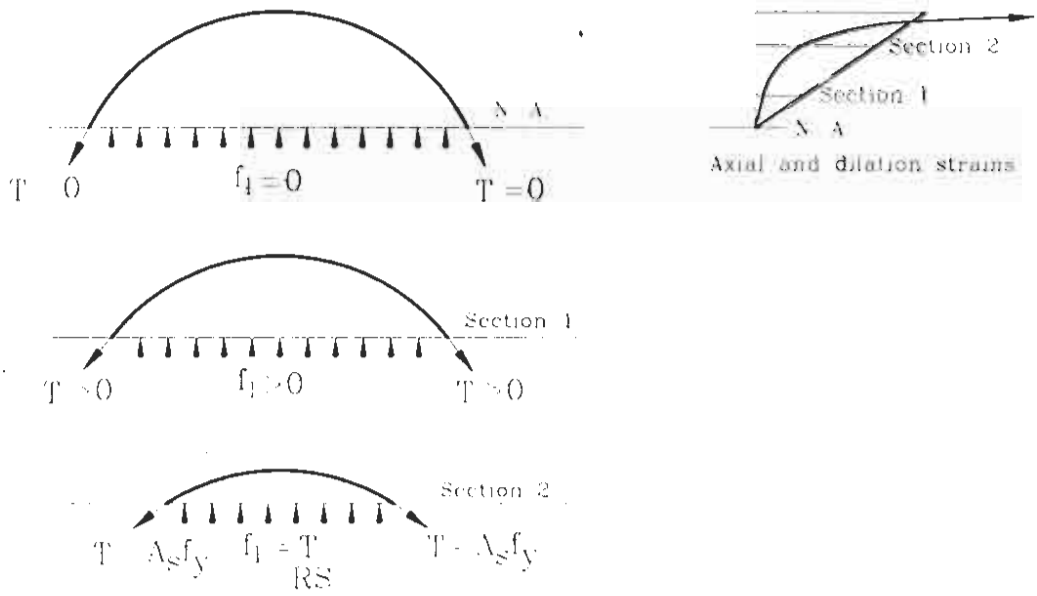

Figure 3.9: Force equilibrium at various sections above the neutral axis

3.4.2 Flexural Parameter Study

Using the analysis procedures discussed in Section 3.4.1 it is possible to calculate maximum hoop strains versus curvature and displacement ductility as well as hoop strains around the section at a given ductility level. For a typical column (assumed here to have 2% longitudinal steel ratio, 1% transverse steel ratio and 5% axial load ratio), this is demonstrated in Figure 3.10a and Figure 3.10b where maximum hoop strain versus curvature and displacement ductilities are shown, and Figure 3.10c where the hoop strains around the section are given at displacement ductility levels of 4, 5 and 8. In Appendix E, hoop strains are given around the section at displacement ductility levels 4, 5 and 6 for both 6 ft and 8 ft diameter columns. In flexure the axial load ratio, longitudinal steel ratio and transverse steel ratio all play important parts on the hoop strain demand. The axial load ratio and longitudinal steel ratio are important because they can significantly shift the neutral axis which changes the axial, dilation and hoop strain demands at the extreme confined elements and has a direct effect on the ductility capacity of the member. The transverse steel ratio is important because it causes the confinement stresses, which reduce dilation and hoop strains and, therefore, also has a direct effect on the ductility capacity of the member.

A parameter study was conducted to determine the curvature ductility capacity at maximum hoop strains of 2% (Figure 3.11), 3% (Figure 3.12) and 4% (Figure 3.13). As the figures indicate the axial load ratio was varied from 0 to 20 percent, the longitudinal steel ratio was varied from 1 to 3 percent and the transverse steel ratio was varied from 0.25 to 2 percent. These limits were chosen because they represent the typical range for most bridge columns.

All of the figures have been presented so that designers may enter the charts with a given axial load ratio, longitudinal steel ratio and transverse steel ratio to determine the curvature ductility capacity of the section at a given hoop strain of 2%, 3% or 4%. The designer can then convert from curvature ductility to displacement ductility as discussed in [14]. Displacement ductility capacities are given in Figure 3.14, Figure 3.15 and Figure 3.16 at maximum hoop strains of 0.02, 0.03 and 0.04, respectively. It should be noted, however, that to convert from curvature ductility (which is based on section information only) to displacement ductility requires knowledge of the ratio of the equivalent plastic hinge length to cantilever member length and will change depending on the size of the primary flexural steel. The value of 0.141 was used here to convert curvature to displacement ductility, which is the value found for TU1 presented in [7], and is a reasonable ratio of plastic hinge length to cantilever length for many columns. For example, a 30 ft tall, 8 ft diameter column with #14 bars would have a ratio of 0.13. If the ratio of plastic hinge length to cantilever length is much different than assumed here, the designer should use the curvature ductility charts provided in Figure 3.11 through Figure 3.13 and convert to displacement ductility based on the correct plastic hinge length to cantilever length ratio, see [14].

From the displacement ductility charts presented, it is possible to determine the transverse steel volume required to reach displacement ductility 4 at hoop strains of 0.02, 0.03 and 0.04, respectively (see Figure 3.17). Thus by entering one of the charts in Figure 3.17 with axial load and longitudinal steel ratios, the required transverse steel ratio to limit hoop strains to either 0.02, 0.03 or 0.04 at displacement ductility 4 can be quickly determined.

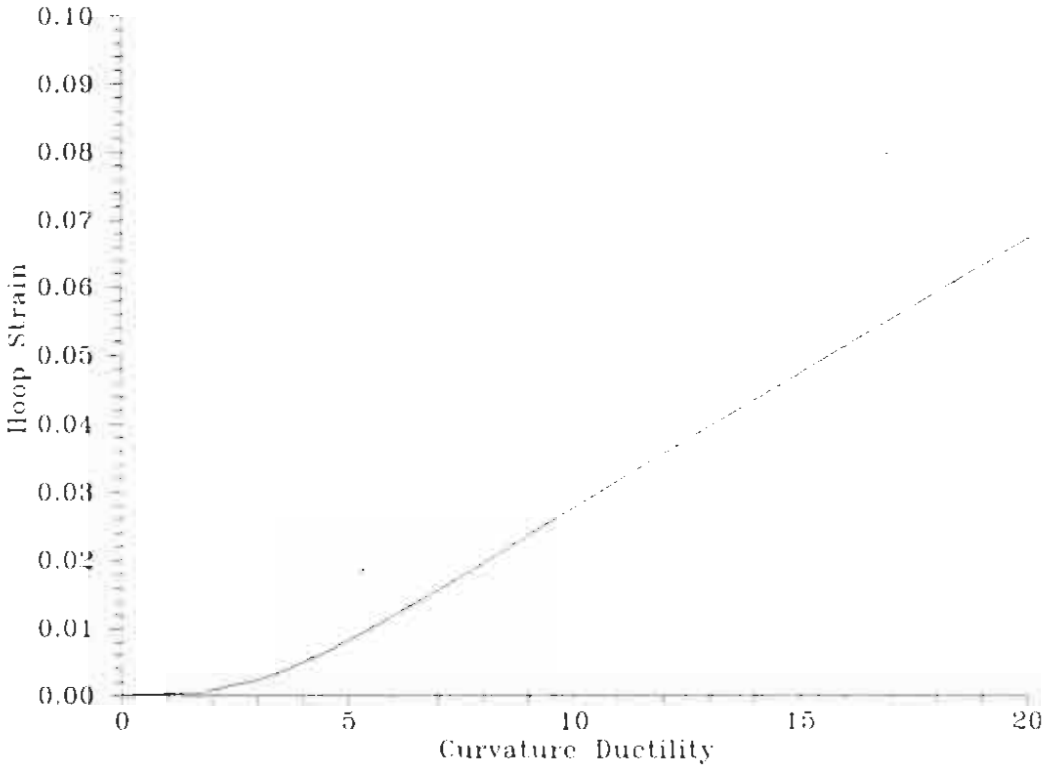

a) Maximum hoop strain versus curvature ductility

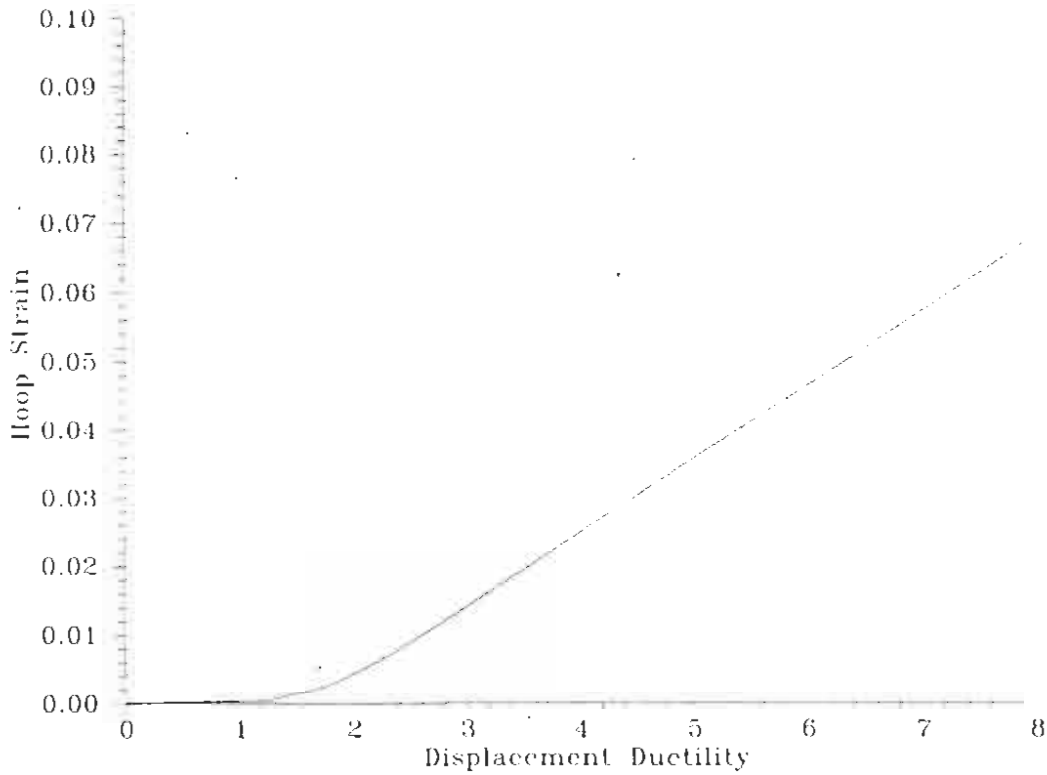

b) Maximum hoop strain versus displacement ductility

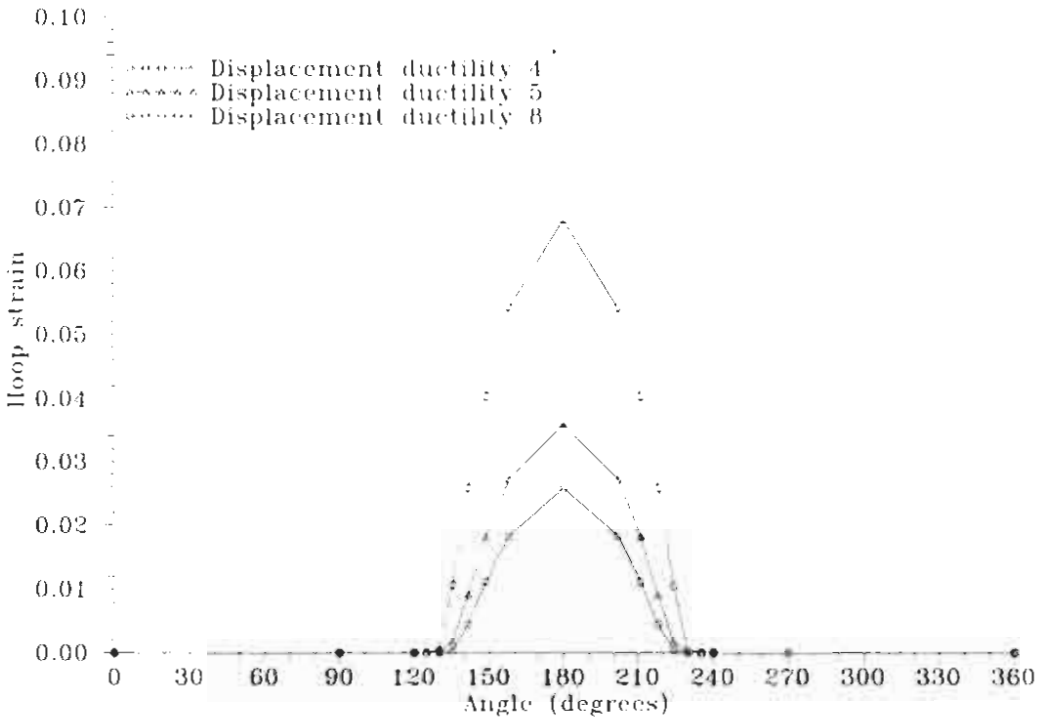

c) Hoop strains around circumference at displacement ductility 4, 5 and 8

Figure 3.10: Hoop strain versus ductility results for typical column

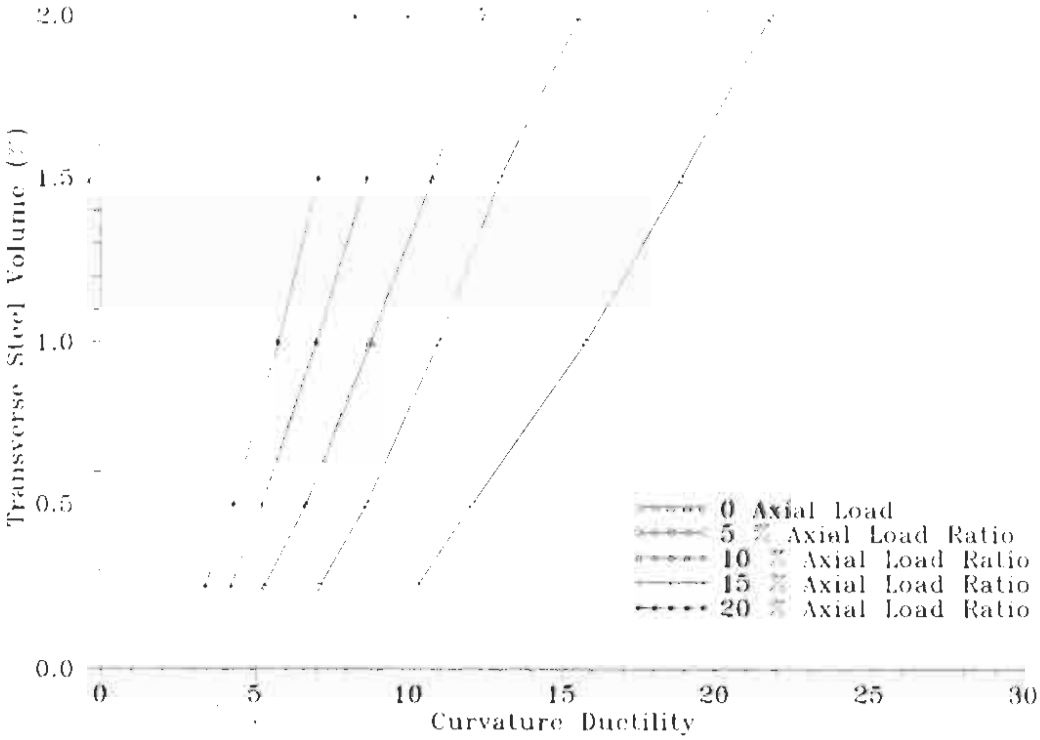

a) 1% Longitudinal steel ratio

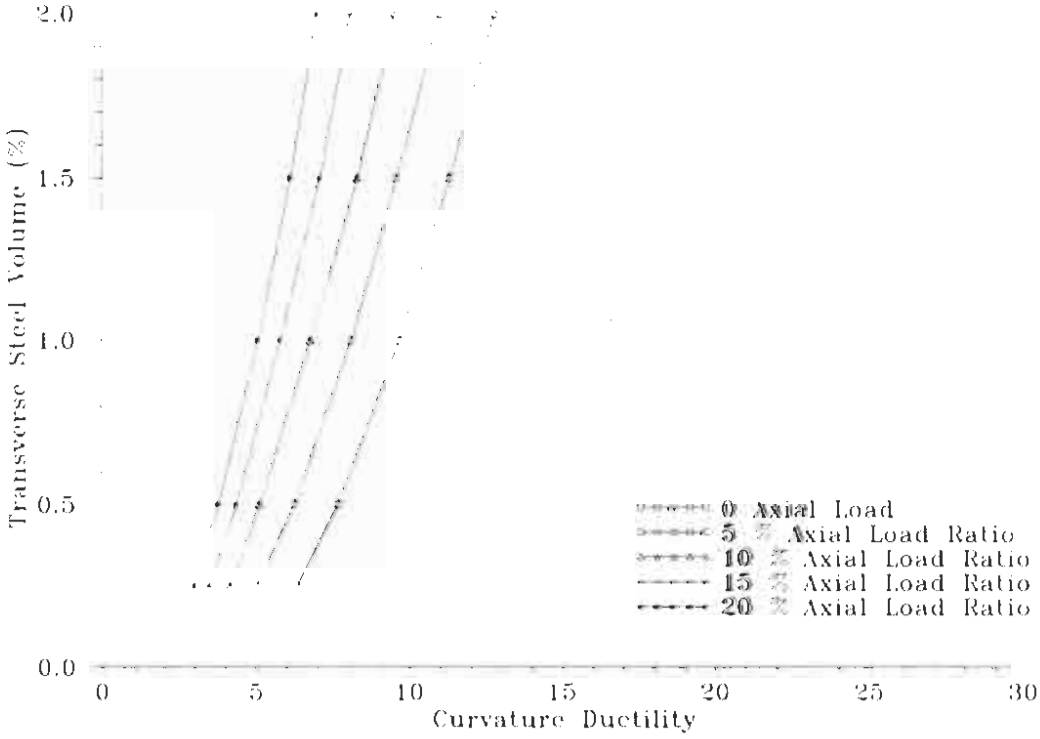

b) 2% Longitudinal steel ratio

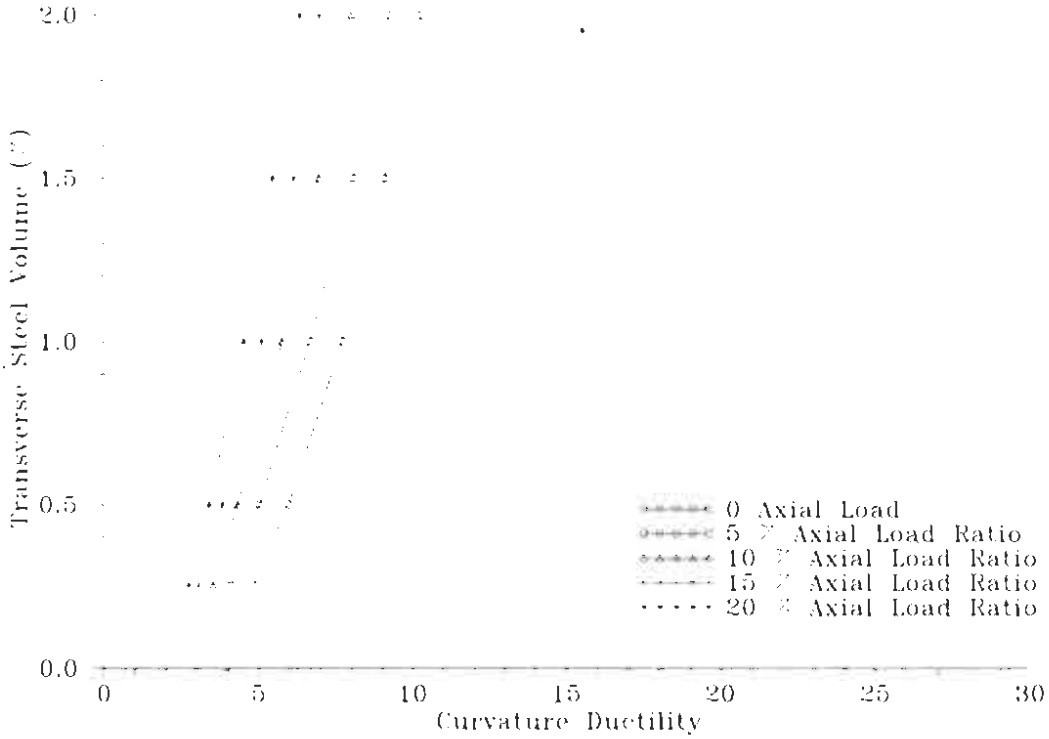

c) 3% Longitudinal steel ratio

Figure 3.11: Curvature ductility at peak hoop strain of 0.02

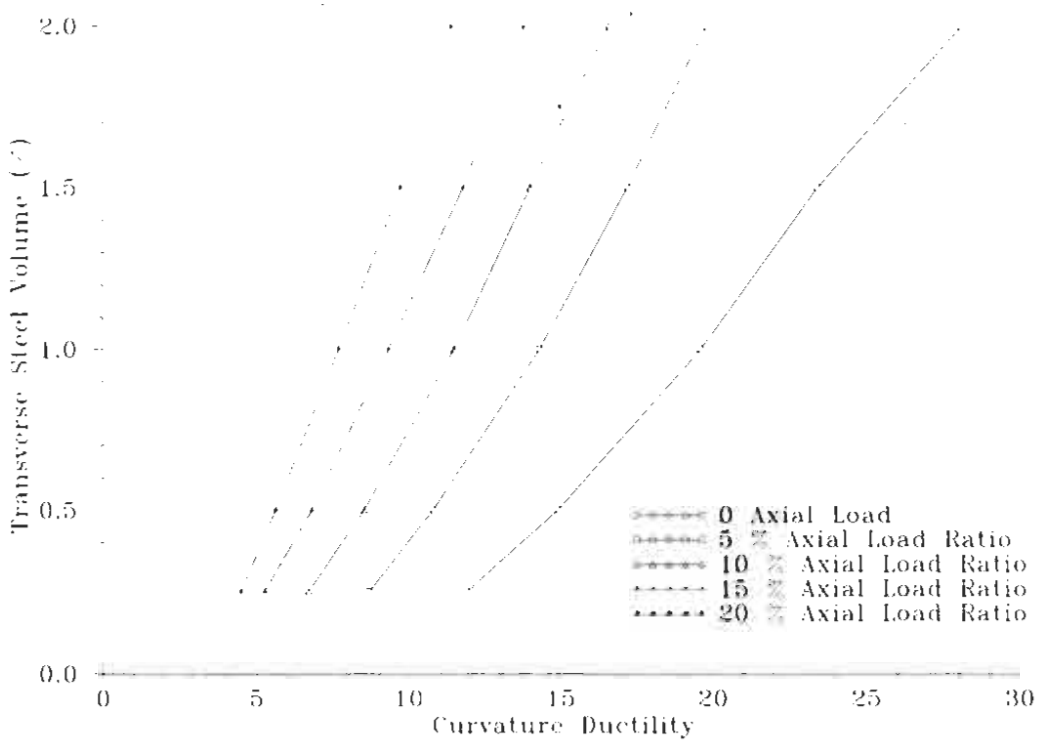

a) 1% Longitudinal steel ratio

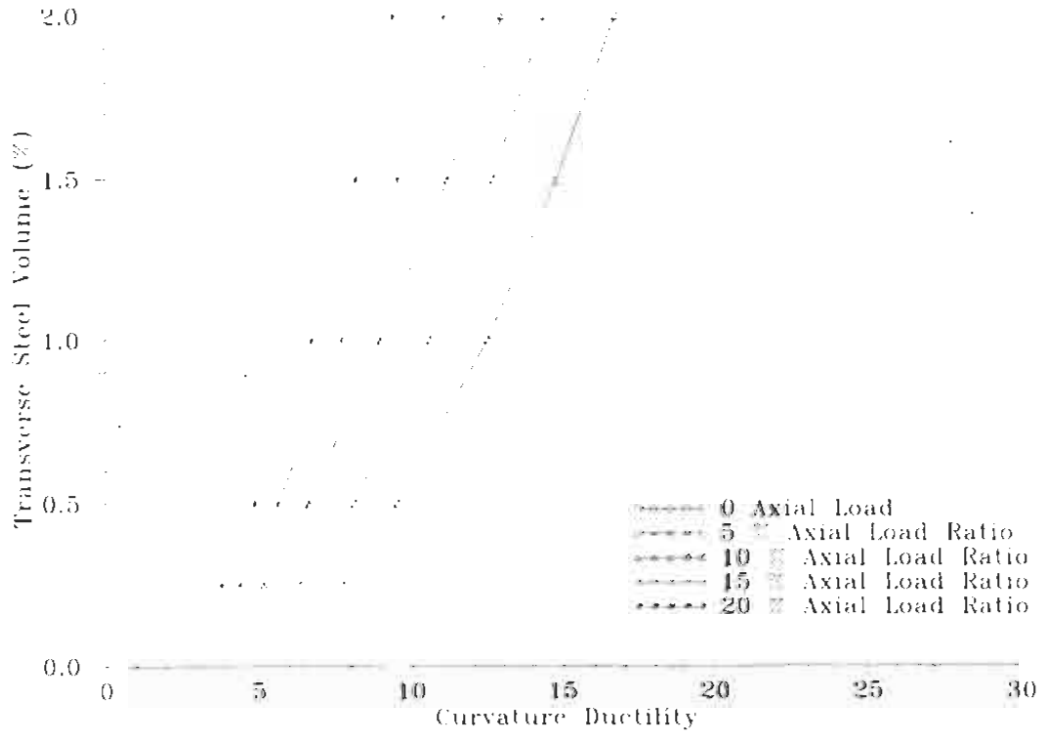

b) 2% Longitudinal steel ratio

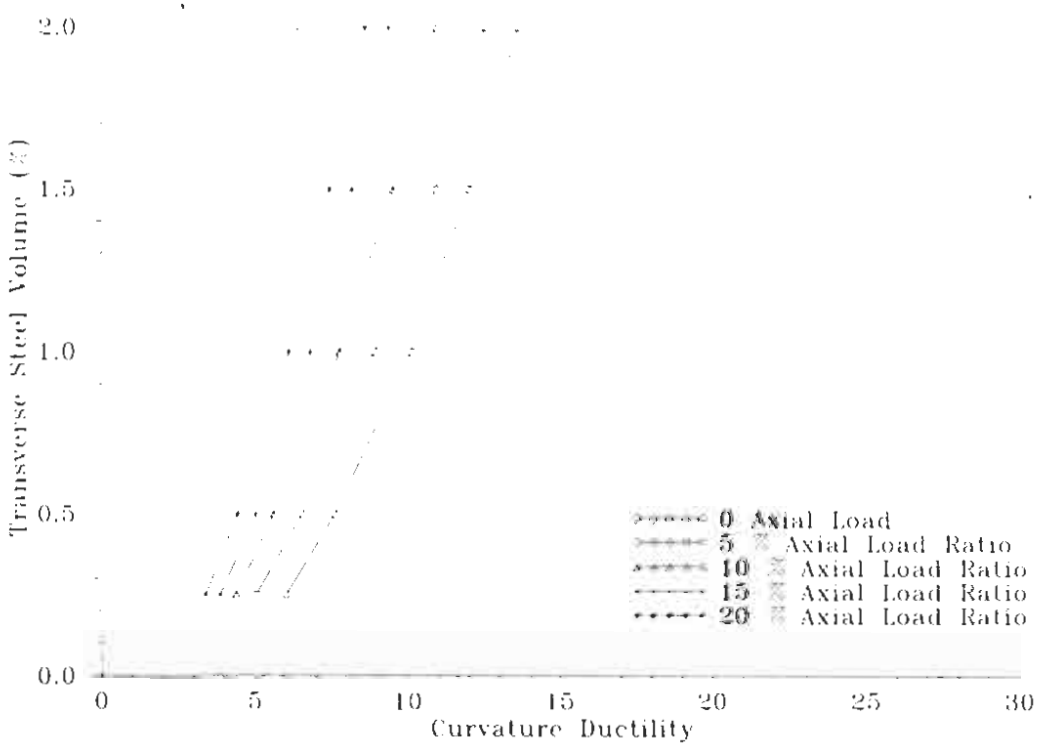

c) 3% Longitudinal steel ratio

Figure 3.12: Curvature ductility at peak hoop strain of 0.03

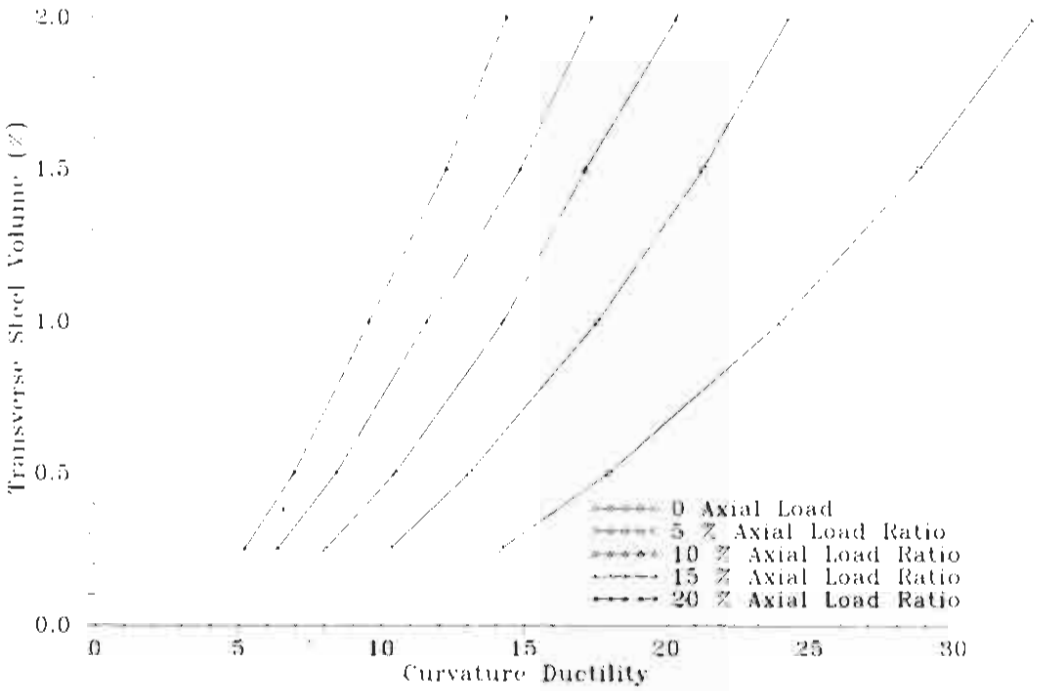

a) 1% Longitudinal steel ratio

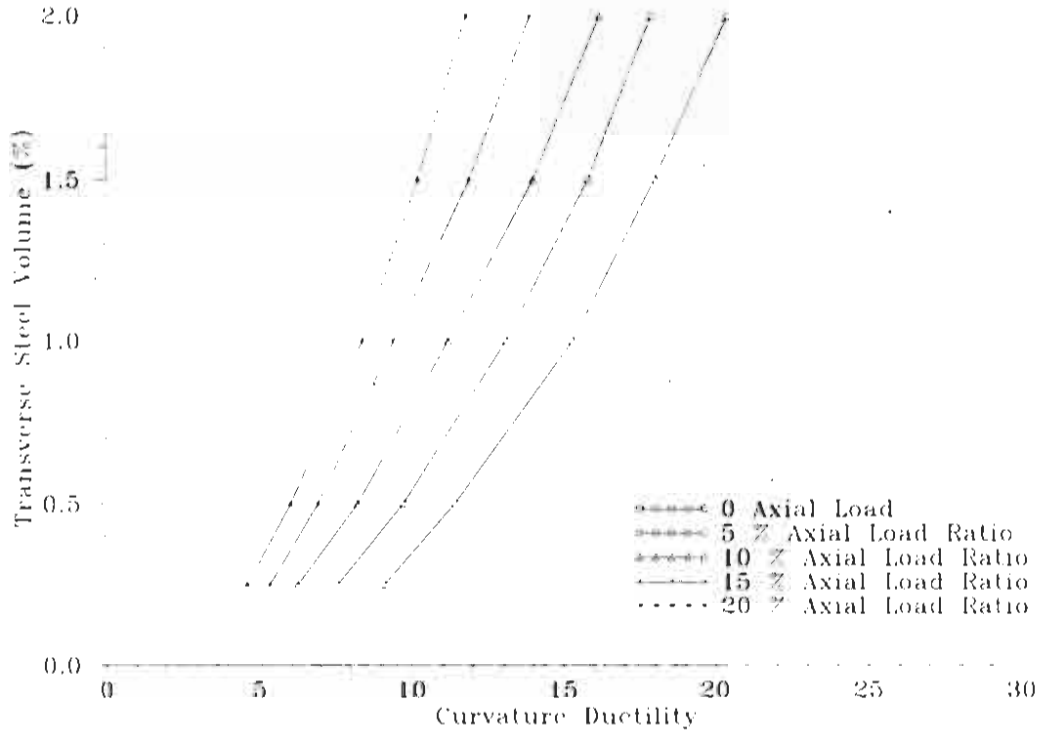

b) 2 % Longitudinal steel ratio

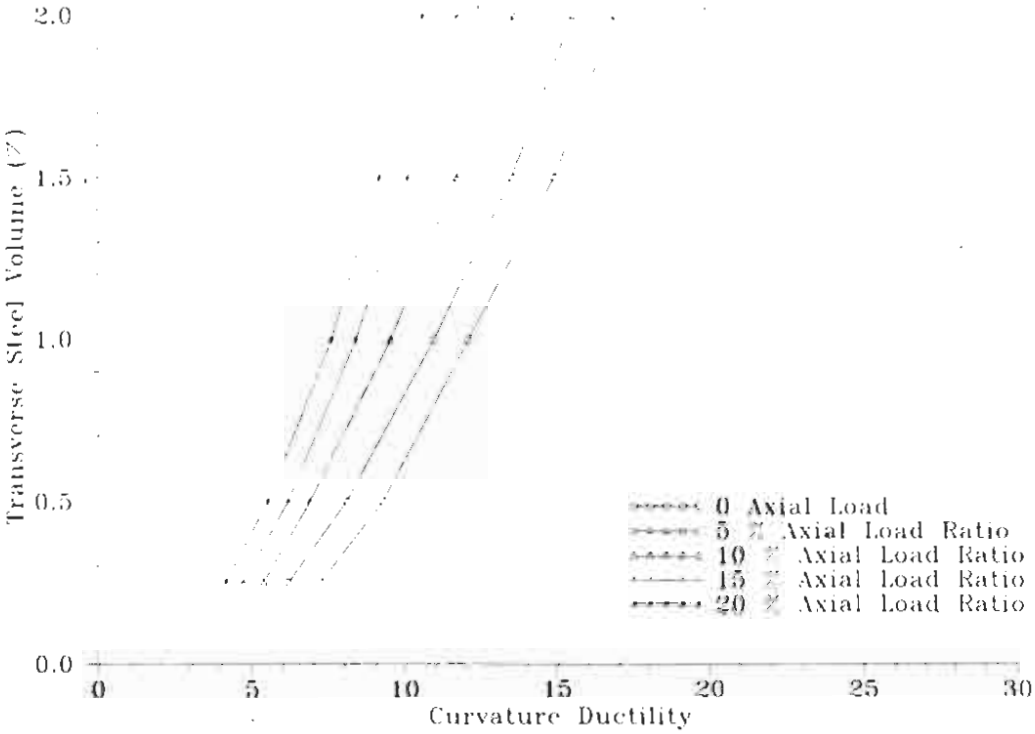

c) 3% Longitudinal steel ratio

Figure 3.13: Curvature ductility at peak hoop strain of 0.04

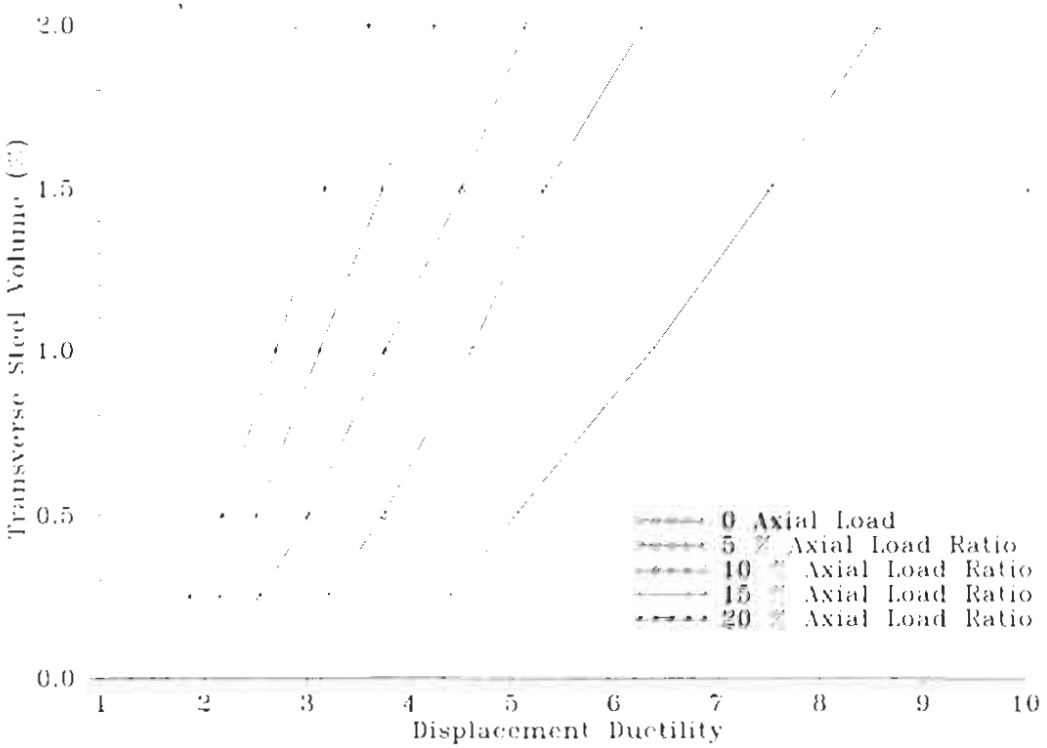

a) 1% Longitudinal steel ratio

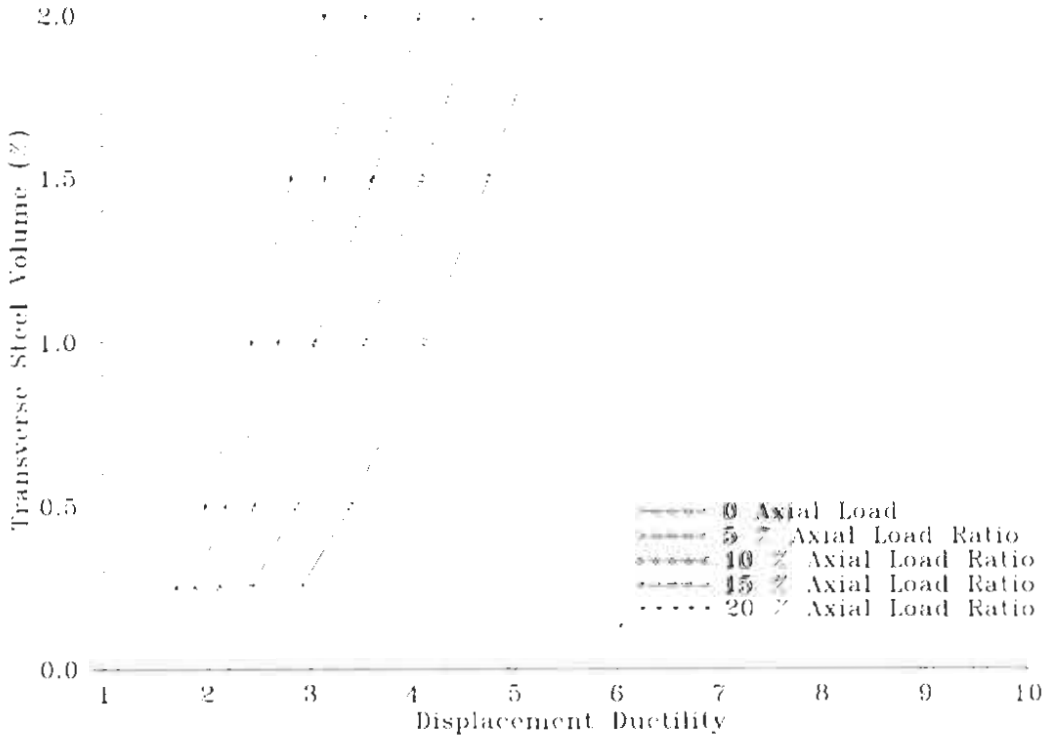

b) 2% Longitudinal steel ratio

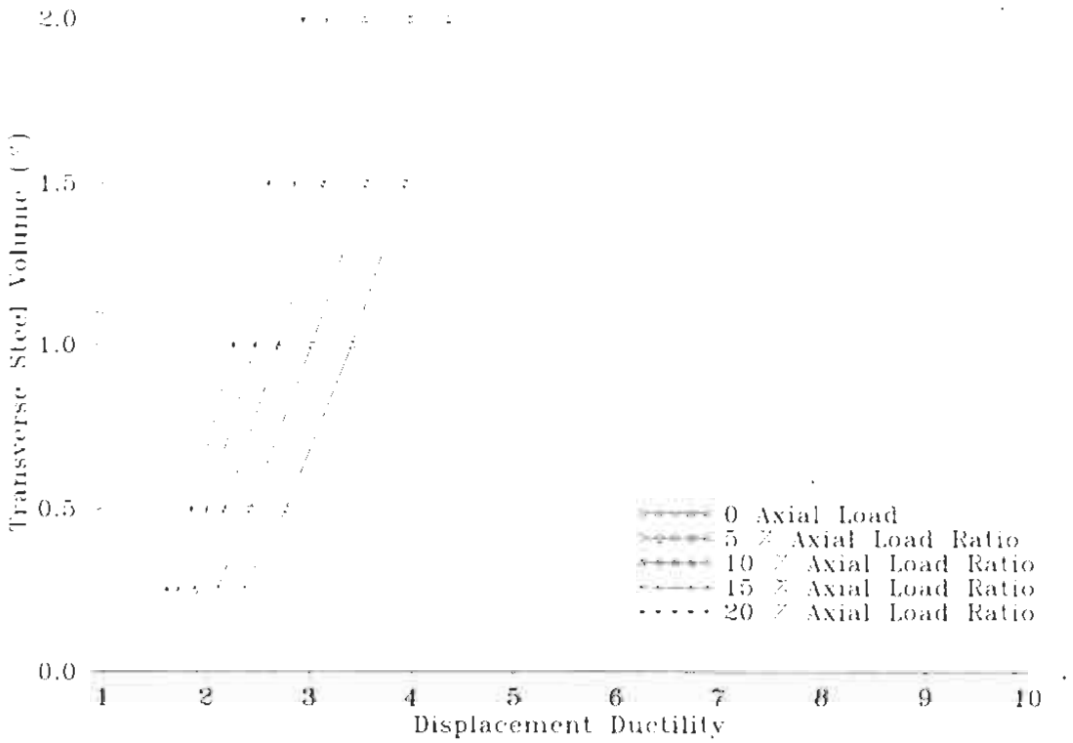

c) 3% Longitudinal steel ratio

Figure 3.14: Displacement ductility at peak hoop strain of 0.02

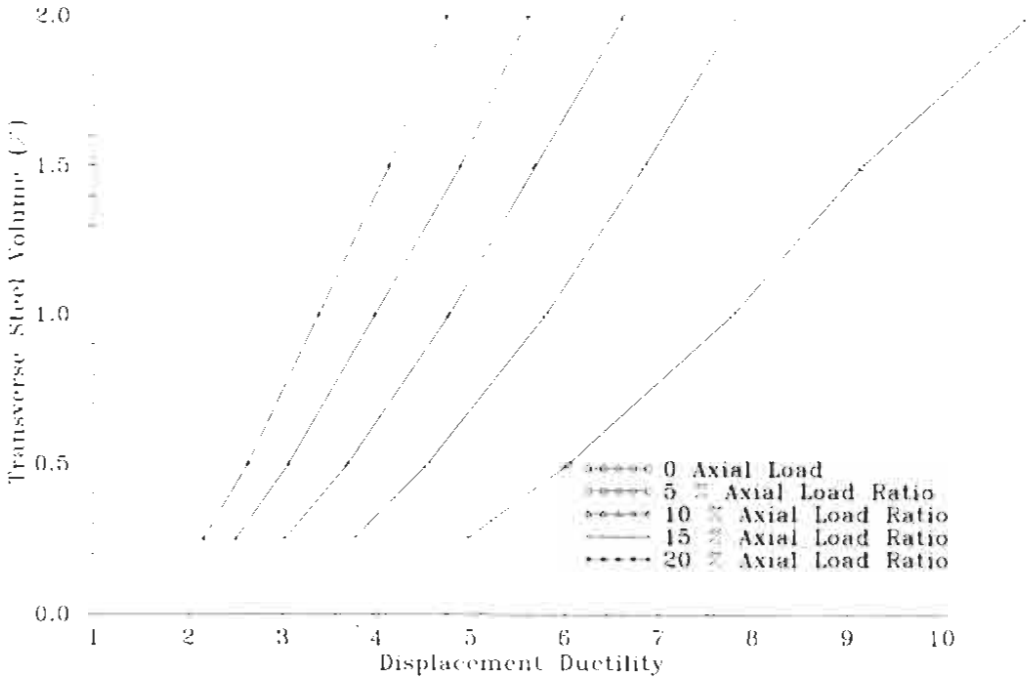

a) 1% Longitudinal steel ratio

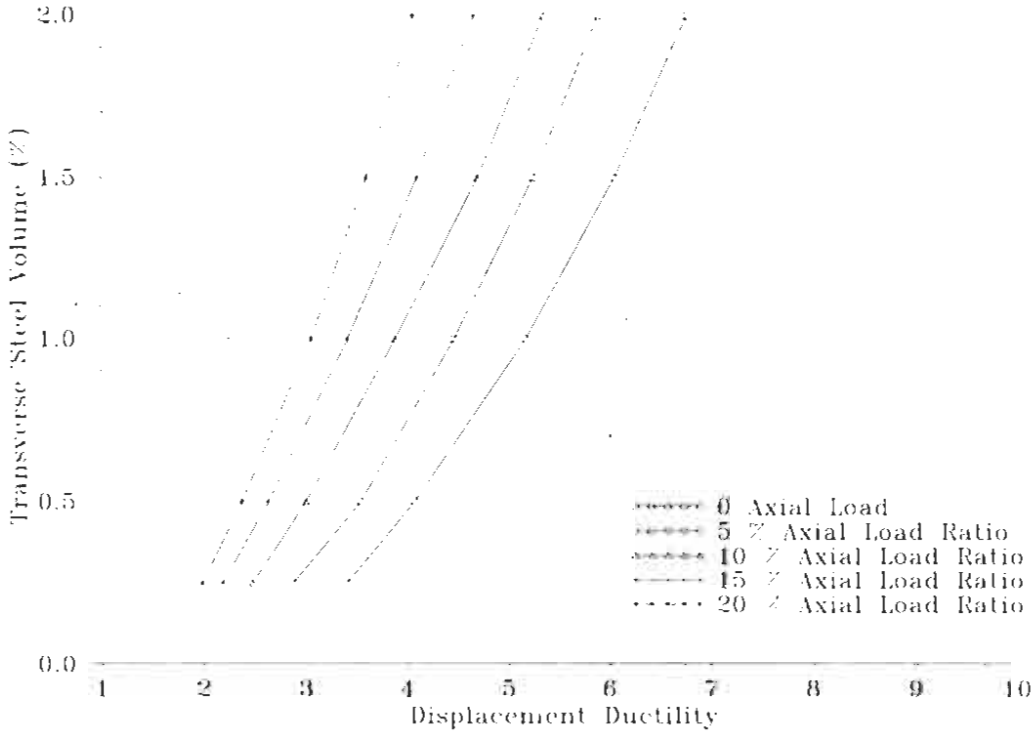

b) 2% Longitudinal steel ratio

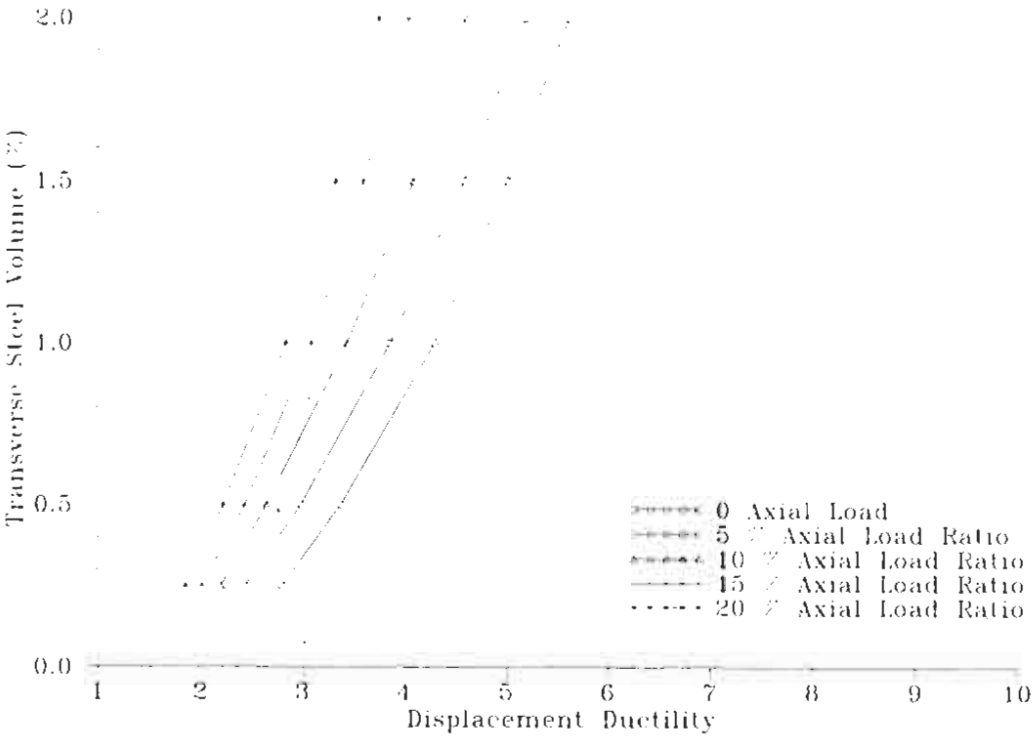

c) 3% Longitudinal steel ratio

Figure 3.15: Displacement ductility at peak hoop strain of 0.03

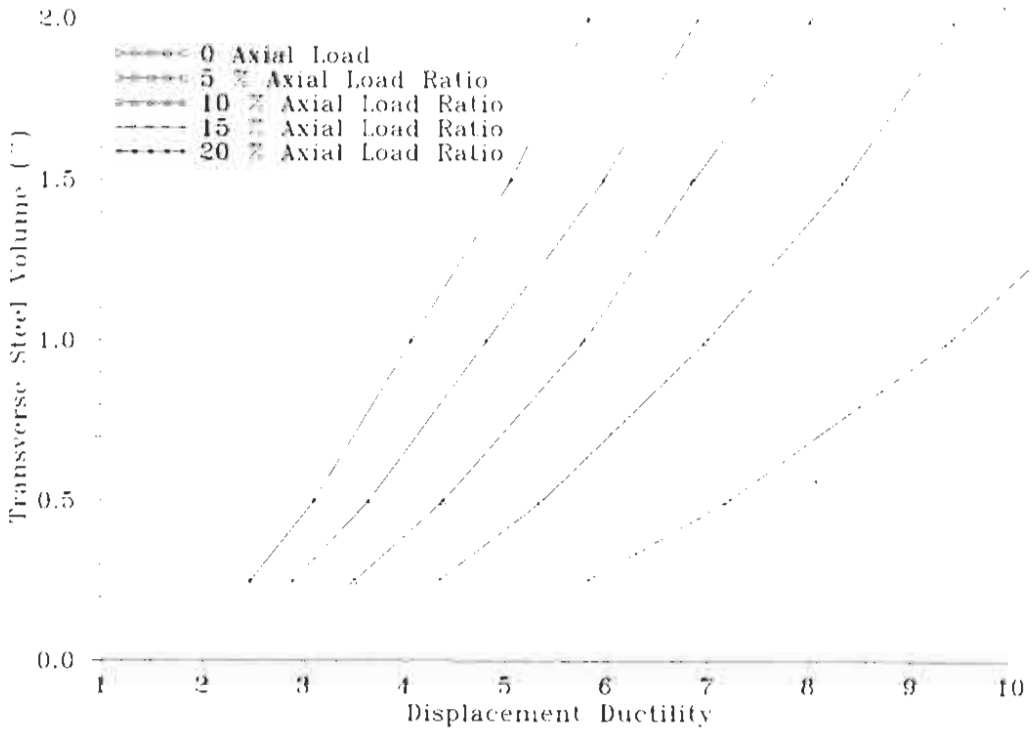

a) 1% Longitudinal steel ratio

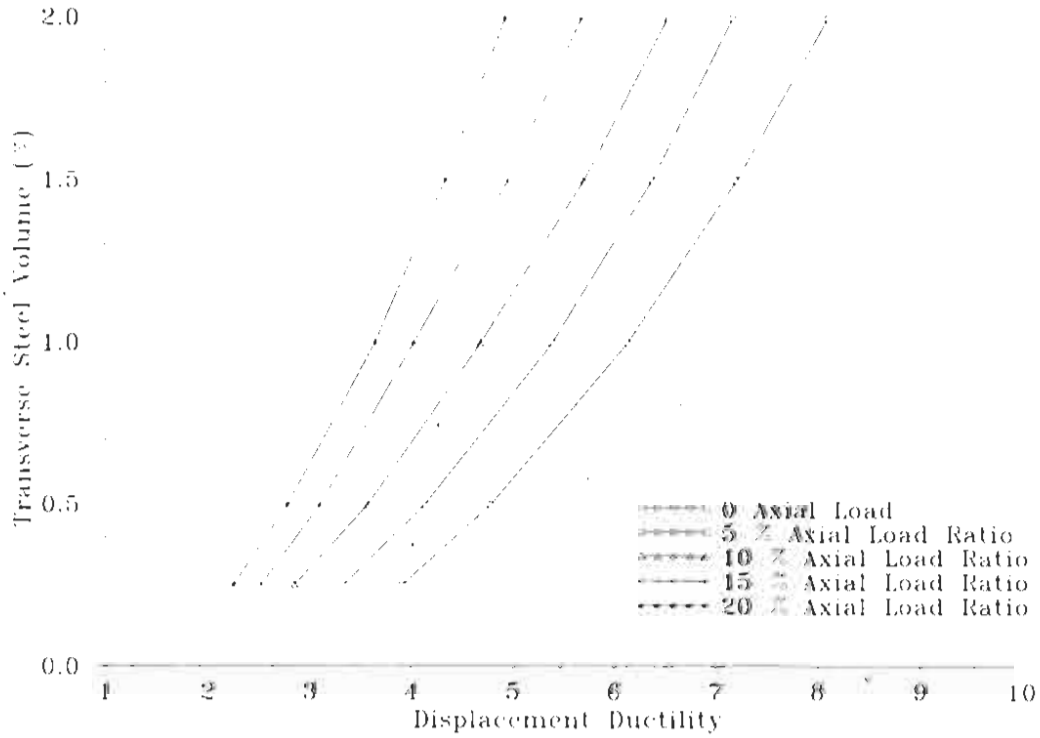

b) 2% Longitudinal steel ratio

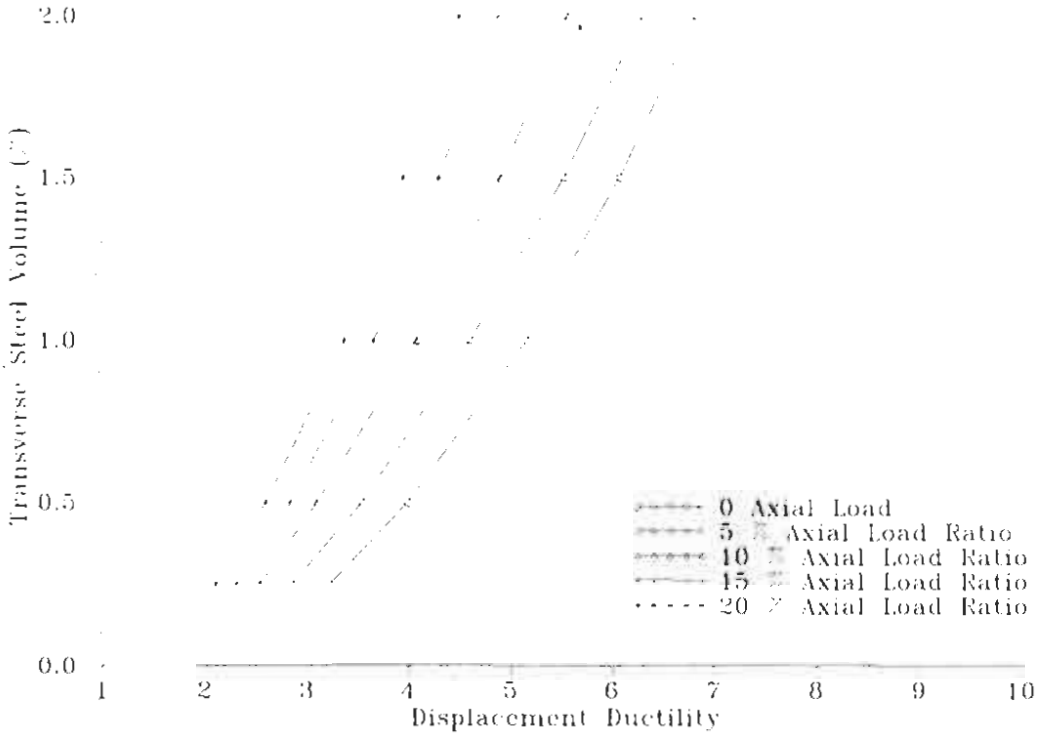

c) 3% Longitudinal steel ratio

Figure 3.16: Displacement ductility at peak hoop strain of 0.04

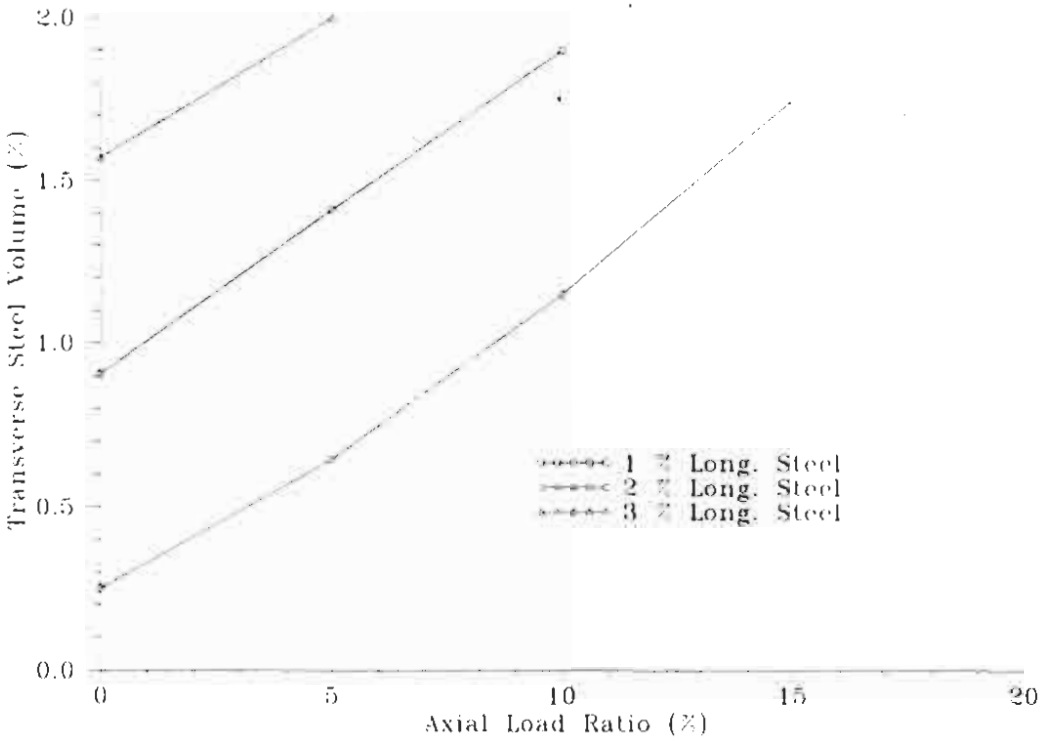

a) Peak hoop strain of 0.02

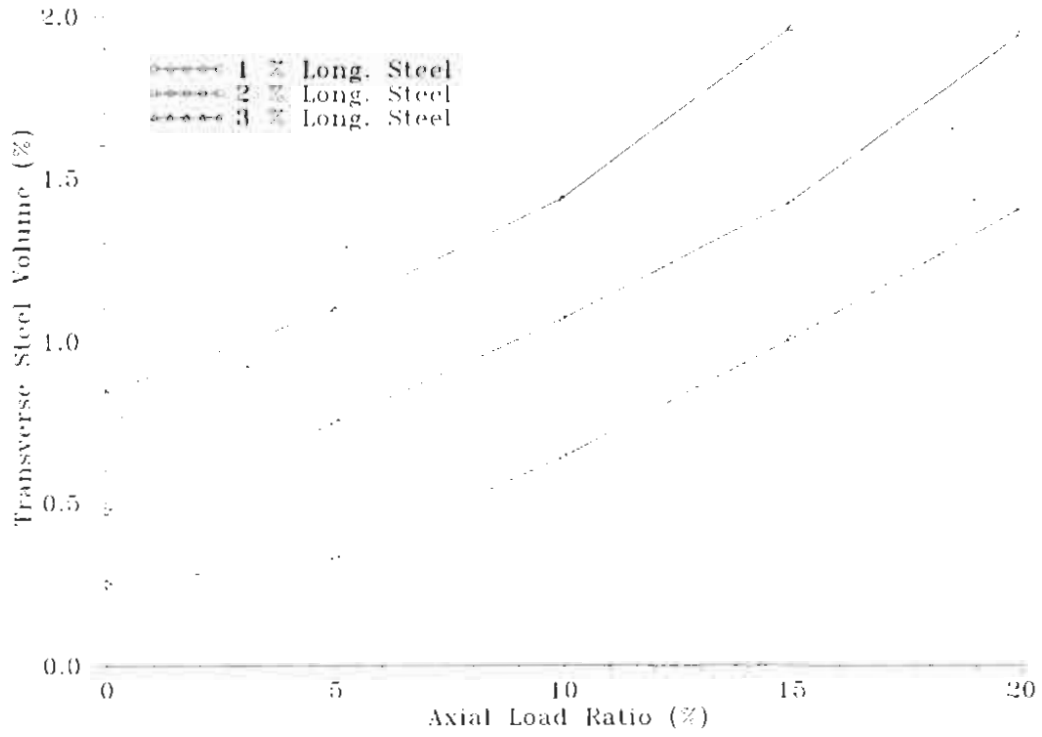

b) Peak hoop strain of 0.03

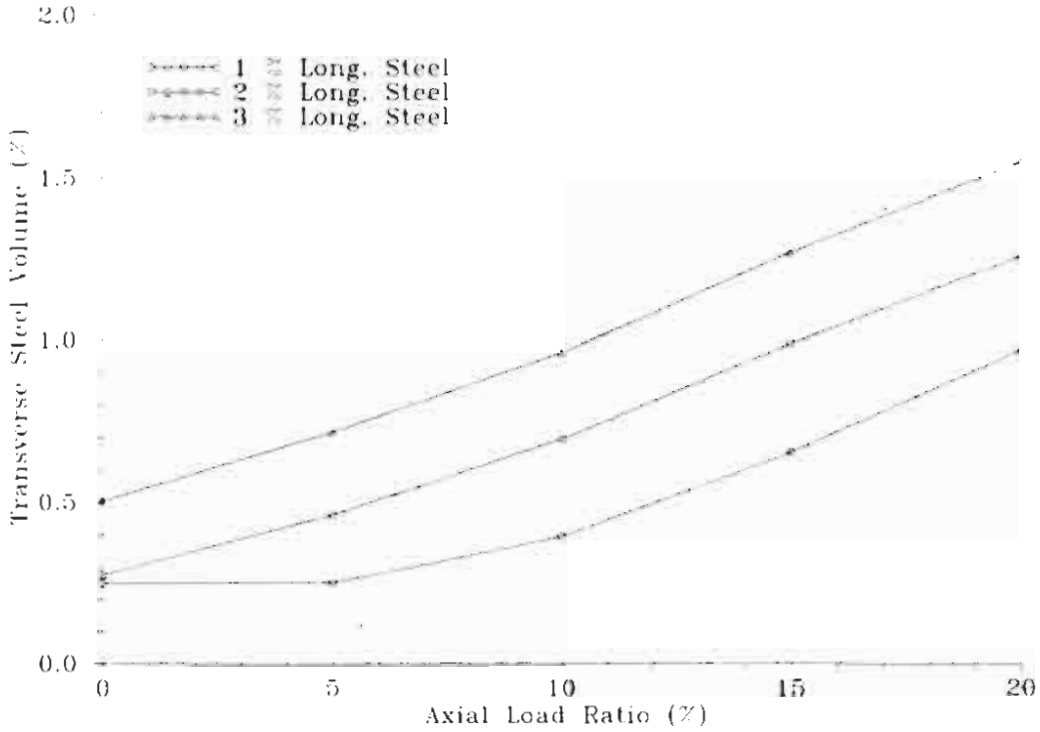

c) **Peak hoop strain of 0.04**

Figure 3.17: Required transverse steel volume to reach displacement ductility 4

4 Design Analysis

The theory behind the modification to the sectional moment-curvature analysis tool was described in Chapter 3. The following chapter validates the new analytical model using test results from some of the columns presented in Chapter 2. As an example calculation the analytical tool is then utilized to determine the amount of transverse steel required to limit the column hoop strains in actual bridge columns to 0.02, 0.03 and 0.04 at displacement ductility 4. The validation of the analytical model is presented in Section 4.1, while the bridge column study is given in Section 4.2.

4.1 Flexural Column Verification

To verify the flexural analysis approach described in Section 3.4 of Chapter 3, hoop strains of five flexural columns tested at UCSD and assessed in Chapter 2 of this report are compared to maximum hoop strains from moment-curvature analyses. The columns are TU1, TU5 and TU7 from SSRP 97/05 [7], and COL 1 and COL 2 from SSRP 94/14 [16]. All of these columns were tested at a slow strain rate. As discussed in Section 3.3, the Mander tests showed that with a fast strain rate the hoop strains are up to twice the values from loading at a slow strain rate. Note that there was only one direct comparison provided by Mander between measured hoop strains from a dynamic and static test and, therefore, this observation of increased hoop strains under dynamic loading should be taken with caution.

The comparison of the analytical and measured hoop strains for the five flexural columns investigated seem to confirm the approximate factor of two between hoop strains from dynamic and static loading as shown in Table 4.1 and Figure 4.1. The measured hoop strains for the statically loaded columns are given in Table 4.1. The measured hoop strains for statically loaded columns are doubled to compare directly with the analytical results and show that the new moment-curvature analysis approach provides realistic maximum hoop strains from dynamic loading. Figure 4.1 shows that for

the five flexural columns investigated the ratios of measured to calculated hoop strains fall near the 0.5 value, which is consistent with the dynamic factor discussed previously.

Table 4.1: Measured and calculated hoop strains from five flexural tests

Column	Reference	Displacement Ductility	Measured Hoop Strains (static)	Measured Hoop Strains (2 x static)	Calculated Hoop Strains (dynamic)
TU1	[7]	2	0.0084	0.017	0.016
TU5		2.8	0.018	0.036	0.033
TU7		3	0.015	0.03	0.038
COL 1	[16]	Drift of 13 in.	0.0021	0.0042	0.0060
COL 2		Drift of 17 in.	0.0046	0.0092	0.0079

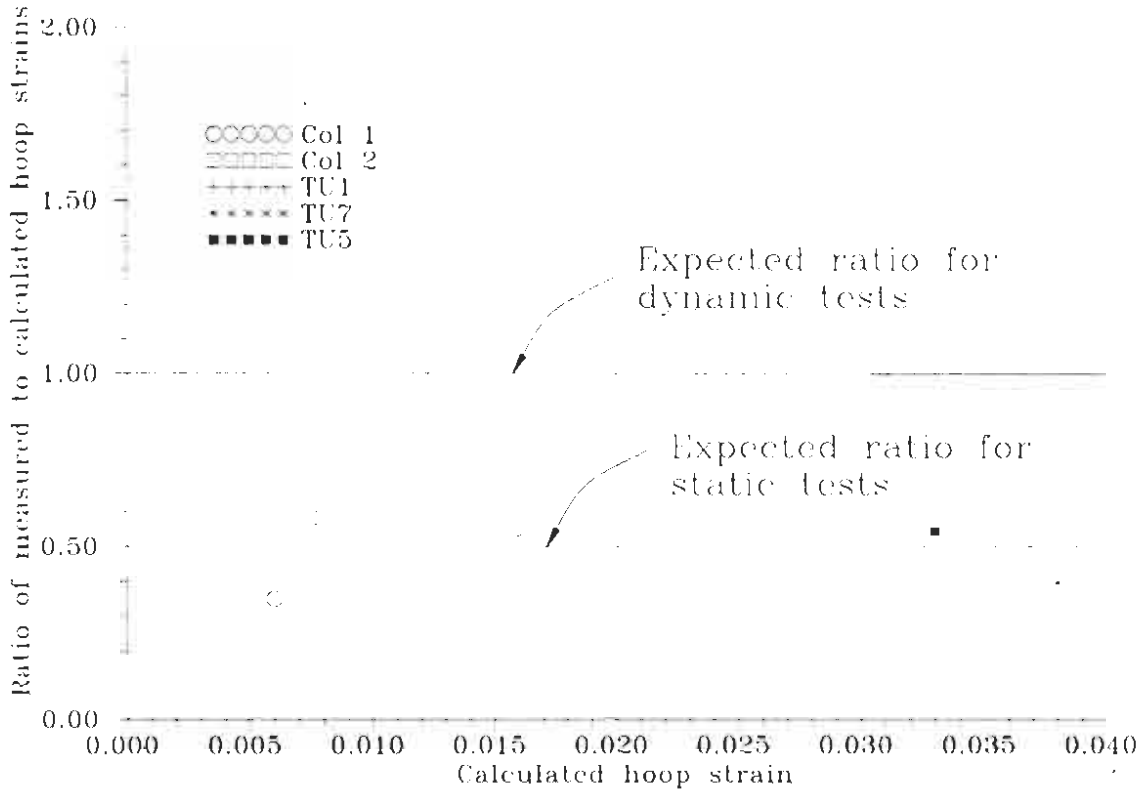

Figure 4.1: Ratio of calculated to measured hoop strains for the five columns

Note that the analyses provide an upper bound to the measured results and are well within the scatter of measured hoop strains. Also, the reduction in hoop strains that occurred in some of the tests at larger ductility levels (probably due to relative slip between the hoops and the concrete) is not modeled, which makes the analysis more

conservative. Furthermore, it should be noted that the increase in hoop strains by a factor of two due to dynamic effects occurs mostly at the smaller ductility levels.

As a final check of the proposed model, the force-displacement responses of two columns that were part of the strategic relocation of the plastic hinge experimental program [7] were calculated to failure (hoops assumed failed at ultimate strain of 0.10). Column TU1, the reference column discussed in Section 2.1.1, was evaluated as well as an additional column, TU2, which was designed to relocate the plastic hinge region 18 inches from the base. For Columns TU1 and TU2 the ultimate displacements at failure were measured to be 12.5 inches and 11.5 inches, respectively. Using the new assessment method presented in Chapter 3, the ultimate displacements were calculated as 12.4 inches and 12.5 inches, respectively, while the predicted ultimate displacements based on the Mander approach were 7.8 inches and 7 inches for TU1 and TU2, respectively. It should be noted that the failure mode for both TU1 and TU2 was given in [7] as buckling of the vertical reinforcement, which fractured on the next half cycle. There was no mention of the hoops failing. Section analysis methods (Mander approach and the new method) do not directly assess longitudinal bar buckling, but it can be assumed that bar buckling and hoop fracture are closely related. Therefore, the predictions based on the Mander model are clearly conservative (as discussed previously) as no buckling occurred until larger displacements.

In Figure 4.2a, the measured response of TU2 is compared to the predicted and new model force-deformation results to failure demonstrating that the new model follows the measured force-deformation response and defines failure more closely than that predicted based on the Mander approach. Figure 4.2a indicates that the termination criteria matches the failure displacement at high displacement ductility levels without requiring a factor to account for dynamic effects. The maximum hoop strains versus displacement from the new analysis approach are given in Figure 4.2b, which shows the assumed ultimate hoop strain of 0.10 at a column displacement of 12.5 inches.

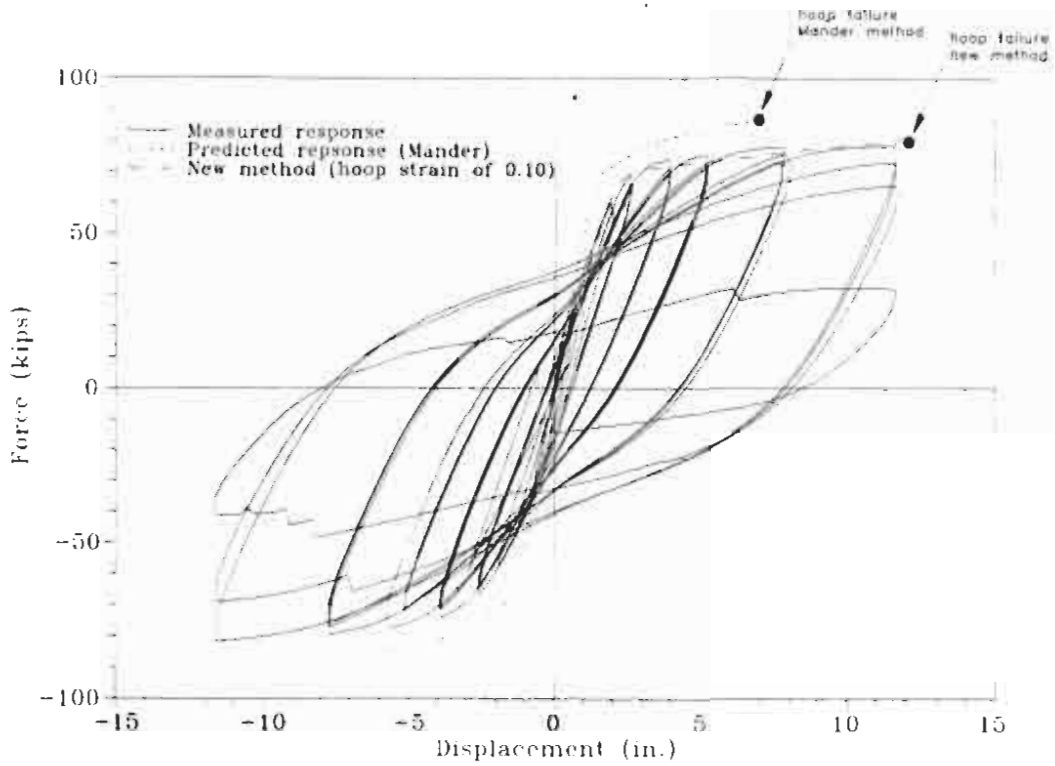

a) Force-displacement responses

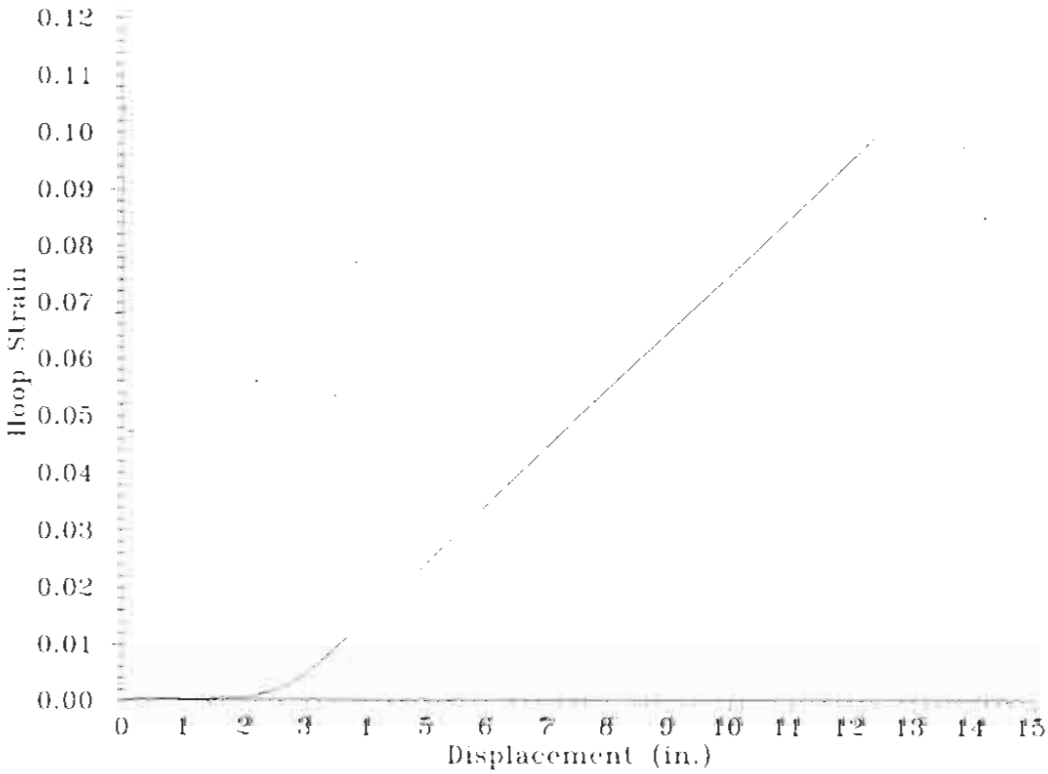

b) Hoop strain versus top displacement

Figure 4.2: Measured and analytical responses of TU2 [7]

4.2 Bridge Column Study

The impetus of this study was Caltrans' interest in the performance of actual bridge columns. As an example, three bridges (55-683F, 55-692E, and 55-681H) and eleven bents of the SR-57/I-5 Interchange given in Table 4.2 were investigated. Also in the table are the axial load, longitudinal steel and transverse steel ratios. The required transverse steel volumes to reach displacement ductility 4 at hoop strains of 0.02, 0.03, and 0.04, respectively, were found from the charts provided in Figure 3.17 of Chapter 3. The results are presented in Table 4.2 and in Figure 4.3. It is clear that all of the columns have been provided with enough transverse reinforcement to limit the hoop strains to less than 0.03 at displacement ductility 4. The columns have close to twice the amount of confinement steel needed to limit the hoop strains to 0.04 at displacement ductility 4. However, only one of the columns investigated had the required amount of transverse reinforcement to limit the strains to 0.02 at displacement ductility 4.

Table 4.2: Required transverse steel ratios for displacement ductility 4 with hoop strains not exceeding 2%, 3%, and 4%

Bridge	Bent	Axial load ratio (%)	ρ_l (%)	ρ_s (%)	Required ρ_s $\varepsilon_{hoop} = 2\%$ (%)	Required ρ_s $\varepsilon_{hoop} = 3\%$ (%)	Required ρ_s $\varepsilon_{hoop} = 4\%$ (%)
55-683F	2	11.5	2.74	1.60	2.45	1.46	0.96
55-683F	3	7.89	2.11	1.33	1.77	1.00	0.62
55-683F	4	6.08	2.11	1.33	1.60	0.88	0.53
55-683F	5	8.49	2.11	1.33	1.82	1.03	0.66
55-692E	2	4.25	2.31	1.44	1.53	0.82	0.52
55-692E	3	7.39	1.06	1.02	0.94	0.52	0.35
55-692E	4	8.11	2.31	1.44	1.90	1.08	0.71
55-681H	2	9.10	2.84	1.78	2.25	1.32	0.87
55-681H	3	7.82	2.84	1.78	2.18	1.19	0.80
55-681H	4	10.5	1.30	1.00	1.42	0.81	0.51
55-681H	5	9.26	1.30	1.14	1.30	0.72	0.46

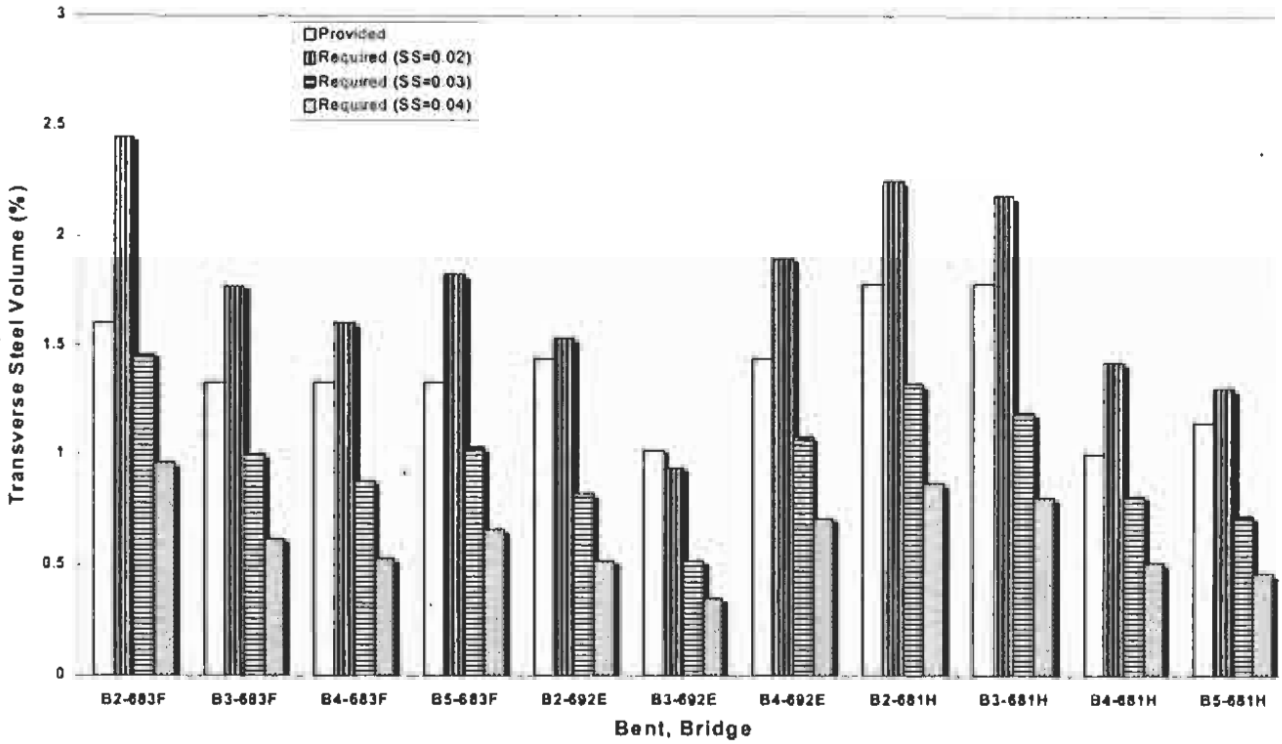

Figure 4.3: Provided and required transverse steel ratios to limit hoop strains to 2%, 3%, and 4% at displacement ductility 4

5 Conclusions and Recommendations

The research presented in this report investigated experimental and analytical strain demands in hoop reinforcement of various bridge columns. Results from recent laboratory tests of a variety of modern columns were assessed to determine strain levels observed in hoop reinforcement during large scale experimental testing. Since strain gages provided on hoop reinforcement are often lost at higher displacement ductility levels, an analytical method to assess transverse strains was developed and presented in Chapters 3 and 4. The experimental strain values presented in Chapter 2 were used to validate this new model.

From a comparison of the experimental column tests in Section 2.3.1, as well as observations from the analytical parameter study in Section 3.4.2, it is apparent that the scale of the column does not affect performance or strain levels of the transverse reinforcement. Furthermore, size and spacing of the transverse reinforcement have little significance on hoops strains. However, they are crucial in preventing premature bar buckling, and therefore, additional anti-buckling checks are recommended.

Specific findings from the review of large and full-scale bridge column tests in Chapter 2 are as follows:

1) Strain levels in the hoop reinforcement in the flexural plastic hinge region of laboratory test columns were found to be significantly smaller than strain levels predicted by common design tools based on Mander's equal energy approach. Most measured hoop strains were less than 1% but premature loss of strain gages at increasing ductilities does not allow a conclusive experiment based hoop strain evaluation.
2) Developments of reliable analytical tools which predict actual strain levels in the hoop reinforcement are needed which can be calibrated and validated with the limited experimental strain data prior to their application in parametric studies to higher

ductility levels. Experimental hoop strains from jacket retrofitted columns can also be used for model validation.

3) Experimental column tests evaluated considered test specimens with 40% scale or full-scale. At the 40% scale, conventional rebar and aggregates can still be used without affecting test results. Both 40% scale columns and full-scale test specimens show consistent results, indicating that scaling to the 40% scale level provides fully representative results.
4) From the evaluated measured hoop strain data it was observed that hoop strains were only reliably measured to displacement ductility levels of $\mu_\Delta = 3$ or 4 for conventionally reinforced columns and to $\mu_\Delta = 6$ or 8 in jacket retrofitted columns.
5) Hoop strains were also found to decrease at higher ductilities once the cover concrete in the plastic hinge region has spalled off due to debonding and slip of the hoop reinforcement.

Specific findings from the analytical parameter studies consist of the following:

1) Mander's model overestimates the actual strain rate in the hoop reinforcement by a factor of 3 to 4 compared with more rational analytical tools.
2) Three dimensional finite element models with plasticity theory based constitutive models significantly underestimate hoop strain levels.
3) The new adaptive Poisson's ratio section model agrees very well with measured hoop strain data based on axial tests performed by Mander. Dynamic axial loading rates equivalent to rates experienced in typical bridge columns during seismic events may increase hoop strains by up to a factor of 2. Note: only one test by Mander was available to validate these findings.
4) Flexural column response comparisons for maximum hoop strains show good agreement between experimental and the new analytical model considering the large scatter in experimental results.

The analysis results in Chapter 4 show that all of the columns in bridges 55-683F, 55-692E and 55-681H have adequate transverse confinement to prevent hoop strains

from exceeding 3% at a displacement ductility level of 4. Bent 2 of bridge 55-683F was the closest to not having the required transverse steel with an excess of 10%. Furthermore, there is approximately twice the amount of transverse steel required to prevent hoop strains from exceeding 4% and causing weld failure at a displacement ductility level of 4.

Hoop strain limitation of 2% would require additional reinforcement in all columns investigated in the examples. However, it should be noted that (1) not all hoops in an existing prototype column are weld spliced at the extreme compression side (2) not all welds are along a single column generator (line) and (3) even failure of a single hoop weld does not constitute complete column failure. Thus, even the demonstrated maximum hoop strain analysis is not necessarily indicative of hoop failures, which could lead to the full collapse of a plastic hinge (i.e. the formation of an "elephant foot").

For the assessment of other bridge columns and the design of new bridge columns, it is recommended that the procedures and charts outlined in Chapter 3 of this report be used to obtain more realistic performance assessments of hoop strains in flexural bridge column hinge regions. Furthermore, good seismic detailing practice should require that for new columns, splice locations in the hoop reinforcement be staggered around the column perimeter by at least $20d_b$ (hoop reinforcement bar diameters) to reduce the risk of failure propagation in case of a sub-standard hoop splice.

6 References

1. ANATECH, C., *ANACAP-U user's and theory manual*, Version 2.5, 1997.
2. Chai, Y.H., *Steel jacketing of circular reinforced concrete bridge columns for enhanced flexural performance*, University of California, San Diego, La Jolla, Ph.D. Dissertation, 1991.
3. Chai, Y.H., F. Seible, and M.J.N. Priestley, *Flexural retrofit of circular reinforced concrete bridge columns by steel jacketing*, University of California, San Diego, La Jolla, Structural Systems Research Project, 91/06, October, 1991.
4. Dowell, R.K., *ANDRIANNA User's Manual*, Version 1, 1999.
5. Gallagher, D., D. Innamorato, F. Seible, and M.J.N. Priestley, *Carbon fiber jacket repair test of circular flexural column with 5.0% continuous reinforcement*, University of California, San Diego, La Jolla, Test Report, 97/07, May, 1997.
6. Hibbitt, Karlson, and Sorenson, *ABAQUS user's and theory manual*, Version 5.8, 1999.
7. Hose, Y.D., F. Seible, and M.J.N. Priestley, *Strategic relocation of plastic hinges in bridge columns*, University of California, San Diego, La Jolla, Structural Systems Research Project, 97/05, September, 1997.
8. Mahan, M. and C. Pazzi, *Study of continuous and spliced rebar straight and hoop*, California Department of Transportation, Sacramento, Report to Weld Committee, Draft, May 9, 2000.
9. Mander, J.B., *Seismic design of bridge piers*, University of Canterbury, Christchurch, Ph.D. Dissertation, 1983.
10. Ohtaki, T., G.M. Benzoni, and M.J.N. Priestley, *Seismic performance of a full scale bridge column - as built and as repaired*, University of California, San Diego, La Jolla, Structural Systems Research Report, 96/07, November, 1996.
11. Orozco, G., K. Cox, S. Ashford, and F. Seible, *Near field large velocity pulse effects on reinforced concrete bridge columns*, University of California, San Diego, La Jolla, Structural Systems Research Project, 99/08, August, 1999.
12. Paulay, T. and M.J.N. Priestley, *Seismic design of reinforced concrete and masonry buildings*. 1 ed. 1992, New York: John Wiley & Sons, Inc. pp. 744.
13. Priestley, M.J.N., F. Seible, and G.M. Benzoni, *Seismic performance of circular columns with low longitudinal steel ratios*,' University of California, San Diego, La Jolla, Structural Systems Research Report, 94/08, June, 1994.
14. Priestley, M.J.N., F. Seible, and G.M. Calvi, *Seismic Design and Retrofit of Bridges*. First ed. 1996, New York: John Wiley & Sons, Inc. pp. 686.
15. Sánchez, A.V., F. Seible, and M.J.N. Priestley, *Seismic performance of flared bridge columns*, University of California, San Diego, La Jolla, Structural Systems Research Program, 97/06, August, 1997.

16. Seible, F., M.J.N. Priestley, C.T. Latham, and P. Silva, *Full-scale bridge column/superstructure connection tests under simulated longitudinal seismic loads*, University of California, San Diego, La Jolla, Structural Systems Research Program, 94/14, June, 1994.

17. Stone, W.C. and G.S. Cheok, *Inelastic behavior of full-scale bridge columns subjected to cyclic loading*, National Institute of Standards and Technology, US Department of Commerce, Gaithersburg, MD, Building Science Series, NIST BSS 166, January, 1989.

18. Sun, Z., F. Seible, and M.J.N. Priestley, *Flexural retrofit of rectangular reinforced concrete bridge columns by steel jacketing*, University of California, San Diego, La Jolla, Structural Systems Research Project, 93/01, February, 1993.

APPENDIX A

Transverse reinforcement strain values for each experimental column

A Transverse reinforcement strain values for each experimental column

Figure A.1 and Figure A.2 were presented in Chapter 2 to define the degree locations around the circumference of the columns in both the push and pull directions, and the test setups for flexural (single bending) and shear (double bending) columns. It should be noted that some shear tests are still tested in single bending.

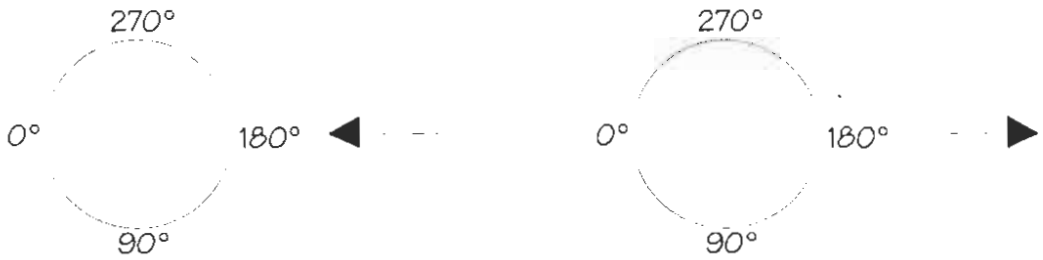

a) Push Loading **b) Pull Loading**

Figure A.1: Degree locations around the circumference of the columns

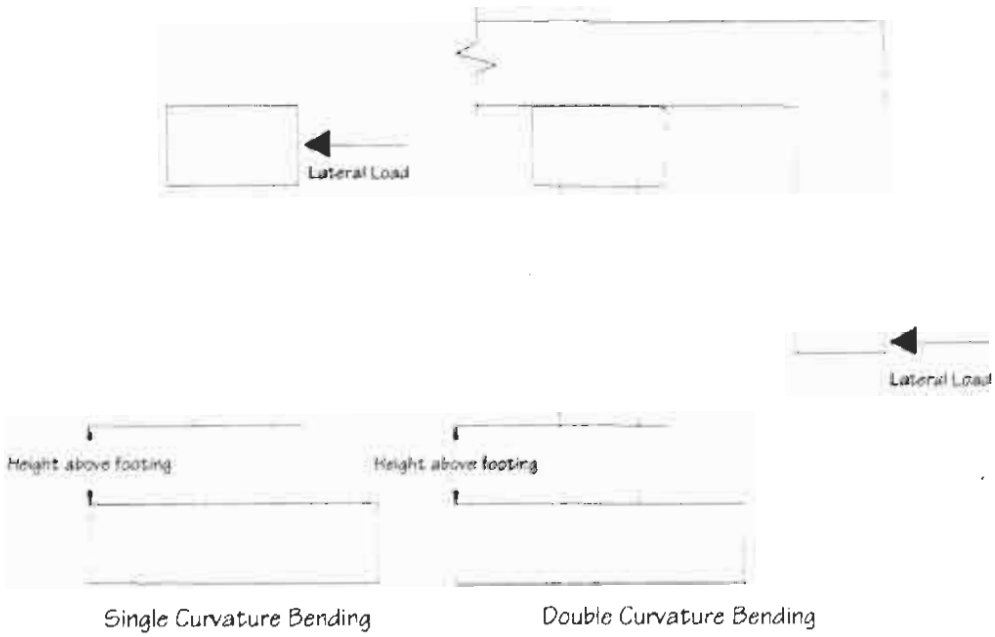

Figure A.2: Flexure and shear test setups

The test matrix, and important column and reinforcement parameters for each test unit are given in Table A.1, Table A.2, and Table A.3 in the following pages. Following these tables, the transverse reinforcement strain profiles for each experimental column are provided.

Table A.1: Test Matrix

Report #	Reference #	Test Unit	Scale	Cross section	Transverse Reinforcement
SSRP 97/05	[7]	TU1	40%	Circular	Spiral
		TU7	40%	Circular	Spiral
SSRP 97/06	[15]	RDS1	40%	Rectangular	Double spiral
		RDS6	40%	Rectangular*	Double spiral
SSRP 94/14	[16]	Col 1	Full	Circular	Spiral
		Col 2	Full	Circular	Spiral
SSRP 96/07	[10]	L1	Full	Circular	Hoops
		L1-R	Full	Circular	Hoops w/ fiberglass jacket
SSRP 93/01	[18]	R5	40%	Rectangular	Stirrups
		R6	40%	Rectangular**	Stirrups w/ steel jacket
SSRP 94/08	[13]	Col 1	40%	Circular	Hoops
		Col 2	40%	Circular	Hoops
SSRP 91/06	[3]	TU3	40%	Circular	Hoops
		TU4	40%	Circular	Hoops w/ steel jacket
SSRP 99/08	[11]	VP1	25%	Circular	Spiral
		VP2	25%	Circular	Spiral
TR 97/07	[5]	Carbon Jacket	40%	Circular	Hoops w/ carbon-fiber jacket
NIST	[17]	Flexure	Full	Circular	Spiral
		Shear	Full	Circular	Spiral

* Flared Column

** Elliptical steel jacket placed on column from base to 48 inches above base

Table A.2: Column Parameters

Report #	Test Unit	L' (ft)	D (in)	Cover (in)	f'_c Day of Testing (ksi)	P (kips)	$P/A_g f'_c$ (%)
SSRP 97/05	TU1	12	24	1	6	400	14.7
	TU7	5*	24	1	5.1	200	8.68
SSRP 97/06	RDS1	13	24x36	1	4.81	400	9.63
	RDS6	13	24x36	1	4.79	400	9.67
SSRP 94/14	Col 1	25	60	2	6.1	600	3.48
	Col 2	25	60	2	4.34	600	4.89
SSRP 96/07	L1	12	72	2.5	4.29	300	1.72
	L1-R	12	72	2.5	4.29	300	1.72
SSRP 93/01	R5	12	19.25x28.75	0.75	4.85	400	14.9
	R6	12	19.25x28.75**	0.75	5.25	400	13.8
SSRP 94/08	Col 1	7.5	24	0.8	4.35	113	5.7
	Col 2	7.5	24	0.8	4.37	113	5.7
SSRP 91/06	TU3	12	24	0.8	4.73	400	18.7
	TU4	12	24	0.8	5.52	400	16
SSRP 99/08	VP1	6	16	0.5	5	0	0
	VP2	6	16	0.5	4.38	0	0
TR-97/07	Carbon Jacket	12	24	0.5	6.07	400	14.57
NIST	Flexure	30	60	2	4.14	1000	8.54
	Shear	15	60	2	5.2	1000	6.8

* $L' = L_{eff}$: plastic hinge was relocated 2 ft up from column/footing interface. $L_{total} = 7$ ft

** Elliptical steel jacket was placed on column changing cross-section. See reference.

Table A.3: Reinforcement Parameters

Report #	Test Unit	ρ_l (%)	$d_{b,l}$ (in)	# bars	$f_{y,l}$ (ksi)	ρ_s (%)	d_{sp} (in)	s (in)	$f_{y,t}$ (ksi)
SSRP 97/05	TU1	2.66	0.875	20	66	0.87	0.375	2.25	Gr 60
	TU7	2.66	0.875	20	67	0.87	0.375	2.25	Gr 60
SSRP 97/06	RDS1	1.53	0.75	30	68.5	0.44	0.375	2	68.5
	RDS6	1.53	0.75	30	70.8	0.44	0.375	2	Gr 60
SSRP 94/14	Col 1	4.07	2.257	20	77.5	0.89	0.75	3.5	62.3
	Col 2	4.07	2.257	20	70	0.89	0.75	3.5	66.8
SSRP 96/07	L1	1.33	1.693	24	73.8	0.09	0.5	12	43.3
	L1-R	1.33	1.693	24	73.8	0.09	0.5	12	43.3
SSRP 93/01	R5	5.03	1*	14	47.7	0.17	0.25	5	51
			0.875*	28	40.6				
	R6	5.03	1*	14	47.7	0.17	0.25	5	51
			0.875*	28	40.6				
SSRP 94/08	Col 1	0.53	0.5	12	67	0.29	0.25	3	52.3
	Col 2	1.06	0.5	24	67	0.17	0.25	3	52.3
SSRP 91/06	TU3	2.53	0.75	26	45.7	0.174	0.25	5	51
	TU4	2.53	0.75	26	45.7	0.174	0.25	5	51
99/08	VP1	1.2	0.5	12	64.6	0.52	0.178	1.25	Gr 80
	VP2	1.2	0.5	12	64.6	0.52	0.178	1.25	Gr 80
TR-97/07	Carbon Jacket	5.1	1.128**	16	Gr 60	0.17***	0.25	5	50
			0.75**	16	70.5				
NIST	Flexure	2	1.693	25	68.9	0.633	0.625	3.5	71.5
	Shear	2	1.693	25	68.9	1.479	0.75	2.125	63.1

* Columns had 28 #7's around the perimeter of the column with two additional rows of 7 #8's directly outside the main longitudinal reinforcement cage on the 19.25"edges of the column

** Columns had bundled longitudinal bars: 14 #8 and then 14 #7 directly inside the #8's

*** Number shown for transverse reinforcement ratio does not include carbon jacket

97/05

STRAIN (all Ductility values in/in) * value likely higher at another location, but gage was lost

TU1

spiral			**Push**				**Pull**			
	Degrees		0	90	180	270	0	90	180	270
	Height above footing	(in)	7	7	0	20	7	0	0	20
	Ductility 1		0.00015	0.0001	0.0005	0	0.0003	0.0004	0.0002	0.0001
	Height (in)				7					
	Ductility 2		0.0004	0.0004	0.001	0.0001	0.0009	0.0029	0.0084	0.0004
	Height (in)				7					
	Ductility 3		0.0007	0.0008	0.0024	0.0004*	0.0015	0.001*	0.0046	0.0012*
	Height (in)			14				14		
	Ductility 4		0.0008	0.0009*	0.0025	0.0009*	0.0023	0.0008*	0.0043	0.0014*
	Height (in)			0				7		

STRAIN (all Ductility values in/in) * value likely higher at another location, but gage was lost

TU7

spiral			**Push**				**Pull**			
	Degrees		0	90	180	270	0	90	180	270
	Height above footing	(in)	32	28	28	28	32	28	28	28
	Ductility 1		0.001	0.0017	0.002	0.0017	0.0023	0.002	0.001	0.0022
	Height (in)		28		32					
	Ductility 2		0.006	0.0056	0.005	0.006	0.0108	0.0065	0.0027	0.0054
	Height (in)								24	
	Ductility 3		0.0098	0.005	0.0148	0.0093	0.0153	0.0052	0.007	0.008*
	Height (in)			20			28	40		46

97/06

STRAIN (all Ductility values in/in) * value likely higher at another location, but gage was lost

RDS1

spiral			Push				Pull			
	Degrees		60	120	240	300	60	120	240	300
	Height above footing	(in)	0	0	0	0	0	0	0	0
	Ductility 2		0.0003	0.00064	0.00042	0.00024	0.00045	0.0002	0.00016	0.00064
	Height (in)		12	48	48	12		48	48	24
	Ductility 4		0.00076	0.00092	0.00072	0.0008	0.00114	0.0003	0.00046	0.0018
	Height (in)		24	12	24	24	24	24	24	24
	Ductility 6		0.00035	0.00025	0.00025	0.0001	0.0006	0	0.0002	0.00025
	Height (in)									
	Ductility 8		0.0005	0.00025	0.00025	0.0001	0.0004	0	0	0.0003
	Height (in)									
	Ductility 12		0.00197	0.0007	0.0008	0.0008	0.00165	0.00235	0.0013	0.0016
	Height (in)									

STRAIN (all Ductility values in/in) * value likely higher at another location, but gage was lost

"-" = strain gage lost

RDS6

spiral			Push				Pull			
	Degrees		60	120	240	300	60	120	240	300
	Height above footing	(in)	72	72	0	12	0	12	12	0
	Ductility 1		0.00015	0.00017	0.00024	0.00034	0.00024	0.0002	0.0003	0.0003
	Height (in)		12	24						12
	Ductility 2		0.0004	0.0003	0.0004	0.0005	0.0003	0.00075	0.0007	0.00035
	Height (in)		12	0						
	Ductility 4		0.0008	0.0004	0.0009	0.0008	0.0006	-	1.4	0.0005
	Height (in)		12				12			
	Ductility 6		0.00015	0.0005	0.001	0.00035	0.0005	-	0.0006	0.0005
	Height (in)					24			24	
	Ductility 8		0.00025	0.0006	0.0007	0.00045	-	-	-	0.00045
	Height (in)					24				24
	Ductility 12		0.0003	0.0006	0.0007	0.0005	-	-	-	0.00075
	Height (in)				48	24				24

94/14

STRAIN

* value likely higher at another location, but gage was lost

"-" = lost strain gage

Col 1 spiral			Push				Pull			
Degrees			0	90	180	270	0	90	180	270
Height above footing		(in)	10	10	10	10	10	10	10	10
Drift = 4" Height (in)	Ductility 0.7		0.00065	0	0	0.00015	0.0001	0.00005	0.0006	0.00005
Drift = 6" Height (in)	Ductility 1.05		0.0009	0	0	0.0004	0.00017	0.0003	0.0009	0.0002
Drift = 9" Height (in)	Ductility 1.57		0.00135	0.0004	0.00025	0.0011	0.00035	0.0006	0.002	0.0005
Drift = 13.5 Height (in)	Ductility 2.36		0.0021	0.0008	-	0.0017	-	0.001	-	0.0008
Drift = 17" Height (in)	Ductility 3		-	-	-	0.00225	-	-	-	0.001

"-" = lost strain gage

STRAIN

Col 2 spiral			Push				Pull			
Degrees			0	90	180	270	0	90	180	270
Height above footing		(in)	10	10	10	10	10	10	10	10
Drift = 4" Height (in)	Ductility 1		0.0003	0.0002	0.00008	0.0004	0.0003	0.0002	0.0003	0
Drift = 6" Height (in)	Ductility 1.5		0.0007	0.0005	0.0004	0.00058	0.0006	0.0004	0.0001	0.0004
Drift = 9" Height (in)	Ductility 2.25		0.002	0.0007	0	0.0007	0.0013	0.0007	0.0006	0.0004
Drift = 13.5 Height (in)	Ductility 3.38		0.00335	0.001	0.0005	0.0008	0.0023	0.00039	0.00085	0.0005
Drift = 17" Height (in)	Ductility 4.25		0.0046	0.001	0.0006	0.001	0.00285	0.00041	0.0006	0.0006

96/07 **STRAIN** (all Ductility values in/in) ** data acquisition limit strain at 0.02 in/in

L1 hoops								
			Push					
	Degrees		45	90	135	225	270	315
	Height above footing	(in)	48	60, 72	48, 60, 72	48, 60, 84, 96	96	36
	Ductility 1		0.02**	0.02	0.02	0.02	0.02	0.02**
			Pull					
	Degrees		45	90	135	225	270	315
	Height above footing	(in)	48	60, 72	48, 60, 72	48, 60	96	36
	Ductility 1		0.02**	0.02	0.02	0.02	0.02	0.02**

96/07 **STRAIN** (all Ductility values in/in) ** data acquisition limit strain at 0.02 in/in

L1-R fiberglass jacket								
	Push							
	Degrees		45	90	135	225	270	315
	Height above footing	(in)	37	37	53	37	53	53
	Ductility 1		0.0013	0.0015	0.001	0.0015	0.0018	0.0009
	Height (in)			53				
	Ductility 2		0.0025	0.0023	0.0014	0.0023	0.0026	0.0014
	Height (in)							
	Ductility 3		0.003	0.0029	0.002	0.0025	0.0028	0.0015
	Height (in)							
	Ductility 4		0.0031	0.0032	0.0028	0.0029	0.0035	0.0023
	Height (in)			53	22	22		22
	Ductility 6		0.0047	0.0041	0.0042	0.0039	0.0047	0.0037
	Height (in)					22		
	Pull							
	Degrees		45	90	135	225	270	315
	Height above footing	(in)	53	37	22	22	37	37
	Ductility 1		0.0008	0.001	0.0009	0.0008	0.0014	0.0011
	Height (in)					105	76	76
	Ductility 2		0.0012	0.002	0.0015	0.0015	0.0019	0.002
	Height (in)					105		
	Ductility 3		0.0017	0.0027	0.0024	0.0013	0.0026	0.0028
	Height (in)							22
	Ductility 4		0.0023	0.0038	0.0028	0.0018	0.0035	0.0029
	Height (in)							
	Ductility 6		0.0053	0.0051	0.0042	0.0025	0.0045	0.0042
	Height (in)		37		37			

93/01

STRAIN (all Ductility values in/in)

* value likely higher at another location, but gage was lost

"-" = strain gage lost

R5 stirrup			Push				Pull			
	Degrees		0	90	180	270	0	90	180	270
	Height above footing	(in)	7	12	12	7	7	32	12	12
	Ductility 1		0.00056	0.0003	0.00016	0.00036	0.00028	0.00109	0.00064	0.0005
	Height (in)		12							
	Ductility 2		0.00102	0.0008	0.00035	0.0013	0.0012	0.00197	0.0011	0.00117
	Height (in)			7						
	Ductility 3		-	0.0028*	-	0.0026	0.0018	0.00275	0.00165	0.00255
	Height (in)			12			12			7

STRAIN (all Ductility values in/in)

* value likely higher at another location, but gage was lost

"-" = strain gage lost

R6 steel jacket			Push				Pull			
	Degrees		0	90	180	270	0	90	180	270
	Height above footing	(in)	2.5	2.5	2.5	8	2.5	48	2.5	2.5
	Ductility 1		0.0002	0.00018	0.0002	0.00015	0.00015	0.0003	0.00035	0.00015
	Height (in)			48	18					8
	Ductility 2		0.0004	0.00025	0.0002	0.00021	0.00025	0.0004	0.00055	0.0002
	Height (in)			48	18					8
	Ductility 3		0.0006	0.00032	0.0003	0.00037	0.0006	0.00045	0.00087	0.00035
	Height (in)									
	Ductility 4		0.0009	0.00046	0.0004	0.0006	0.0006	0.00048	0.00125	0.00054
	Height (in)							2.5		
	Ductility 6		0.0016	0.00068	0.0008	0.00089	0.001	0.00085	0.0023	0.00097
	Height (in)					2.5		2.5		
	Ductility 8		0.0025	-	0.001	-	-	-	-	-
	Height (in)									

94/08 STRAIN (all Ductility values in/in) * value likely higher at another location, but gage was lost

Col 1

hoops			Push				Pull			
	Degrees		0	90	180	270	0	90	180	270
	Height above footing	(in)	60	60	60	72	12	12	0	72
	Ductility 1		0	0.00054	0.00027	0.00037	0.00019	-	0.00032	0.00015
	Height (in)				0					
	Ductility 2		0.0006	0.00088	0.00045	0.00062	0.0003	0.0004	0.00042	0.00039
	Height (in)		72		0			0		
	Ductility 3		0.0009	0.0011	0.00051	0.00105	0.00056	0.0015	0.0005	0.00042
	Height (in)							60		
	Ductility 4		0.00125	0.00204	0.00072	0.0015	0.00092	0.00061	0.00059	0.00058
	Height (in)							60		
	Ductility 6		0.0019	0.00273	0.00117	0.0019	0.00143	0.0005	0.00016*	0.00112
	Height (in)		72		12				60	
	Ductility 8		0.00245	0.00265	0.00112	0.0025	0.00172	0.00065	0.00036*	0.0019
	Height (in)		12						60	
	Ductility 10		0.00165*	0.00255	0.00095	0.0037	0.00102*	0.00205	0.00075	-
	Height (in)		24				24	12	72	

94/08 STRAIN (all Ductility values in/in) * value likely higher at another location, but gage was lost

Col 2

hoops			Push				Pull			
	Degrees		0	90	180	270	0	90	180	270
	Height above footing	(in)	20	15	60	70	20	25	15	60
	Ductility 1		0	0.00025	0.0034	0.00046	0	0.0006	0	0.00015
	Height (in)							0		24
	Ductility 2		0.01	0.00073	0.00845	0.00072	0.0105	0.00118	0.0066	0.00062
	Height (in)								60	
	Ductility 3		0.012	0.00109	0.008	0.0012	0.0124	0.00162	0.0082	0.00089
	Height (in)			45						
	Ductility 4		0.0116	0.00131	0.0115	0.0017	0.0105	0.00233	0.0127	0.0016
	Height (in)			70				70		0

91/06

STRAIN (all Ductility values in/in) * value likely higher at another location, but gage was lc

TU3

hoops			Push				Pull			
	Degrees		0	90	180	270	0	90	180	270
	Height above footing	(in)	18	2	2	2	8	2	18	2
	Ductility 1		-0.0001	0.00068	-0.00013	0.00018	-0.00009	0.00012	-0.00012	0.00053
	Height (in)		2	18		28		28		18
	Ductility 2		0.00034	0.00126	0.0002	0.00042	0.00008	0.0005	0.00009	0.00125
	Height (in)								2	
	Ductility 3		0.00063	0.00202	0.00032	0.00051	0.0005	0.00128	0.0002	0.00139
	Height (in)				12				12	
	Ductility 4		0.00112	0.00288	0.00108	0.00051	0.0006	0.002	-0.00043	0.00156
	Height (in)				18			12		

STRAIN (all Ductility values in/in) * value likely higher at another location, but gage was lc

NA = test not performed at this location

TU4

hoops			Push				Pull			
	Degrees		0	90	180	270	0	90	180	270
	Height above footing	(in)	2	7	68	2	2	7	7	2
	Ductility 1		-0.00009	0.0005	0.00007	0.0002	0.00008	0.00034	-0.00006	0.00057
	Height (in)		28				48		58	
	Ductility 2		0.00033	0.00082	0.00024	0.00089	0.00041	0.00065	0.00026	0.00134
	Height (in)									
	Ductility 3		0.00039	0.00155	0.00041	0.00073	0.00073	0.00105	0.00023	0.0009
	Height (in)			2						8
	Ductility 4		0.00031	0.00013	0.0002	0.00076	0.00031	0.0019	-0.00006	0.00115
	Height (in)		7		7		7		28	8
	Ductility 6		0.00085	NA	-0.00025	NA	0.00073	NA	-0.00007	NA
	Height (in)		7		7		7		28	

91/06

STRAIN (all Ductility values in/in)

* value likely higher at another location, but gage lost
NA = test not performed at this location

TU4 steel jacket			Push				Pull			
	Degrees		0	90	180	270	0	90	180	270
	Height above footing	(in)	2	NA	2	NA	2	NA	2	NA
	Ductility 1		0.00026	NA	0.00023	NA	0.00027	NA	0.0002	NA
	Height (in)									
	Ductility 2		0.00038	NA	0.00044	NA	0.00046	NA	0.00029	NA
	Height (in)									
	Ductility 3		0.00049	NA	0.00063	NA	0.0007	NA	0.00048	NA
	Height (in)									
	Ductility 4		0.00062	NA	0.00082	NA	0.00088	NA	0.00054	NA
	Height (in)									
	Ductility 6		0.00069	NA	0.00095	NA	0.00109	NA	0.00062	NA
	Height (in)									

99/08 **STRAIN** (all Ductility values in/in) "-" = strain gage lost

VP1 spiral			Push				Pull			
	Degrees		0	90	180	270	0	90	180	270
	Height above footing	(in)	-3	-3	-3	-3	-3	-3	-3	-3
	Pulse		-0.0005	0.0003	0.0003	-0.0004	-0.00099	0.0004	-0.0002	-0.0002
	Height (in)									
	Ductility 0.5		0.00018	0.00028	-0.0002	0.00027	-0.00003	0.0002	-0.0005	0.0001
	Height (in)									
	Ductility 1		0.0003	0.000306	-0.00062	0.00021	-0.00028	0.00012	-0.0006	-0.00005
	Height (in)									
	Ductility 1.5		0.00047	0.00027	-0.00073	0.00016	-0.00033	0.000395	-0.0007	-0.00005
	Height (in)									
	Ductility 2		0.00081	0.000214	-0.0012	0.0002	-0.00057	0.00035	-0.00125	-0.0006
	Height (in)									
	Ductility 3		0.0006	0.0001	-0.002	0.0003	-0.0006	0.00016	-0.0018	-0.00004
	Height (in)									
	Ductility 4		0.0028	0.00008	-0.0045	0.0004	-0.00045	0.00006	-0.0035	-0.0001
	Height (in)									
	Ductility 5		0.0024	-0.005	-0.0075	-0.0002	0.003	-0.001	-0.006	-0.0002
	Height (in)									
	Ductility 6		-	0.001	-0.009	-0.0003	-	-0.001	-0.0075	-0.0003
	Height (in)									

99/08 **STRAIN** (all Ductility values in/in) "-" = strain gage lost

VP2 spiral			Push				Pull			
	Degrees		0	90	180	270	0	90	180	270
	Height above footing	(in)	0	0	0	0	0	0	0	0
	Pulse		0.003	0.00075	0.0022	0.00072	0.0002	-0.00045	0.0018	0.00067
	Height (in)									
	Ductility 0.5		0.0004	0.0002	0.00175	0.0011	0.0002	-0.00035	0.00175	0.00077
	Height (in)									
	Ductility 1		0.0004	0.0003	0.0018	0.0011	0.0001	-0.00028	0.0013	0.00022
	Height (in)									
	Ductility 1.5		0.0005	0.00036	0.00175	0.00114	-0.0001	-0.0003	0.00132	0.00023
	Height (in)									
	Ductility 2		-0.0006	0.0004	0.00185	0.00114	-0.00075	-0.00026	0.0013	0.00021
	Height (in)									
	Ductility 3		-0.0007	0.0005	0.00188	0.00115	-0.00085	-0.00028	0.0012	0.000256
	Height (in)									
	Ductility 4		-0.0008	0.0006	0.0019	0.00128	-0.0008	-0.00028	0.001	0.00041
	Height (in)									
	Ductility 5		-0.00085	0.0008	0.002	0.0016	-0.0013	-0.0002	0.001	0.00076
	Height (in)									
	Ductility 6		-0.0012	0.00083	0.0022	0.0022	-0.00135	0.00038	-0.006	0.0013
	Height (in)									
	Ductility 7		-0.0018	-	0.0005	-0.0049	-0.0022	-	0.0005	-0.0016
	Height (in)									

TR-97/07 STRAIN (all Ductility values in/in)

carbon fiber jacket

		Push				Pull			
Degrees		0	90	180	270	0	90	180	270
Height above footing	(in)	9	39	39	39	39	39	39	39
Ductility 1		0.00048	0.00032	0.00038	0.00051	0.00053	0.00061	0.00053	0.00038
Height (in)		39							
Ductility 2		0.00072	0.00091	0.0007	0.00342	0.0007	0.00118	0.00079	0.00466
Height (in)				15	15			21	15
Ductility 3		0.00126	0.0023	0.00126	0.00117*	0.00063	0.00239	0.00112	0.001*
Height (in)			15	15		21	15	21	
Ductility 4		0.00156	0.00146*	0.00137	0.00141*	0.0009	0.00132*	0.00167	0.00118*
Height (in)			57	15		21			
Ductility 6		0.00226	0.00158*	0.0016	0.00205*	0.00131	0.002*	0.00283	0.00171*
Height (in)		6	75						57
Ductility 8		0.00298	0.00192*	0.00173	0.0022*	0.0016	0.00224*	0.00299	0.00199*
Height (in)		6	75						57

* value likely higher at another location, but gage was lost:
15 " above base is plastic hinge region, but data beyond ductility 3 was unreliable due to jacket splitting

TR-97/07 STRAIN (all Ductility values in/in)

hoops

		Push				Pull			
Degrees		0	90	180	270	0	90	180	270
Height above footing	(in)	6	15	39	15	39	15	39	15
Ductility 1		0.00022	0.00001	0.00039	0.00001	0.00058	0.00003	0.00049	0.00005
Height (in)									
Ductility 2		0.00071	0.00061	0.00071	0.0034	0.00063	0.00043	0.00081	0.00468
Height (in)				15					
Ductility 3		0.00123	0.0023	0.000105	NA	0.00058	0.00024	0.0011	NA
Height (in)				15					
Ductility 4		0.0015	-	0.001*	-	0.00063	-	0.00166*	-
Height (in)				21					
Ductility 6		0.00223	-	0.0016*	-	0.00137	-	0.0028*	-
Height (in)									
Ductility 8		0.00297	-	0.00174*	-	0.00162	-	0.00293*	-
Height (in)									

* value likely higher at another location, but gage was lost:
15 " above base is plastic hinge region, but data beyond ductility 3 was unreliable due to jacket splitting
NA = strain value exceeded gage limit of 0.006 in/in

NIST

STRAIN (all Ductility values in/in)

* value likely higher at another location, but gage lost

"-" = strain gage lost

Flexure

spiral

		Push		Pull	
Degrees		90	270	90	270
Height above footing	(in)	56	7	56	7
Ductility 1		0.00021	0.00027	0.00022	0.00213
Height (in)		0		0	
Ductility 2		0.00109	0.00289	0.00097	0.00298
Height (in)		0			
Ductility 3		0.00184	0.00342	0.00223	0.00369
Height (in)			56		
Ductility 4		0.00333	0.00662	0.00385	0.00609
Height (in)			56		56
Ductility 5		0.00392	-	0.00472	-
Height (in)					
Ductility 6		-	0.01	-	0.00876
Height (in)			28		28

NIST

STRAIN (all Ductility values in/in)

* value likely higher at another location, but gage lost

"-" = strain gage lost

Shear

spiral

		Push		Pull	
Degrees		90	270	90	270
Height above footing	(in)	9	7	28	7
Ductility 1		0.00014	0.00018	0.00014	0.00014
Height (in)		27			
Ductility 2		0.0008	0.00074	0.00046	0.0005
Height (in)		13		5	28
Ductility 3		-	-	-	-
Height (in)					
Ductility 4		0.00503	0.00175	0.00086	0.00105
Height (in)				18	
Ductility 6		-	0.00253	-	0.00183
Height (in)					
Ductility 8		-	0.00518	-	-
Height (in)			-2		
Ductility 10		0.00503	-	0.00223	-
Height (in)					

APPENDIX B

Strain and displacement ductility comparisons at different degree locations

B Strain and displacement ductility comparisons at different degree locations

Figure B.1 and Figure B.2, presented in Chapter 2 and Appendix A, are repeated again to define the degree locations around the circumference of the columns in both the push and pull directions, and to show the test setups for flexural (single bending) and shear (double bending) columns.

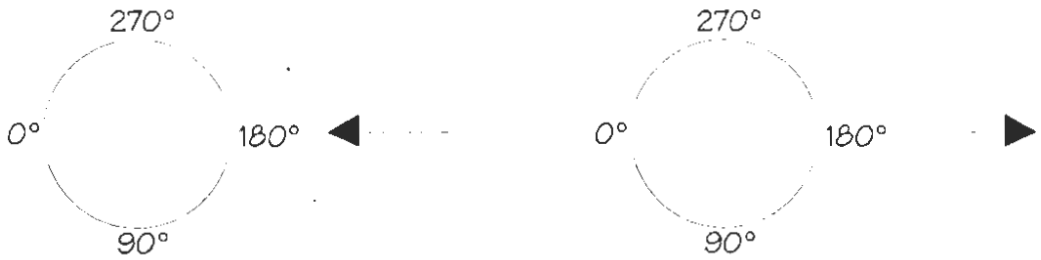

a) Push Loading **b) Pull Loading**

Figure B.1: Degree locations around the circumference of the columns

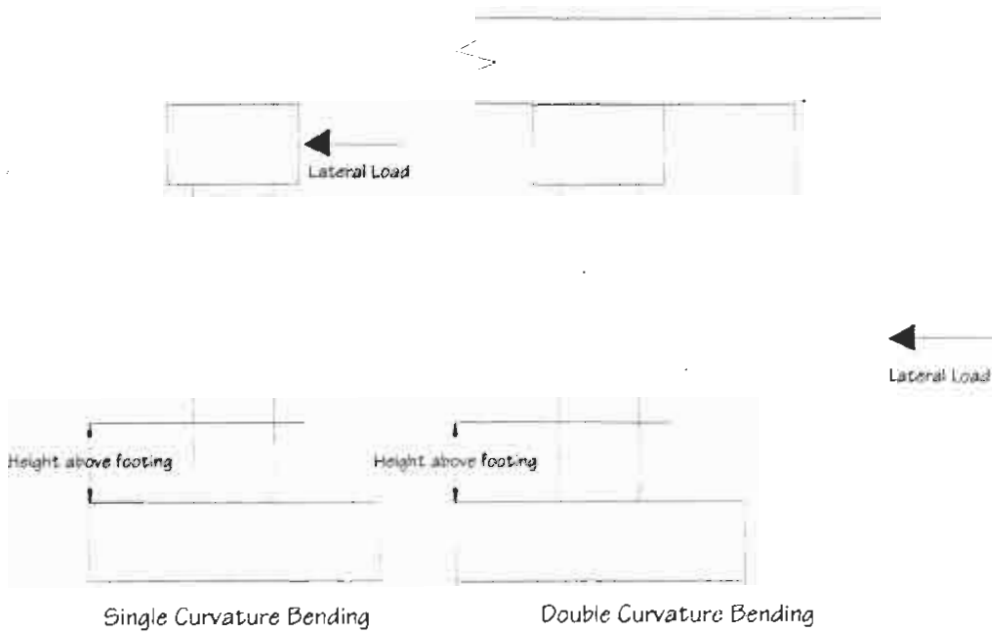

Figure B.2: Flexure and shear test setups

The test matrix, and important column and reinforcement parameters for each test unit are also repeated in Table B.1, Table B.2, and Table B.3 in the following pages. Following these tables, the strain and displacement ductility comparisons at different degree locations are provided.

Table B.1: Test Matrix

Report #	Reference #	Test Unit	Scale	Cross section	Transverse Reinforcement
SSRP 97/05	[7]	TU1	40%	Circular	Spiral
		TU7	40%	Circular	Spiral
SSRP 97/06	[15]	RDS1	40%	Rectangular	Double spiral
		RDS6	40%	Rectangular*	Double spiral
SSRP 94/14	[16]	Col 1	Full	Circular	Spiral
		Col 2	Full	Circular	Spiral
SSRP 96/07	[10]	L1	Full	Circular	Hoops
		L1-R	Full	Circular	Hoops w/ fiberglass jacket
SSRP 93/01	[18]	R5	40%	Rectangular	Stirrups
		R6	40%	Rectangular**	Stirrups w/ steel jacket
SSRP 94/08	[13]	Col 1	40%	Circular	Hoops
		Col 2	40%	Circular	Hoops
SSRP 91/06	[3]	TU3	40%	Circular	Hoops
		TU4	40%	Circular	Hoops w/ steel jacket
SSRP 99/08	[11]	VP1	25%	Circular	Spiral
		VP2	25%	Circular	Spiral
TR 97/07	[5]	Carbon Jacket	40%	Circular	Hoops w/ carbon-fiber jacket
NIST	[17]	Flexure	Full	Circular	Spiral
		Shear	Full	Circular	Spiral

* Flared Column

** Elliptical steel jacket placed on column from base to 48 inches above base

Table B.2: Column Parameters

Report #	Test Unit	L' (ft)	D (in)	Cover (in)	f'_c Day of Testing (ksi)	P (kips)	$P/A_g f'_c$ (%)
SSRP 97/05	TU1	12	24	1	6	400	14.7
	TU7	5*	24	1	5.1	200	8.68
SSRP 97/06	RDS1	13	24x36	1	4.81	400	9.63
	RDS6	13	24x36	1	4.79	400	9.67
SSRP 94/14	Col 1	25	60	2	6.1	600	3.48
	Col 2	25	60	2	4.34	600	4.89
SSRP 96/07	L1	12	72	2.5	4.29	300	1.72
	L1-R	12	72	2.5	4.29	300	1.72
SSRP 93/01	R5	12	19.25x28.75	0.75	4.85	400	14.9
	R6	12	19.25x28.75**	0.75	5.25	400	13.8
SSRP 94/08	Col 1	7.5	24	0.8	4.35	113	5.7
	Col 2	7.5	24	0.8	4.37	113	5.7
SSRP 91/06	TU3	12	24	0.8	4.73	400	18.7
	TU4	12	24	0.8	5.52	400	16
SSRP 99/08	VP1	6	16	0.5	5	0	0
	VP2	6	16	0.5	4.38	0	0
TR-97/07	Carbon Jacket	12	24	0.5	6.07	400	14.57
NIST	Flexure	30	60	2	4.14	1000	8.54
	Shear	15	60	2	5.2	1000	6.8

* L' = L_{eff}: plastic hinge was relocated 2 ft up from column/footing interface. L_{total} = 7 ft

** Elliptical steel jacket was placed on column changing cross-section. See reference.

Table B.3: Reinforcement Parameters

Report #	Test Unit	ρ_l (%)	$d_{b,l}$ (in)	# bars	$f_{y,l}$ (ksi)	ρ_t (%)	d_{sp} (in)	s (in)	$f_{y,t}$ (ksi)
SSRP 97/05	TU1	2.66	0.875	20	66	0.87	0.375	2.25	Gr 60
	TU7	2.66	0.875	20	67	0.87	0.375	2.25	Gr 60
SSRP 97/06	RDS1	1.53	0.75	30	68.5	0.44	0.375	2	68.5
	RDS6	1.53	0.75	30	70.8	0.44	0.375	2	Gr 60
SSRP 94/14	Col 1	4.07	2.257	20	77.5	0.89	0.75	3.5	62.3
	Col 2	4.07	2.257	20	70	0.89	0.75	3.5	66.8
SSRP 96/07	L1	1.33	1.693	24	73.8	0.09	0.5	12	43.3
	L1-R	1.33	1.693	24	73.8	0.09	0.5	12	43.3
SSRP 93/01	R5	5.03	1*	14	47.7	0.17	0.25	5	51
			0.875*	28	40.6				
	R6	5.03	1*	14	47.7	0.17	0.25	5	51
			0.875*	28	40.6				
SSRP 94/08	Col 1	0.53	0.5	12	67	0.29	0.25	3	52.3
	Col 2	1.06	0.5	24	67	0.17	0.25	3	52.3
SSRP 91/06	TU3	2.53	0.75	26	45.7	0.174	0.25	5	51
	TU4	2.53	0.75	26	45.7	0.174	0.25	5	51
99/08	VP1	1.2	0.5	12	64.6	0.52	0.178	1.25	Gr 80
	VP2	1.2	0.5	12	64.6	0.52	0.178	1.25	Gr 80
TR-97/07	Carbon Jacket	5.1	1.128**	16	Gr 60	0.17***	0.25	5	50
			0.75**	16	70.5				
NIST	Flexure	2	1.693	25	68.9	0.633	0.625	3.5	71.5
	Shear	2	1.693	25	68.9	1.479	0.75	2.125	63.1

* Columns had 28 #7's around the perimeter of the column with two additional rows of 7 #8's directly outside the main longitudinal reinforcement cage on the 19.25"edges of the column

** Columns had bundled longitudinal bars: 14 #8 and then 14 #7 directly inside the #8's

*** Number shown for transverse reinforcement ratio does not include carbon jacket

ZERO DEGREE LOCATION

(all ductility values reported as in/in)

PUSH

Height above footing (in)	**97/05 TU1** spiral	**97/05 TU7** spiral	**94/14** Col 1** spiral	**94/14** Col 2** spiral	**93/01 R5** stirrup	**93/01 R6** steel jacke	**94/08 Col 1** hoops	**94/08 Col 2** hoops	**91/06 TU3** hoops	**91/06 TU4** hoops	**91/06 TU4** steel jacket	**99/08 VP1**	**99/08 VP2**	**TR 97/07** carbon jacket	**TR 97/07** hoops
	7	32	10	10	7	2.5	60	20	18	2	2	-3	0	9	6
Ductility 1	0.00015	0.001	0.0008	0.0003	0.00056	0.0002	0	0	-0.0001	-9E-05	0.00026	0.0003	0.0004	0.00048	0.00022
Height (in)		28			12				2	28				39	
Ductility 2	0.0004	0.006	0.0018	0.0016	0.00102	0.0004	0.0006	0.01	0.00034	0.00033	0.00038	0.00081	-0.0006	0.00072	0.00071
Height (in)							72								
Ductility 3	0.0007	0.0098	-	0.0029	-	0.0006	0.0009	0.012	0.00063	0.00039	0.00049	0.0006	-0.0007	0.00126	0.00123
Height (in)															
Ductility 4	0.0008	-	-	0.0043	-	0.0009	0.00125	0.0116	0.00112	0.00031	0.00062	0.0028	-0.0008	0.00156	0.0015
Height (in)										7					
Ductility 6	-	-	-	-	-	0.0016	0.0019	-	-	0.00085	0.00069	-	-0.0012	0.00226	0.00223
Height (in)							72			7				6	
Ductility 8	-	-	-	-	-	0.0025	0.00245	-	-	-	-	-	-	0.00298	0.00297
Height (in)							12							6	
Ductility 10	-	-	-	-	-	-	0.00165*	-	-	-	-	-	-	-	-
Height (in)							24								

* value likely higher at another location, but gage was lost

** 94/14 strains were interpolated from graphs because the original strains were recorded in drift, not ductility

"-" = strain information not available

ZERO DEGREE LOCATION

(all ductility values reported as in/in)

PULL

Height above	**97/05 TU1** spiral	**97/05 TU7** spiral	**94/14** Col 1** spiral	**94/14** Col 2** spiral	**93/01 R5** stirrup	**93/01 R6** steel jacke	**94/08 Col 1** hoops	**94/08 Col 2** hoops	**91/06 TU3** hoops	**91/06 TU4** hoops	**91/06 TU4** steel jacket	**99/08 VP1**	**99/08 VP2**	**TR 97/07** carbon jacket	**TR 97/07** hoops
footing (in)	7	32	10	10	7	2.5	12	20	8	2	2	-3	0	39	39
Ductility 1	0.0003	0.0023	0.00015	0.0003	0.00028	0.00015	0.00019	0	-9E-05	0.00008	0.00027	-0.0003	0.0001	0.00053	0.00058
Height (in)										48					
Ductility 2	0.0009	0.0108	-	0.0011	0.0012	0.00025	0.0003	0.0105	0.00008	0.00041	0.00046	-0.0006	-0.0008	0.0007	0.00063
Height (in)															
Ductility 3	0.0015	0.0153	-	0.002	0.0018	0.0006	0.00056	0.0124	0.0005	0.00073	0.0007	-0.0006	-0.0009	0.00063	0.00058
Height (in)		28			12									21	
Ductility 4	0.0023	-	-	0.0027	-	0.0006	0.00092	0.0105	0.0006	0.00031	0.00088	-0.0005	-0.0008	0.0009	0.00063
Height (in)										7				21	
Ductility 6	-	-	-	-	-	0.001	0.00143	-	-	0.00073	0.00109	-	-0.0014	0.00131	0.00137
Height (in)										7					
Ductility 8	-	-	-	-	-	-	0.00172	-	-	-	-	-	-	0.0016	0.00162
Height (in)															
Ductility 10	-	-	-	-	-	-	0.00102*	-	-	-	-	-	-	-	-
Height (in)							24								

* value likely higher at another location, but gage was lost

** 94/14 strains were interpolated from graphs because the original strains were recorded in drift, not ductility

"-" = strain information not available

90 DEGREE LOCATION

(all ductility values reported as in/in)

PUSH

Height above	97/05 TU1 spiral	97/05 TU7 spiral	94/14** Col 1 spiral	94/14** Col 2 spiral	96/07 L1 hoops	96/07 L1-R fg jacket	93/01 R5 stirrup	93/01 R6 steel jacke	94/08 Col 1 hoops	94/08 Col 2 hoops	91/06 TU3 hoops	91/06 TU4 hoops	91/06 TU4 steel jacket	99/08 VP1	99/08 VP2	TR 97/07 carbon jacket	TR 97/07 hoops	NIST Flexure spiral	NIST Shear spiral
footing (in)	7	28	10	10	60, 72	37	12	2.5	60	15	2	7	-	-3	0	39	15	56	9
Ductility 1	0.0001	0.0017	0	0.0002	0.02	0.0015	0.0003	0.00018	0.00054	0.00025	0.00068	0.0005	-	0.00031	0.0003	0.00032	0.00001	0.00021	0.00014
Height (in)						53		48			18							0	27
Ductility 2	0.0004	0.0056	0.00062	0.00063	-	0.0023	0.0008	0.00025	0.00088	0.00073	0.00126	0.00082	-	0.00021	0.0004	0.00091	0.00061	0.00109	0.0008
Height (in)							7	48										0	13
Ductility 3	0.0008	0.005	-	0.0009	-	0.0029	0.0028*	0.00032	0.0011	0.00109	0.00202	0.00155	-	0.0001	0.0005	0.0023	0.0023	0.00184	-
Height (in)	14	20					12			45		2				15			
Ductility 4	0.0009*	-	-	0.001	-	0.0032	-	0.00046	0.00204	0.00131	0.00288	0.00013	-	0.00008	0.0006	0.00146*	-	0.00333	0.00503
Height (in)	0					53				70						57			
Ductility 6	-	-	-	-	-	0.0041	-	0.00068	0.00273	-	-	-	-	0.001	0.00083	0.00158*	-	-	-
Height (in)																75			
Ductility 8	-	-	-	-	-	-	-	-	0.00265	-	-	-	-	-	-	0.00192*	-	-	-
Height (in)																75			
Ductility 10	-	-	-	-	-	-	-	-	0.00255	-	-	-	-	-	-	-	-	-	0.00503
Height (in)																			

* value likely higher at another location, but gage was lost

** 94/14 strains were interpolated from graphs because the original strains were recorded in drift, not ductility

"-" = strain information not available

"fg" = fiberglass

90 DEGREE LOCATION

(all ductility values reported as in/in)

PULL

Height above footing (in)	97/05 TU1 spiral 0	97/05 TU7 spiral 28	94/14** Col 1 spiral 10	94/14** Col 2 spiral 10	96/07 L1 hoops 60, 72	96/07 L1-R fg jacket 37	93/01 R5 stirrup 32	93/01 R6 steel jacke 48	94/08 Col 1 hoops 12	94/08 Col 2 hoops 25	91/06 TU3 hoops 2	91/06 TU4 hoops 7	91/06 TU4 steel jacket -	99/08 VP1 -3	99/08 VP2 0	TR 97/07 carbon jacket 39	TR 97/07 hoops 15	NIST Flexure spiral 56	NIST .Shear spiral 27
Ductility 1	0.0004	0.002	0.00027	0.0002	0.02	0.001	0.00109	0.0003	-	0.0006	0.00012	0.00034	-	0.00012	-0.0003	0.00061	0.00003	0.00022	0.00014
Height (in)										0	28							0	
Ductility 2	0.0029	0.0065	0.00082	0.0006	-	0.002	0.00197	0.0004	0.0004	0.00118	0.0005	0.00065	-	0.00035	-0.0003	0.00118	0.00043	0.00097	0.00046
Height (in)									0										5
Ductility 3	0.001*	0.0052	-	0.00052	-	0.0027	0.00275	0.00045	0.0015	0.00162	0.00128	0.00105	-	0.00016	-0.0003	0.00239	0.00024	0.00223	-
Height (in)	14	40							60							15			
Ductility 4	0.0008*	-	-	0.00042	-	0.0038	-	0.00048	0.00061	0.00233	0.002	0.0019	-	0.00006	-0.0003	0.00132*	-	0.00385	0.00086
Height (in)	7							2.5	60	70	12								18
Ductility 6	-	-	-	-	-	0.0051	-	0.00085	0.0005	-	-	-	-	-0.001	0.00038	0.002*	-	-	-
Height (in)								2.5											
Ductility 8	-	-	-	-	-	-	-	-	0.00065	-	-	-	-	-	-	0.00224*	-	-	-
Height (in)																			
Ductility 10	-	-	-	-	-	-	-	-	0.00205	-	-	-	-	-	-	-	-	-	0.00223
Height (in)									12										

* value likely higher at another location, but gage was lost

** 94/14 strains were interpolated from graphs because the original strains were recorded in drift, not ductility

"-" = strain information not available

"fg" = fiberglass

180 DEGREE LOCATION

(all ductility values reported as in/in)

PUSH

Height above footing (in)	97/05 TU1 spiral	97/05 TU7 spiral	94/14** Col 1 spiral	94/14** Col 2 spiral	93/01 R5 stirrup	93/01 R6 steel jacke	94/08 Col 1 hoops	94/08 Col 2 hoops	91/06 TU3 hoops	91/06 TU4 hoops	91/06 TU4 steel jacket	99/08 VP1	99/08 VP2	TR 97/07 carbon jacket	TR 97/07 hoops
	0	28	10	10	12	2.5	60	60	2	68	2	-3	0	39	39
Ductility 1	0.0005	0.002	0	0.0008	0.00016	0.0002	0.00027	0.0034	-0.0001	0.00007	0.00023	-0.0006	0.0018	0.00038	0.00039
Height (in)	7	32				18	0								
Ductility 2	0.001	0.005	-	0.00013	0.00035	0.0002	0.00045	0.00845	0.0002	0.00024	0.00044	-0.0012	0.00185	0.0007	0.00071
Height (in)	7					18	0							15	15
Ductility 3	0.0024	0.0148	-	0.00032	-	0.0003	0.00051	0.0115	0.00032	0.00041	0.00063	-0.002	0.00188	0.00126	0.00011
Height (in)									12					15	15
Ductility 4	0.0025	-	-	0.00057	-	0.0004	0.00072	0.008	0.00108	0.0002	0.00082	-0.0045	0.0019	0.00137	0.001*
Height (in)									18	7				15	21
Ductility 6	-	-	-	-	-	0.0008	0.00117	-	-	-0.0003	0.00095	-0.009	0.0022	0.0016	0.0016*
Height (in)							12			7					
Ductility 8	-	-	-	-	-	0.001	0.00112	-	-	-	-	-	-	0.00173	0.00174*
Height (in)															
Ductility 10	-	-	-	-	-	-	0.00095	-	-	-	-	-	-	-	-
Height (in)															

* value likely higher at another location, but gage was lost

** 94/14 strains were interpolated from graphs because the original strains were recorded in drift, not ductility

"-" = strain information not available

180 DEGREE LOCATION

(all ductility values reported as in/in)

PULL

Height above footing (in)	97/05 TU1 spiral	97/05 TU7 spiral	94/14** Col 1 spiral	94/14** Col 2 spiral	93/01 R5 stirrup	93/01 R6 steel jacke	94/08 Col 1 hoops	94/08 Col 2 hoops	91/06 TU3 hoops	91/06 TU4 hoops	91/06 TU4 steel jacket	99/08 VP1	99/08 VP2	TR 97/07 carbon jacket	TR 97/07 hoops
	0	28	10	10	12	2.5	0	15	18	7	2	-3	0	39	39
Ductility 1	0.0002	0.001	0.00086	0.0003	0.00064	0.00035	0.00032	0	-0.0001	-6E-05	0.0002	-0.0006	0.0013	0.00053	0.00049
Height (in)										58					
Ductility 2	0.0084	0.0027	-	0.00043	0.0011	0.00055	0.00042	0.0066	0.00009	0.00026	0.00029	-0.0013	0.0013	0.00079	0.00081
Height (in)		24						60	2					21	
Ductility 3	0.0046	0.007	-	0.00078	0.00165	0.00087	0.0005	0.0082	0.0002	0.00023	0.00048	-0.0018	0.0012	0.00112	0.0011
Height (in)									12					21	
Ductility 4	0.0043	-	-	0.00067	-	0.00125	0.00059	0.0127	-0.0004	-6E-05	0.00054	-0.0035	0.001	0.00167	0.00166*
Height (in)										28					
Ductility 6	-	-	-	-	-	0.0023	0.00016*	-	-	-7E-05	0.00062	-0.0075	-0.006	0.00283	0.0028*
Height (in)							60			28					
Ductility 8	-	-	-	-	-	-	0.00036*	-	-	-	-	-	-	0.00299	0.00293*
Height (in)							60								
Ductility 10	-	-	-	-	-	-	0.00075	-	-	-	-	-	-	-	-
Height (in)							72								

* value likely higher at another location, but gage was lost

** 94/14 strains were interpolated from graphs because the original strains were recorded in drift, not ductility

"-" = strain information not available

270 DEGREE LOCATION

(all ductility values reported as in/in)

PUSH

Height above footing (in)	97/05 TU1 spiral 20	97/05 TU7 spiral 28	94/14** Col 1 spiral 10	94/14** Col 2 spiral 10	96/07 L1 hoops 96	96/07 L1-R fg jacket 53	93/01 R5 stirrup 7	93/01 R6 steel jacke 8	94/08 Col 1 hoops 72	94/08 Col 2 hoops 72	91/06 TU3 hoops 2	91/06 TU4 hoops 2	91/06 TU4 steel jacket -	99/08 VP1 -3	99/08 VP2 0	TR 97/07 carbon jacket 39	TR 97/07 hoops 15	NIST Flexure spiral 7	NIST Shear spiral 7
Ductility 1 Height (in)	0	0.0017	0.00037	0.0004	0.02	0.0018	0.00036	0.00015	0.00037	0.00046	0.00018 28	0.0002	-	0.00021	0.0011	0.00051	0.00001	0.00027	0.00018
Ductility 2 Height (in)	0.0001	0.006	0.00143	0.00065	-	0.0026	0.0013	0.00021	0.00062	0.00072	0.00042	0.00089	-	0.0002	0.00114	0.00342 15	0.0034	0.00289	0.00074
Ductility 3 Height (in)	0.0004*	0.0093	0.00184	0.00076	-	0.0028	0.0026	0.00037	0.00105	0.0012	0.00051	0.00073	-	0.0003	0.00115	0.00117*	-	0.00342 56	-
Ductility 4 Height (in)	0.0009*	-	0.00205	0.00095	-	0.0035	-	0.0006	0.0015	0.0017	0.00051	0.00076	-	0.0004	0.00128	0.00141*	-	0.00662 56	0.00175
Ductility 6 Height (in)	-	-	-	-	-	0.0047	-	0.00089 2.5	0.0019	-	-	-	-	-0.0003	0.0022	0.00205*	-	0.01 28	0.00253
Ductility 8 Height (in)	-	-	-	-	-	-	-	-	0.0025	-	-	-	-	-	-	0.0022*	-	-	0.00518 -2
Ductility 10 Height (in)	-	-	-	-	-	-	-	-	0.0037	-	-	-	-	-	-	-	-	-	-

* value likely higher at another location, but gage was lost

** 94/14 strains were interpolated from graphs because the original strains were recorded in drift, not ductility

"-" = strain information not available

"fg" = fiberglass

270 DEGREE LOCATION

(all ductility values reported as in/in)

PULL

Height above footing (in)	97/05 TU1 spiral 20	97/05 TU7 spiral 28	94/14** Col 1 spiral 10	94/14** Col 2 spiral 10	96/07 L1 hoops 96	96/07 L1-R fg jacket 37	93/01 R5 stirrup 12	93/01 R6 steel jacke 2.5	94/08 Col 1 hoops 72	94/08 Col 2 hoops 58	91/06 TU3 hoops 2	91/06 TU4 hoops 2	91/06 TU4 steel jacket -	99/08 VP1 -3	99/08 VP2 0	TR 97/07 carbon jacket 39	TR 97/07 hoops 15	NIST Flexure spiral 7	NIST Shear spiral 7
Ductility 1	0.0001	0.0022	0.00018	0	0.02	0.0014	0.0005	0.00015	0.00015	0.00015	0.00053	0.00057	-	-5E-05	0.00022	0.00038	0.00005	0.00213	0.00014
Height (in)						76		8		24	18								
Ductility 2	0.0004	0.0054	0.00067	0.0004	-	0.0019	0.00117	0.0002	0.00039	0.00062	0.00125	0.00134	-	-0.0006	0.00021	0.00466	0.00468	0.00298	0.0005
Height (in)								8								15			28
Ductility 3	0.0012*	0.008*	0.00085	0.00047	-	0.0026	0.00255	0.00035	0.00042	0.00089	0.00139	0.0009	-	-4E-05	0.00026	0.001*	-	0.00369	-
Height (in)		46					7					8							
Ductility 4	0.0014*	-	0.00093	0.00057	-	0.0035	-	0.00054	0.00058	0.0016	0.00156	0.00115	-	-0.0001	0.00041	0.00118*	-	0.00609	0.00105
Height (in)										0		8						56	
Ductility 6	-	-	-	-	-	0.0045	-	0.00097	0.00112	-	-	-	-	-0.0003	0.0013	0.00171*	-	0.00876	0.00183
Height (in)																57		28	
Ductility 8	-	-	-	-	-	-	-	-	0.0019	-	-	-	-	-	-	0.00199*	-	-	-
Height (in)																57			
Ductility 10	-	-	-	-	-	-	-	-	-	-	-	-	-	-	-	-	-	-	-
Height (in)																			

* value likely higher at another location, but gage was lost

** 94/14 strains were interpolated from graphs because the original strains were recorded in drift, not ductility

"-" = strain information not available

"fg" = fiberglass

APPENDIX C

C Graphs depicting strain vs. displacement ductility at each degree location

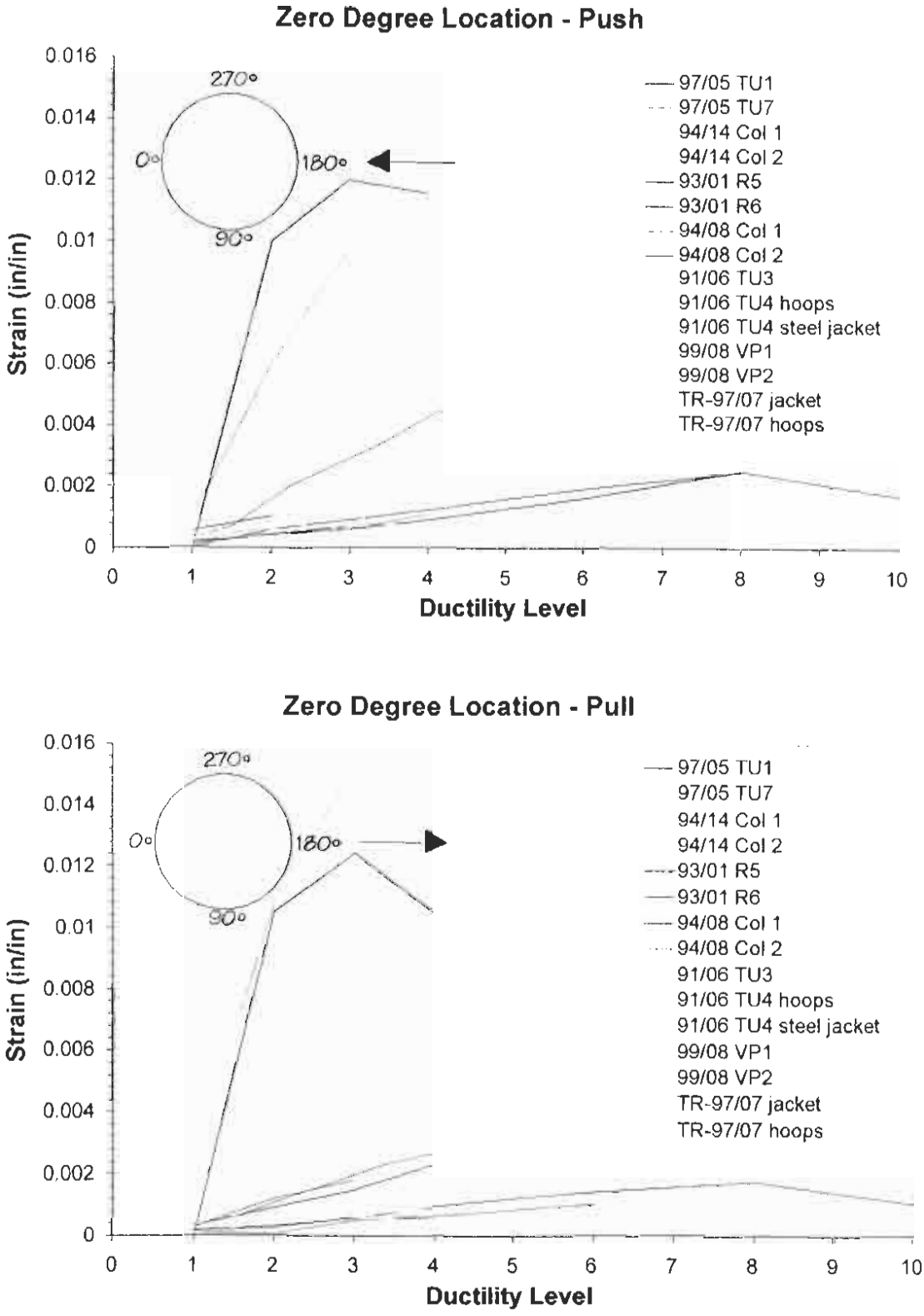

Figure C.1: Comparison of transverse strains at 0° location

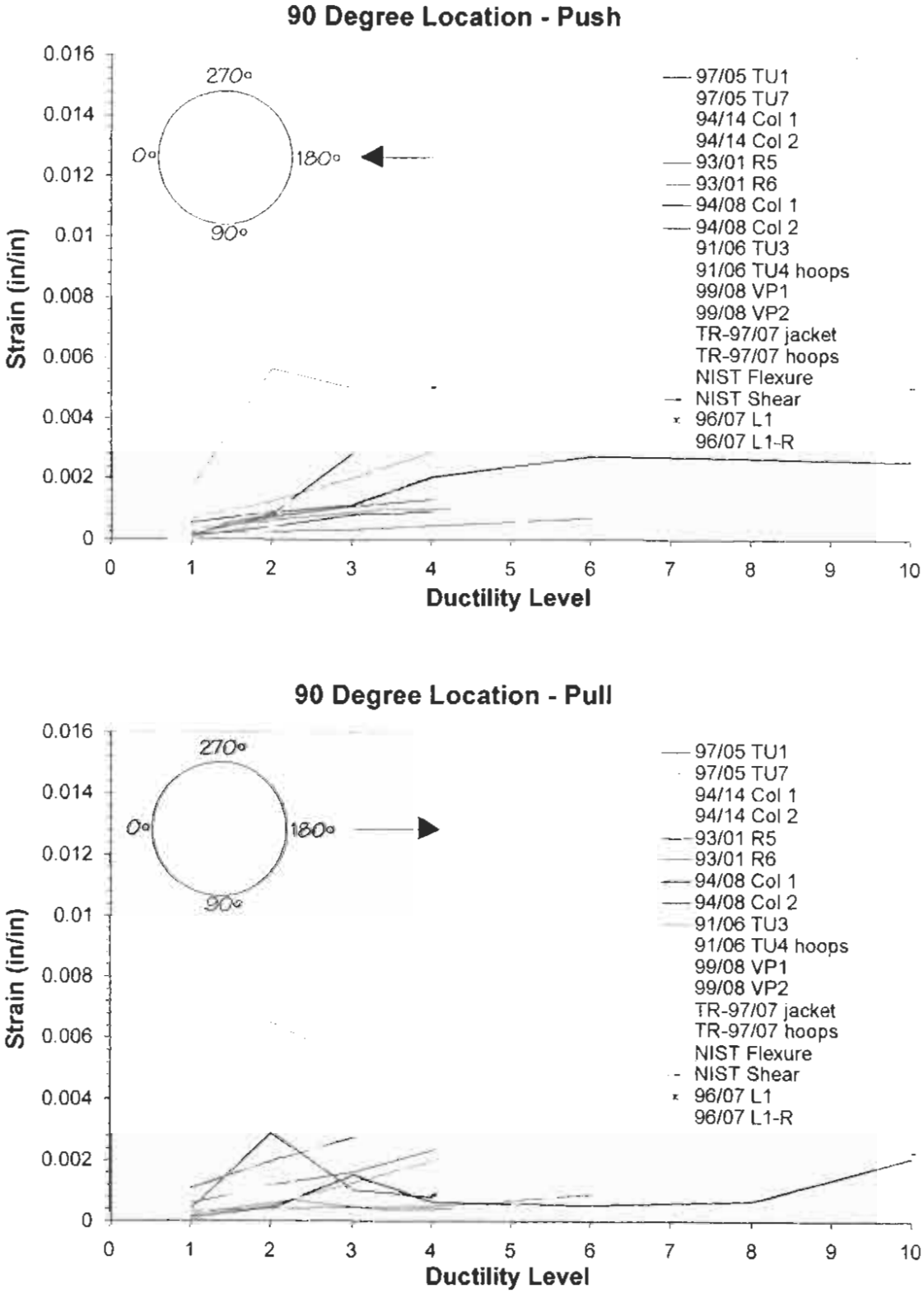

Figure C.2: Comparison of transverse strains at 90° location

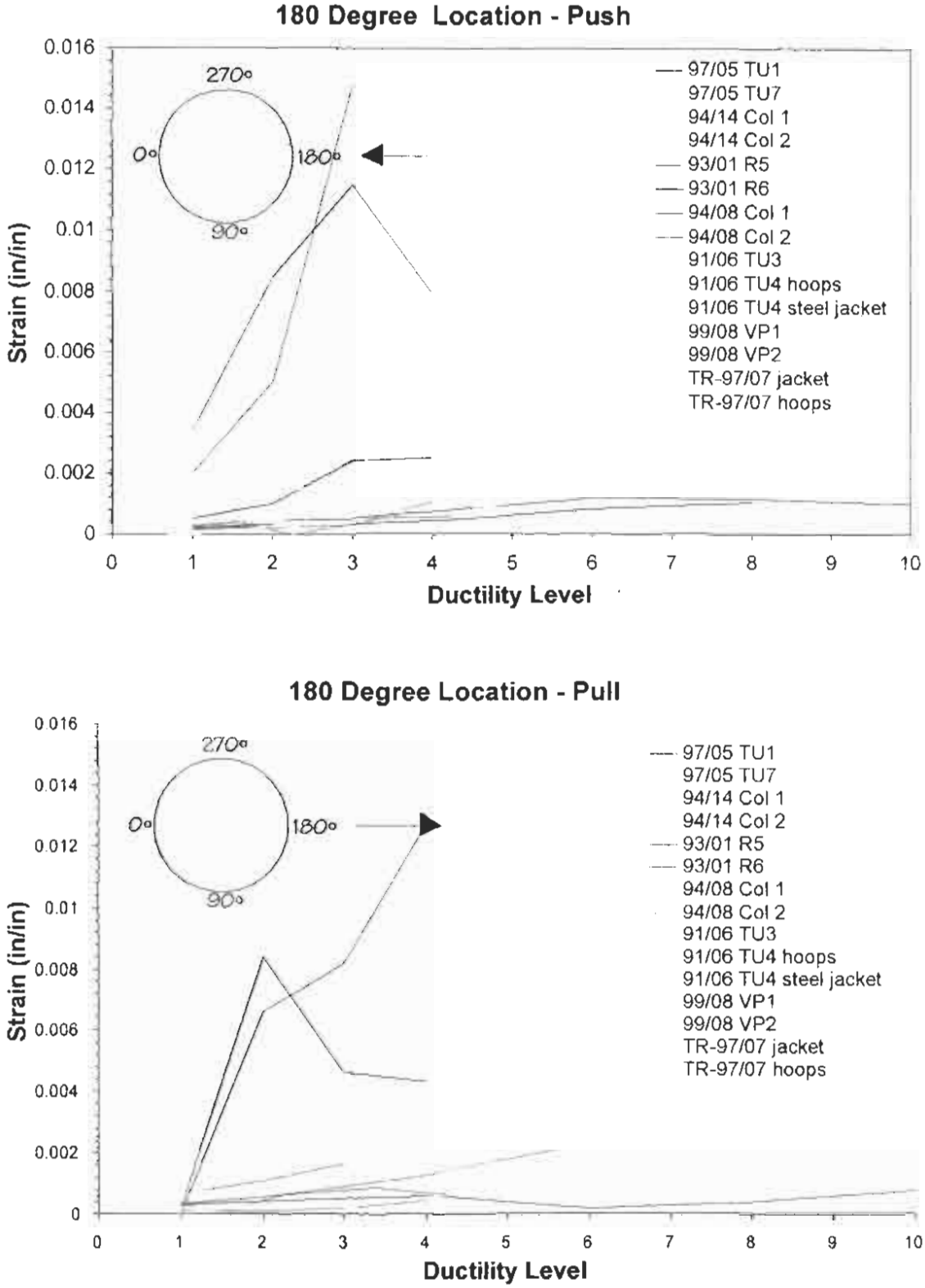

Figure C.3: Comparison of transverse strains at 180° location

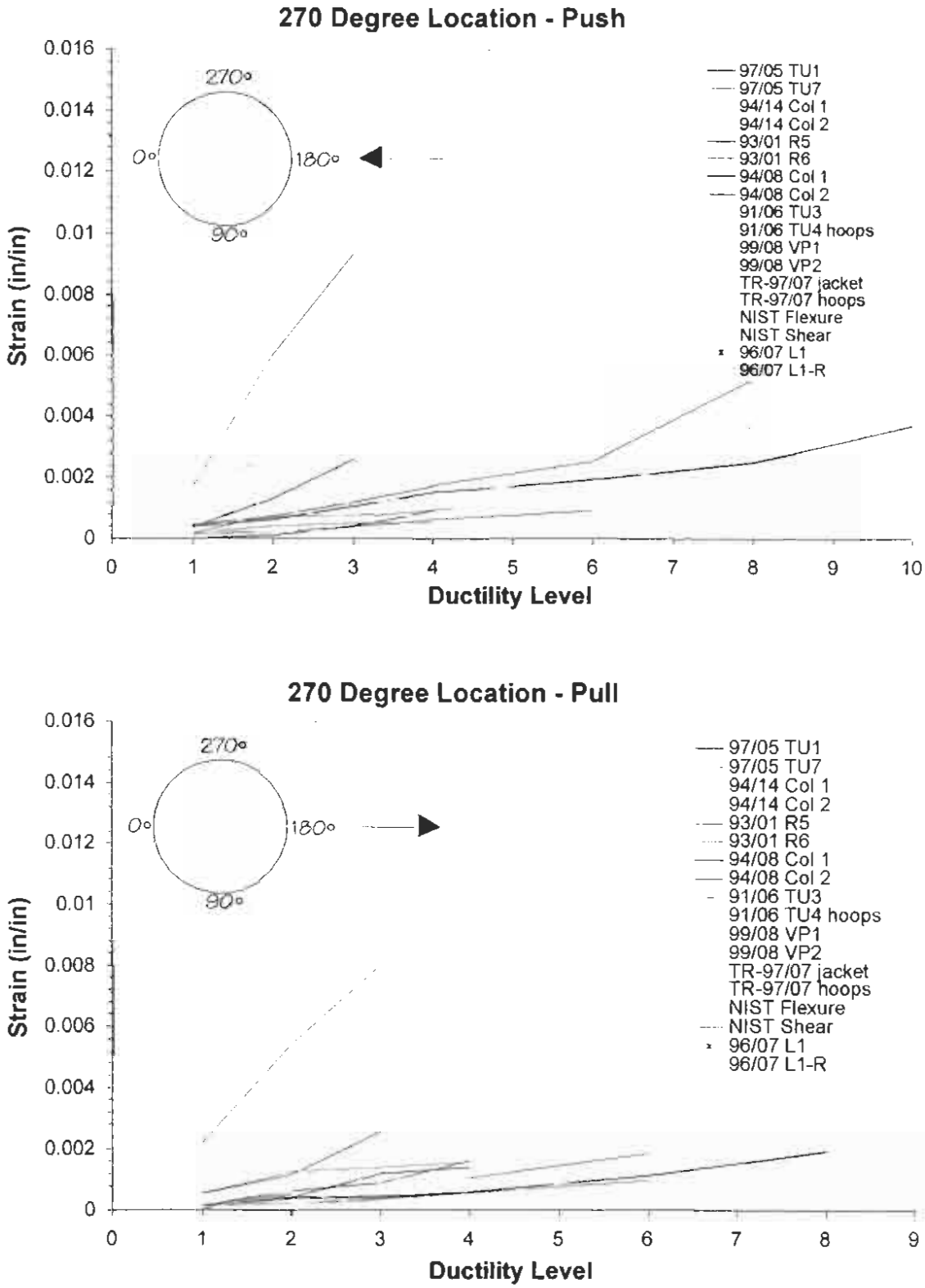

Figure C.4: Comparison of transverse strains at 270° location

APPENDIX D

D Graphs of circumferential strain profiles at various displacement ductility levels

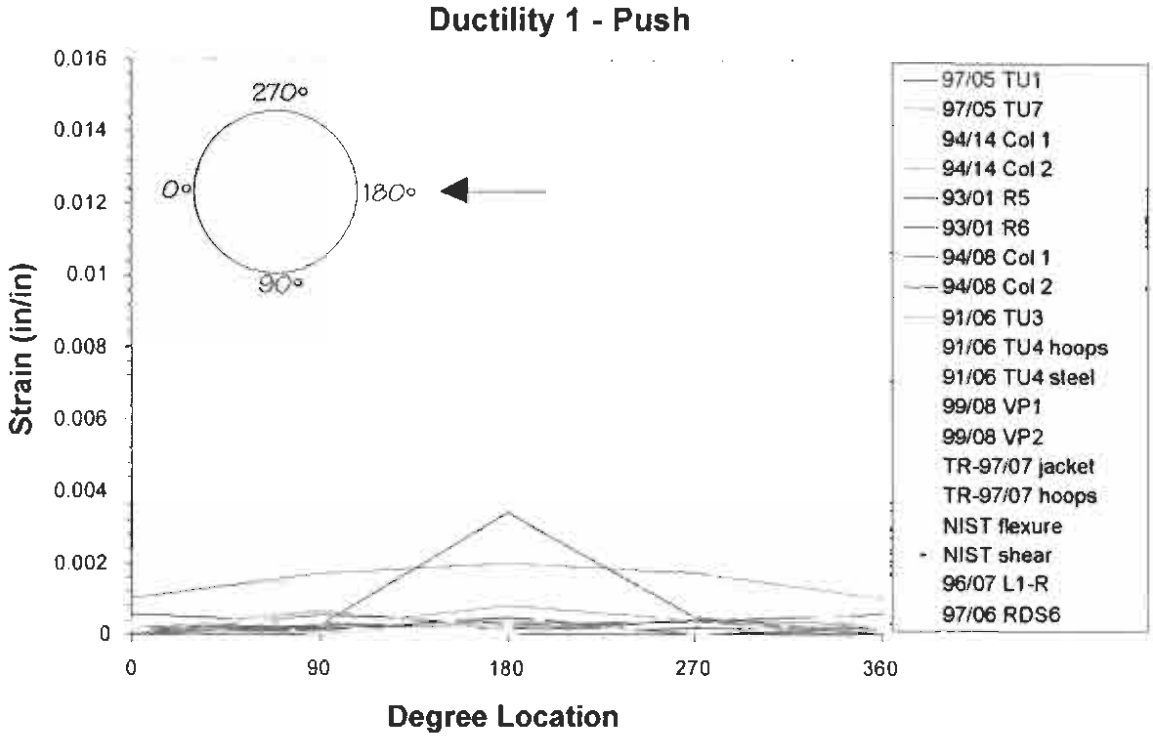

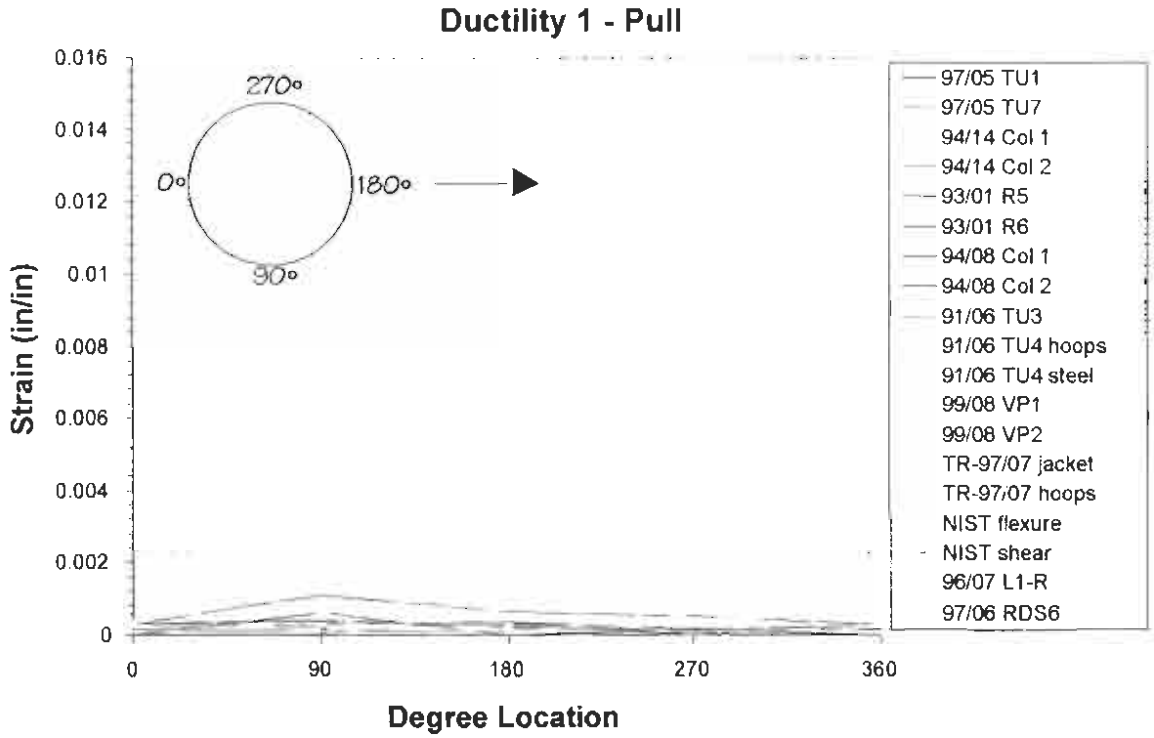

Figure D.1: Comparison of transverse strains at displacement ductility 1

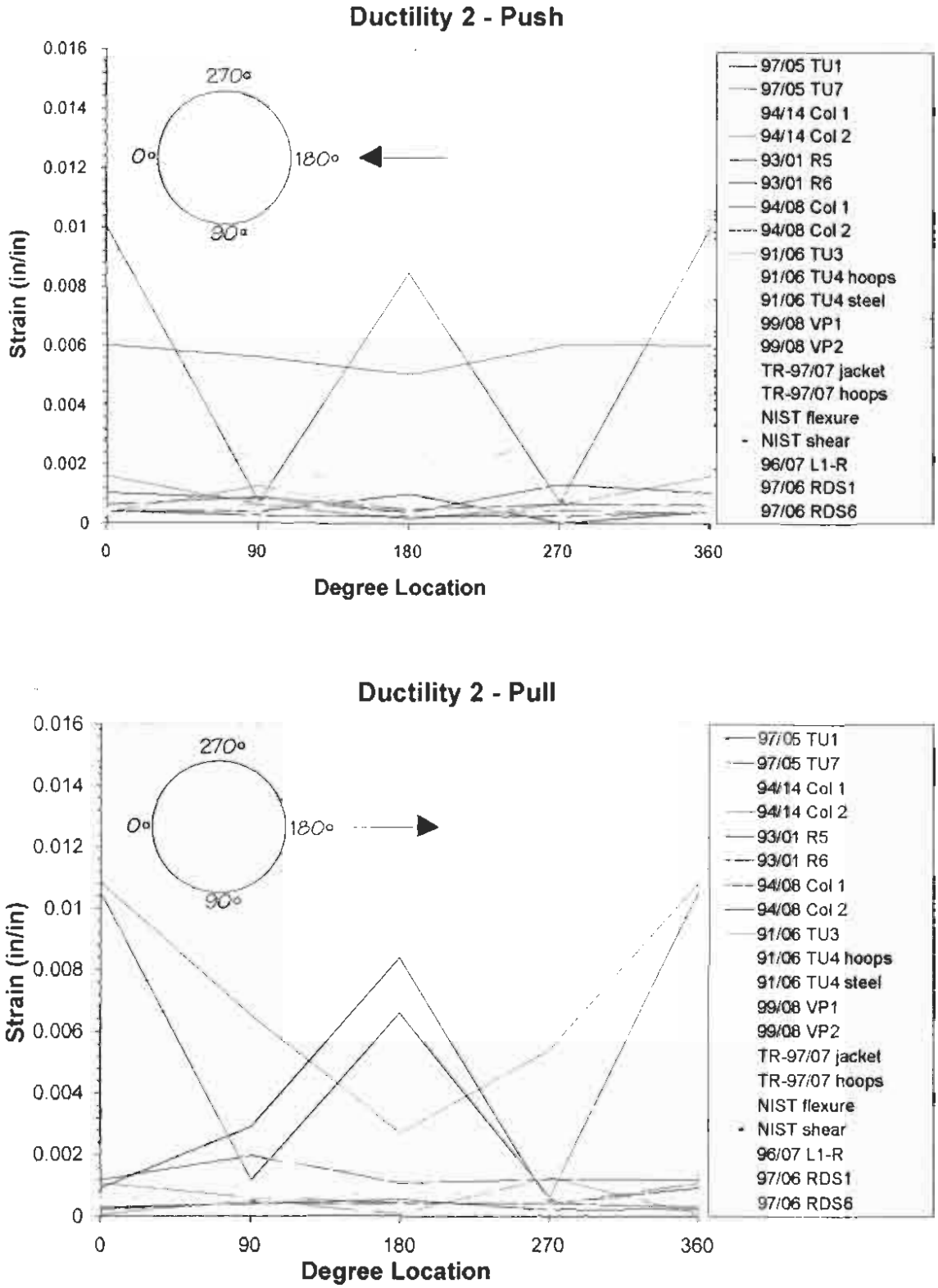

Figure D.2: Comparison of transverse strains at displacement ductility 2

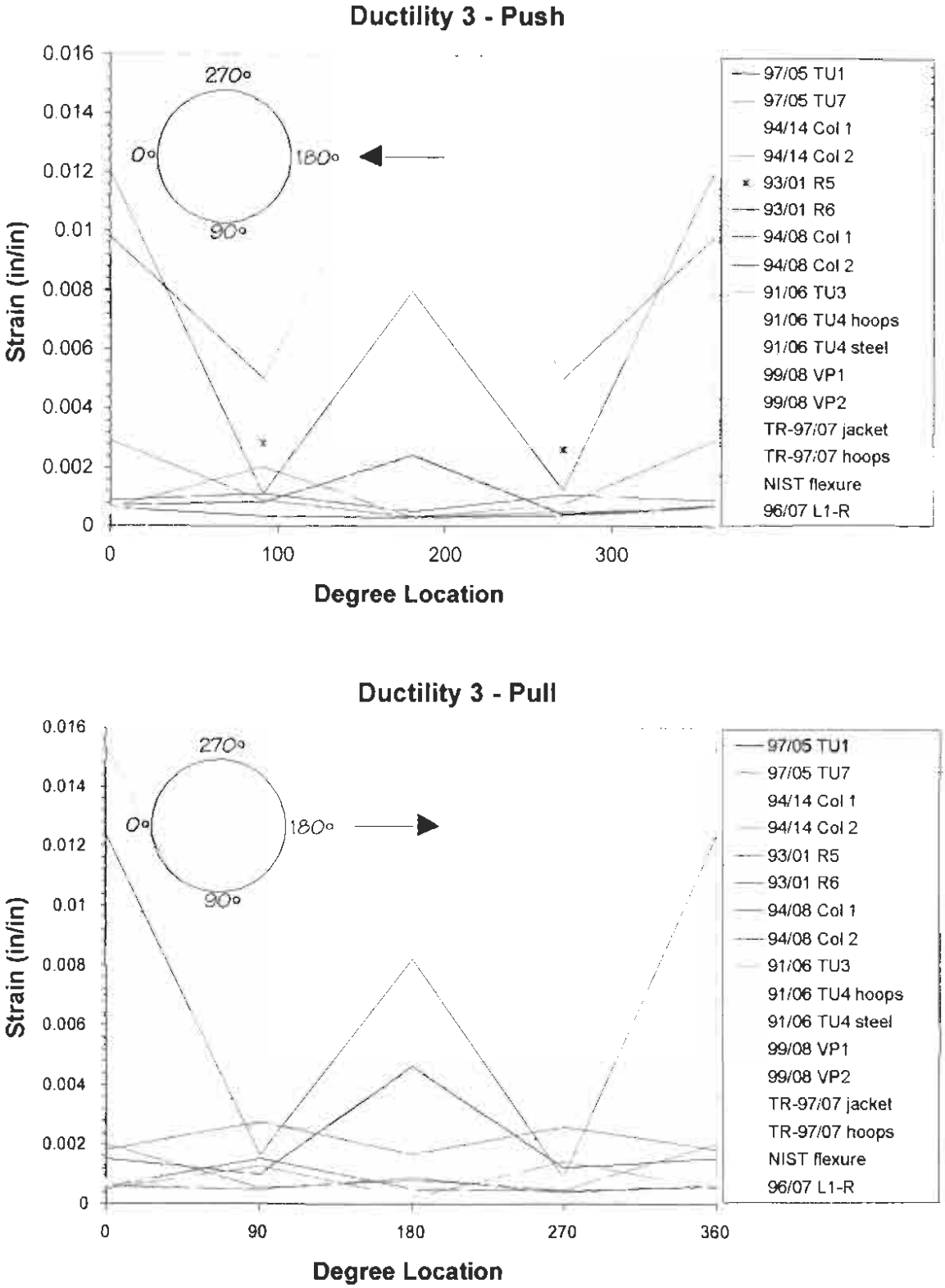

Figure D.3: Comparison of transverse strains at displacement ductility 3

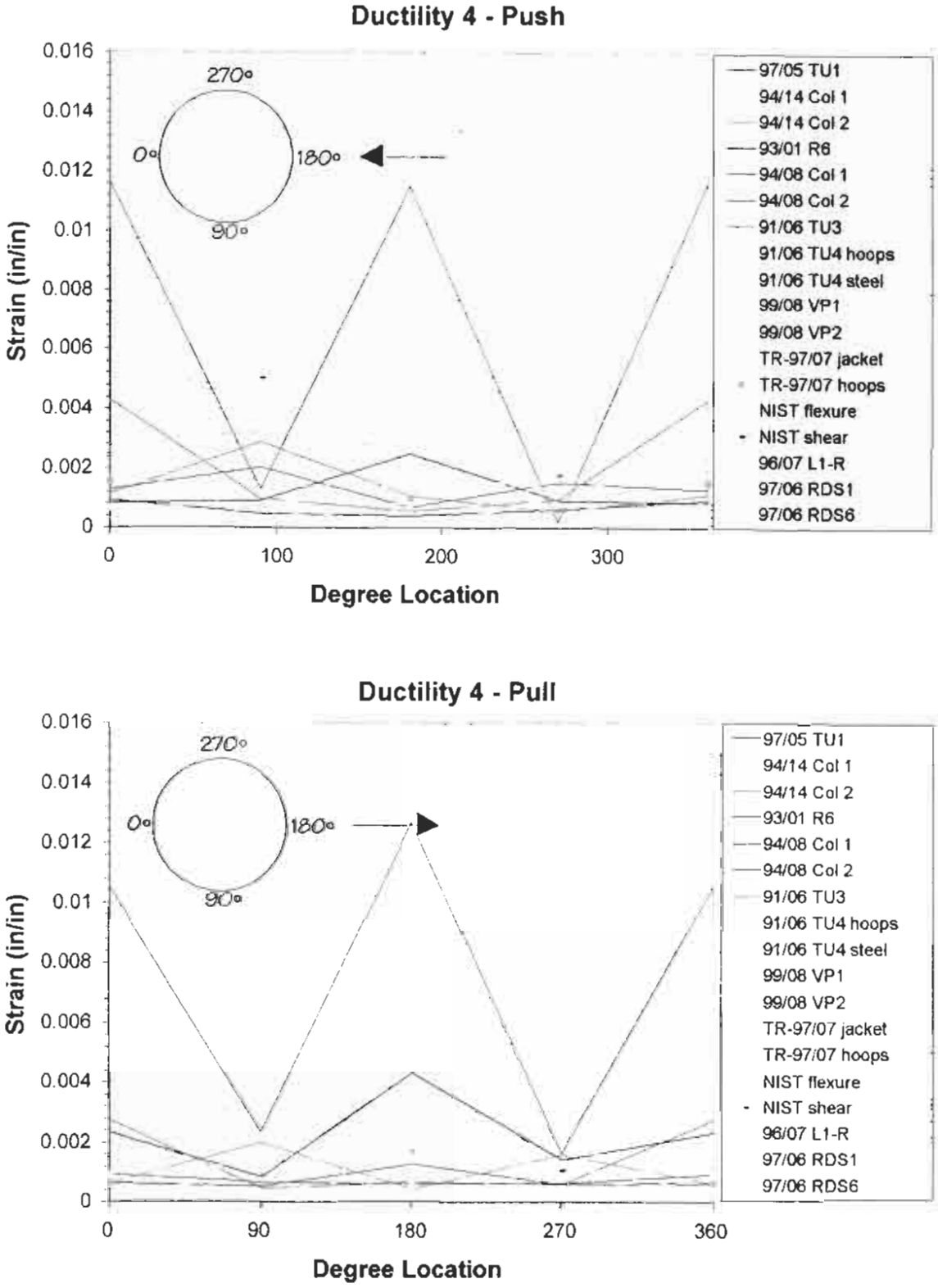

Figure D.4: Comparison of transverse strains at displacement ductility 4

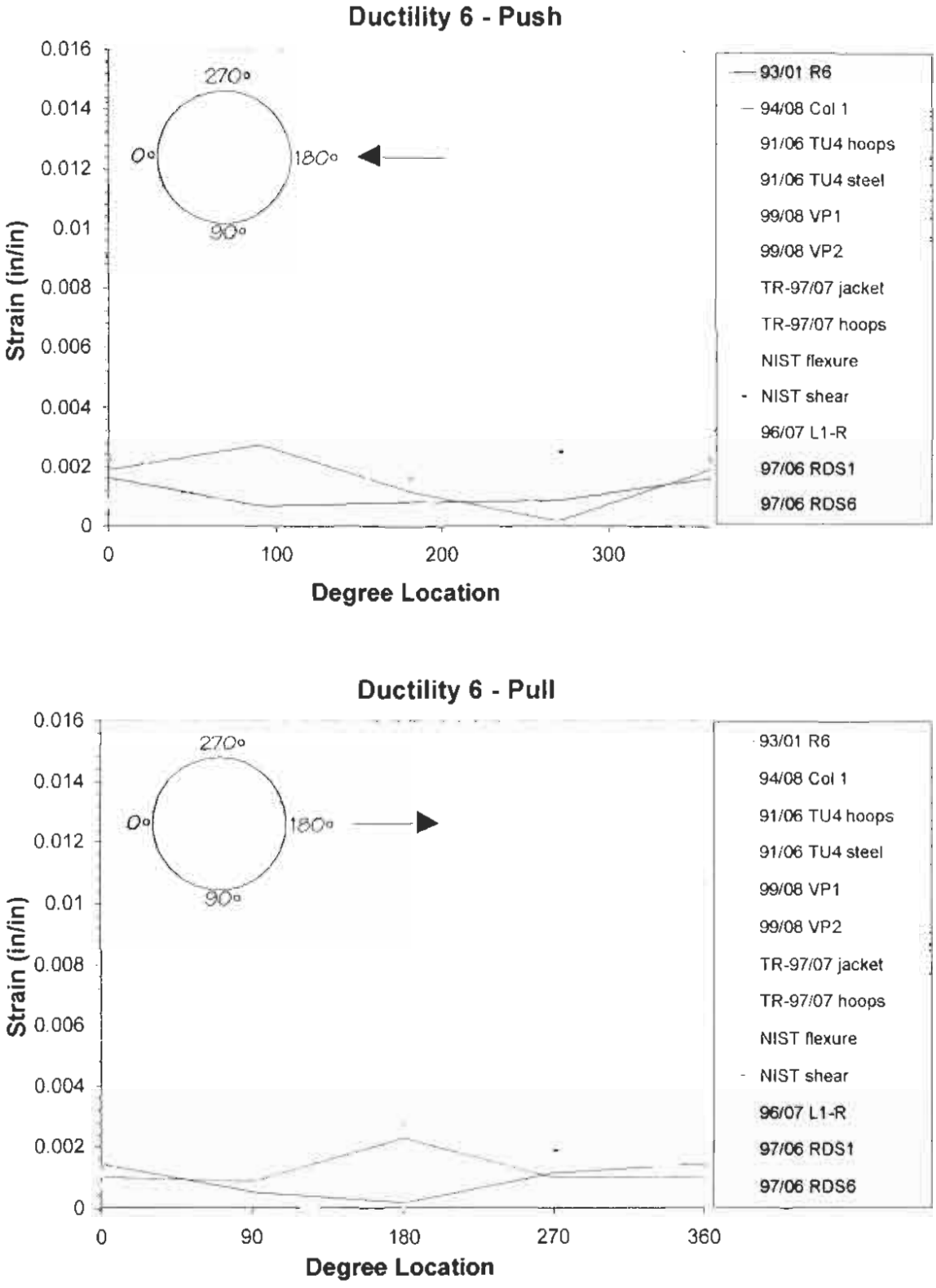

Figure D.5: Comparison of transverse strains at displacement ductility 6

APPENDIX E

Graphs of circumferential strain profiles from moment-curvature analyses at displacement ductility levels 4, 5 and 6 for 6 ft and 8 ft columns

E Graphs of circumferential strain profiles from moment-curvature analyses at displacement ductility levels 4, 5 and 6 for 6ft and 8ft columns

Moment-curvature analyses were conducted for a 6 ft diameter column with an axial load ratio of 5 percent and an 8 ft diameter column with an axial load ratio of 10 percent. In all cases the longitudinal steel ratio was taken as 2 percent. Transverse steel ratios of 0.5 % and 1 % were investigated for each size column. The analysis results are presented in terms of hoop strain around the section at displacement ductility levels 4, 5 and 6 in Figures E.1 through E.4. An aspect ratio of 4 was assumed to calculate the equivalent plastic hinge length, required to convert curvature to displacement ductility, resulting in plastic hinge length to column length ratios of 0.139 and 0.124 for the 6 ft and 8 ft columns, respectively. For the 6 ft column, 36 #14 bars were used for the longitudinal steel with # 6 hoops. For the 8 ft column, a total of 66 # 14 bars (bundled radially) were used for the longitudinal steel with # 8 hoops. Clear cover of 2 inches to the hoops was used.

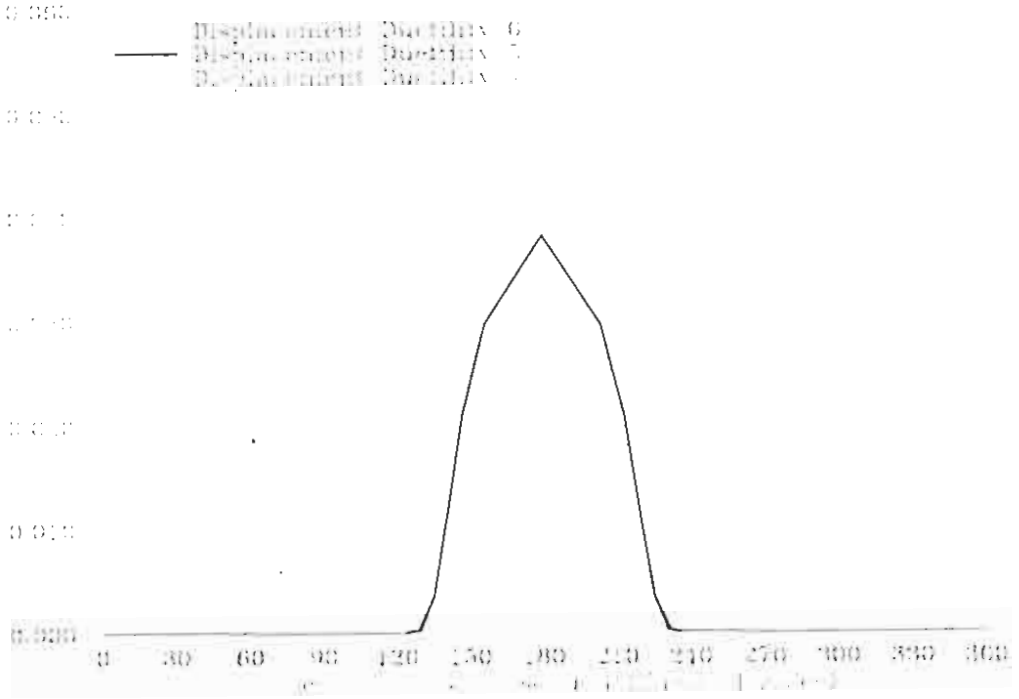

Figure E.1: Hoop strains for 6 ft column with axial load ratio = 5 %, ρ_l = 2 % and ρ_S = 1 %.

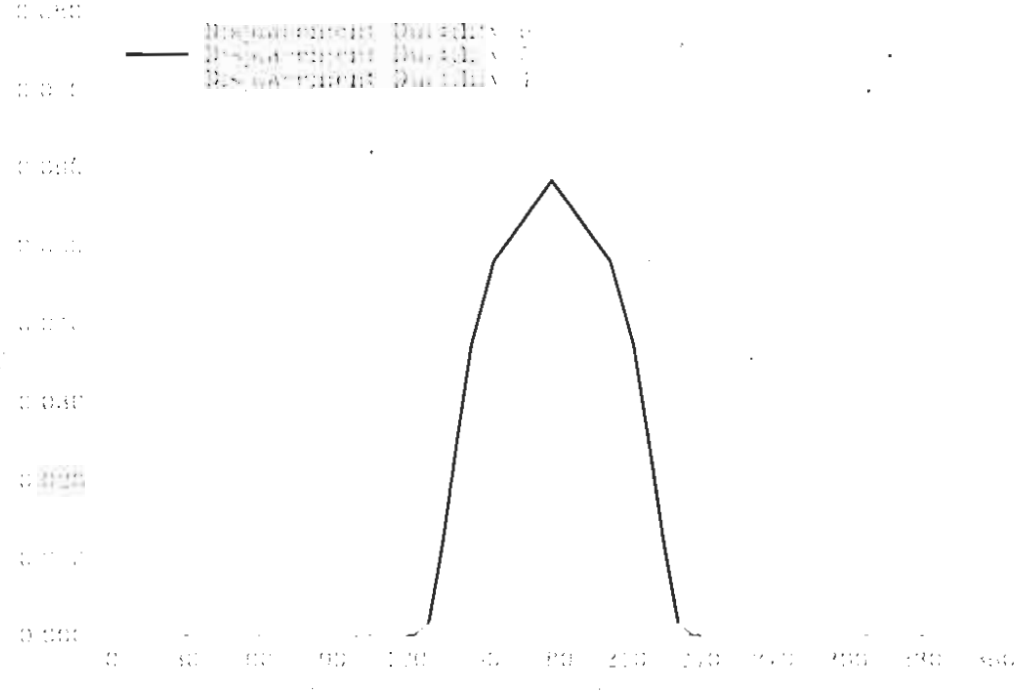

Figure E.2: Hoop strains for 6 ft column with axial load ratio = 5 %, ρ_l = 2 % and ρ_S = 0.5 %.

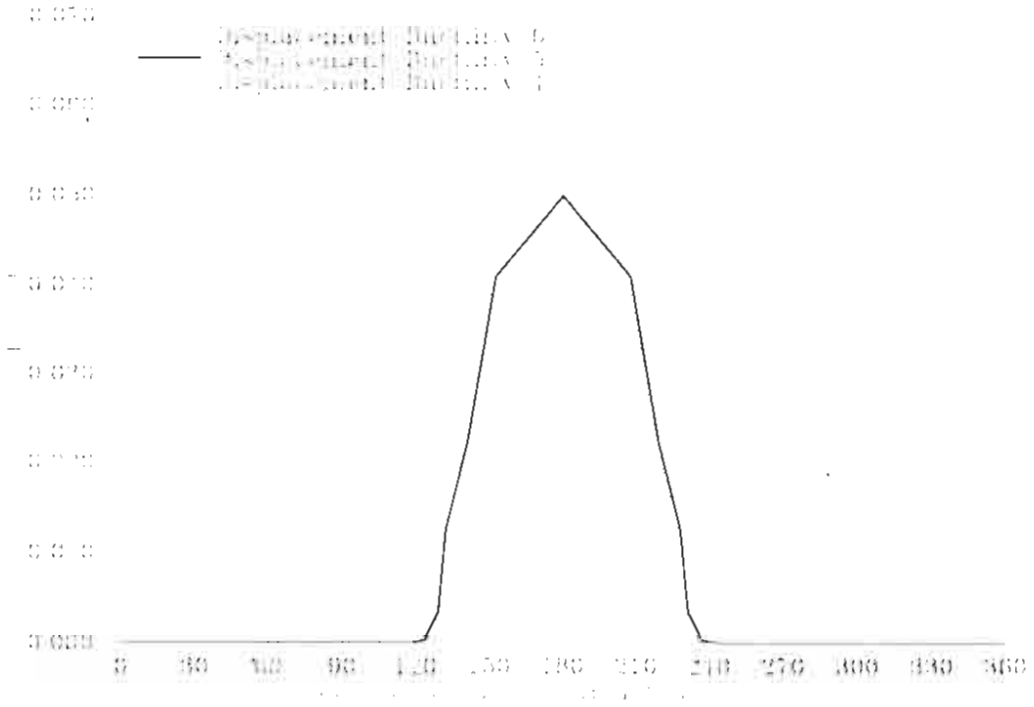

Figure E.3: Hoop strains for 8 ft column with axial load ratio = 10 %, ρ_l = 2 % and ρ_S = 1 %.

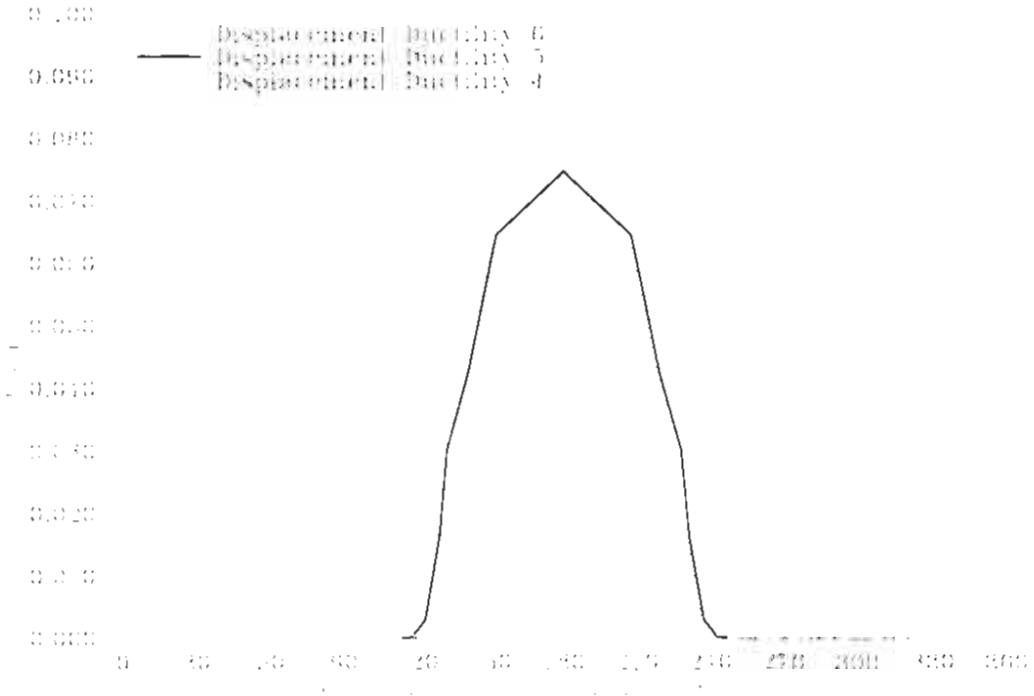

Figure E.4: Hoop strains for 8 ft column with axial load ratio = 10 %, ρ_l = 2 % and ρ_S = 0.5 %.